INVESTIGATION OF CHARACTERISTICS AND PERFORMANCE OF POLYVINYLCHLORIDE (PVC) ULTRAFILTRATION MEMBRANES IMPREGNATED WITH SILICA ORIENTED CARBON NANOTUBES

Degree of Master of Science

Chahrazed MAHMOUDI

Eskişehir, 2019

INVESTIGATION OF CHARACTERISTICS AND PERFORMANCE OF POLYVINYLCHLORIDE (PVC) ULTRAFILTRATION MEMBRANES IMPREGNATED WITH SILICA ORIENTED CARBON NANOTUBES

Chahrazed MAHMOUDI

DEGREE OF MASTER OF SCIENCE

Chemical Engineering Department

Supervisor: Assist. Prof. Dr. Elif DEMİREL

Eskişehir

Eskişehir Technical University

Institute of Graduate Programmes

August, 2019

This thesis has been supported by the Scientific Research Project Commission of Eskisehir Technical University under the project number of 1706F384.

FINAL APPROVAL FOR THESIS

This thesis titled “Investigation of Characteristics and Performance of Polyvinylchloride (PVC) Ultrafiltration Membranes Impregnated With Silica Oriented Carbon Nanotubes” has been prepared and submitted by Chahrazed Mahmoudi in partial fulfillment of the requirements in “Eskişehir Technical University Directive On Graduate Education and Examination” for the Degree of Master of Science in Chemical Engineering Department has been examined and approved on…../…../……

Committee Members	**Title, Name and Surname**	**Signature**
Member (Supervisor)	: Assist.Prof.Dr. Elif DEMİREL	……
Member	: Prof.Dr. Süleyman KAYTAKOĞLU	……
Member	: Assoc.Prof.Dr. Selçuk ÖZCAN	……

Prof.Dr. Murat TANIŞLI
Director of Institute of Graduate Programmes

ABSTRACT

INVESTIGATION OF CHARACTERISTICS
AND PERFORMANCE OF POLYVINYLCHLORIDE (PVC) ULTRAFILTRATION
MEMBRANES IMPREGNATED WITH SILICA ORIENTED CARBON NANOTUBES

Chahrazed MAHMOUDI

Department of Chemical Engineering
Eskişehir Technical University, Institute of Graduate Programmes, August, 2019

Supervisor: Assist. Prof. Dr. Elif DEMİREL

In this thesis, silica oriented multi-walled carbon nanotubes (Si-MWCNT) were synthesized by sol-gel method and characterized using several analytical techniques. Novel polyvinyl chloride (PVC) ultrafiltration membranes were fabricated by incorporation of Si-MWCNT nanoparticles with varying loading levels (0-2 wt.%) using phase inversion method. Membrane morphology, chemical composition, thermal behavior, crystallinity, roughness, hydrophilicity and mechanical strength of the membranes were characterized using several analytical techniques and instruments. Membrane filtration performance was tested in terms of water flux, solute rejection, and anti-fouling characteristics and the results were compared to those of pristine PVC membrane. The results revealed that addition of 0.5% Si-MWCNT nanoparticles into the casting solution exhibited the highest flux (400 L/m^2h), sodium alginate rejection rate (%96) and flux recovery ratio (93%) due to having the highest hydrophilicity, an improved structure and surface properties revealed by the surface morphology and bulk property analysis. Furthermore, dynamic mechanical and nanoindentation analysis results confirmed that mechanical properties such as hardness, Young's modulus and stiffness of the pristine membrane were significantly improved by the addition of Si-MWCNT nanoparticles.

Key Words: Membrane, Ultrafiltration, Nanoparticle, Silica, Carbon nanotube

ÖZET

SİLİKA KAPLI KARBON NANOTÜP İÇEREN POLİVİNİLKLORÜR (PVC) ULTRAFİLTRASYON MEMBRANLARIN ÖZELLİKLERİ VE PERFORMANSININ ARAŞTIRILMASI

Chahrazed MAHMOUDI

Kimya Mühendisliği Anabilim Dalı
Eskişehir Teknik Üniversitesi, Lisansüstü Eğitim Enstitüsü

Danışman: Dr.Öğr.Üyesi Elif DEMİREL

Bu tez çalışmasında, silika kaplı karbon nanotüpler (Si-MWCNT) sol-jel yöntemiyle sentezlenmiş ve çeşitli analiz yöntemleriyle karakterize edilmiştir. Farklı oranlarda Si-MWCNT nanotaneciklerin kullanılmamasıyla (%0-2, a/a) faz dönüşüm tekniği ile yeni polivinil klorür (PVC) ultrafiltrasyon membranlar hazırlanmıştır. Hazırlanan membanların, yüzey ve kesit morfolojisi, kimyasal kompozisyonu, ısıl davranışı, pürüzlülüğü, hidrofilikliği ve mekanik dayanımı, çeşitli analitik yöntem ve cihazlar kullanılarak araştırılmıştır. Membran su akısı, madde giderimi ve antitıkanma gibi filtrasyon özellikleri belirlenerek saf PVC membranın özellikleriyle karşılaştırılmıştır. Elde edilen sonuçlara göre, yüzey morfoloji ve yığın özellikleri ile kanıtlanmış olan yüksek hidrofilikliği, iyileştirilmiş yapı ve yüzey özelliklerine bağlı olarak membran döküm çözeltisine 0,5% Si-MWCNT nanotaneciği ilave edilmesiyle saf su akışı (400 L/m^2h), sodyum aljinat giderimi (%96) ve antitıkanma özelliği (%93) en yüksek değerlere ulaşmıştır. Ayrıca, dinamik mekanik ve nanosertlik analiz sonuçlarına göre, silika kaplı karbon nanotüpolerin membran matrisine ilavesi, saf PVC membranın sertlik ve Young modülü gibi mekanik özelliklerini önemli derecede iyileştirmiştir.

Anahtar kelimler: Membran, Ultrafiltrasyon, Nanotanecik, Silika, Karbon nanotüp

ACKNOWLEDGMENT

First of all, I would like to express my deepest thanks and gratitude to my supervisor, Assist. Prof. Dr. Elif DEMIREL for the competent and valuable help she has given me, for her patience and encouragement. Her critical eye was very valuable for structuring and improving the quality of this thesis.

A very special gratitude goes out to Bahadır ERDUĞAN and Sakhavat DADASHOV for their friendship and the invaluable help they have given me throughout this work.

I am also deeply grateful to my professor Prof. Dr. Hacene MAHMOUDI for all the help and advices that he has given me since the beginning of my career in Turkey

I especially thank my parents Djilali MAHMOUDI and Khadija CHAFAI for the support, motivation and facilities they have given me throughout my entire education life.

I would like to thank Prof. Dr. İdris AKYÜZ from the Department of Physics at Eskisehir Osmangazi University for carrying out the AFM analysis.

I am thankful to all the faculty members during my studies in Algeria and in Turkey to share their information with me.

I would like to express my gratitude to my sisters and my friends who have given me their moral and intellectual support throughout my journey. A big thanks goes for Hamza for his advice. Finally, I want to express my gratitude to my sister Wissam and my cousins Samah, Houda and Ghaniya, for their trust and their invaluable support.

Chahrazed MAHMOUDI

…./…./20….

STATEMENT OF COMPLIANCE WITH ETHICAL PRINCIPLES AND RULES

I hereby truthfully declare that this thesis is an original work prepared by me; that I have behaved in accordance with the scientific ethical principles and rules throughout the stages of preparation, data collection, analysis and presentation of my work; that I have cited the sources of all the data and information that could be obtained within the scope of this study, and included these sources in the references section; and that this study has been scanned for plagiarism with "scientific plagiarism detection program" used by Eskişehir Technical University, and that "it does not have any plagiarism" whatsoever. I also declare that, if a case contrary to my declaration is detected in my work at any time, I hereby express my consent to all the ethical and legal consequences that are involved.

…….

(Signature)

Chahrazed MAHMOUDI

TABLE OF CONTENTS

LIST OF TABLES

LIST OF FIGURES

LIST OF ABBREVIATION

ε	: Porosity (%)
ρ_w	: Density of water (g/cm^3)
Δt	: Time interval (s)
ΔV	: Volume change of the permeate (L)
A	: Membrane filtration area (m^2)
a	: Mean pore diameter (m)
AFM	: Atomic Force Microscopy
C_f	: Concentration of feed (ppm)
CNT	: Carbon nanotube
C_P	: Concentration of feed (ppm)
DMA	: Dynamic Mechanical Analysis
DMAc	: N,N-dimethylacetamide
DMF	: N,N-dimethylformamide
E	: Young's modulus (GPa)
E'	: Storage modulus (MPa)
E''	: Loss modulus (MPa)
EDX	: Energy-Dispersive X-ray Spectroscopy
FRR	: Flux recovery ratio (%)
FTIR	: Fourier-Transform Infrared Spectroscopy
H	: Hardness (GPa)
HA	: Humic acid
J	: Water flux (L/m^2h)
$J_{w,1}$	: Pure water flux (L/m^2h)
$J_{w,2}$	: Water flux after fouling
$J_{w,3}$	: Water flux after backwashing
l	: Thickness (cm)
MF	: Microfiltration
MWCNT-COOH	: Functionalized multi-walled carbon nanotube

NF : Nanofiltration

PVC : Polyvinyl chloride

R : Rejection (%)

r : Radius (cm)

$\mathbf{R_a}$: Mean surface roughness

$\mathbf{R_{ir}}$: Irreversible fouling resistance (m^{-1})

$\mathbf{R_m}$: Intrinsic membrane resistance (m^{-1})

RO : Reverse osmosis

$\mathbf{R_q}$: Root mean square roughness

$\mathbf{R_r}$: Irreversible fouling resistance (m^{-1})

$\mathbf{R_t}$: Total filtration resistance (m^{-1})

$\mathbf{Q_w}$: Water flux (m^3/s)

SA : Sodium alginate

SEM : Scanning Electron Microscopy

Si-MWCNT : Silica oriented multi-walled carbon nanotubes

$\mathbf{T_g}$: Glass transition temperature (ºC)

TGA : Thermogravimetric Analyzer

TMP : Transmembrane pressure

TOC : Total Organic Carbon Analyzer

UF : Ultrafiltration

XRD : X-ray Diffraction Analyzer

1. INTRODUCTION

Currently, freshwater pollution has become a worldwide problem since there is an increasing evidence of contamination in water resources due to the presence of various pollutants such as macromolecular proteins, oils, humic acids and dust particles (Saraswathi, Nagendran and Rana, 2018). Studies have revealed that only 0.5% of the overall global water is available as fresh water, while the world fresh water demand has increased (Zhou et al., 2015). Researchers focused on the utilization of membrane separation to enhance the water quality and treatment capacity as quality and treatment of contaminated water is becoming critical (Goh et al., 2015). Membrane technology is widely used for water treatment and purification owing to their advantages compared to the other conventional separation processes based on the higher selectivity, controllable pore forming characteristics, flexibility of operation, high separation efficiency and cost effectiveness (Khan et al., 2018).

Recently, membrane technology has gained attention for the treatment of drinking water, wastewater and ground water. Furthermore, membrane technology is an important process to get high quality products in the food and pharmaceutical industries. In order to increase the purity of water, one membrane process is followed by another. Thus, one membrane may improve the role of the other with the aim of producing drinking water from several resources (Strathmann, 2000; Nicolaisen, 2002).

Moreover, some membrane processes including reverse osmosis, forward osmosis and membrane distillation are promising processes for desalination of both seawater and brackish water, while other water treatment processes such as distillation, sedimentation, coagulation, H_2O oxidation, solar water disinfection and microbial water sludge treatment processes have some drawbacks due to their dependence on influent water (Das et al., 2014).

Membrane is a semi-permeable, selective barrier that permits separation of species in a fluid medium (gas or liquid) established on sieving, diffusive and adsorptive mechanisms. The separation of these components depends on the chemical nature and the electrical charge of the membrane material as well as the physical properties of the membrane and occurs due to the driving force generated by the pressure difference, the concentration

difference, the electrical potential difference or the temperature difference. The transport of a component through a membrane is controlled according to size, shape and load separation in porous membranes and sorption and diffusion model in nonporous membranes (Mulder, 1996). The most common membrane processes especially applied for water treatment are microfiltration, ultrafiltration, nanofiltration, reverse osmosis, electrodialysis and membrane distillation. Among these processes, ultrafiltration (UF) has been widely used to remove variety of materials such as suspended solids, proteins, bacteria, gluten and organic materials from different water resources with the aim of producing high quality potable water. Recently, many researchers have concentrated on the enhancement of ultrafiltration membrane process in terms of membrane materials, separation performance, membrane modules, among which, membrane materials still hold the key to enhance membrane performance (Low et al., 2015).

Generally, UF membranes are fabricated from several materials such as organic, inorganic or composite (organic-inorganic) materials (Ulbricht, 2006). Most commonly used commercial materials for the preparation of ultrafiltration membrane are polymers because of their excellent chemical, physical, thermal as well as mechanical properties and also their reasonable cost. The most common polymers used in the fabrication of membranes can be listed as polysulfone (Psf), polyvinyldenefluride (PVDF), polypyrrole (PPy), polyethylenimine (PEI), polyvinyl chloride (PVC) (Jose, Kappen and Alagar, 2018; Goh et al., 2015). Polymeric ultrafiltration membrane has been considered as a promising and an effective aid for the treatment of wastewater and surface water due to its simplicity in operation with good separation performance (Yu et al., 2014). However, the main disadvantage of all these backbone polymer-based materials involves their hydrophobic nature, which induces to a high fouling attraction created by the deposition or the adsorption of foulants on the surface or inside the pores of the membrane matrix (Zhao et al., 2015; Demirel et al., 2017). Membrane fouling often causes a decrease in the filtration performance, which results in more frequent membrane cleaning. In addition, the mechanical property is an important issue for polymeric UF membranes in terms of long-duration stable performance. In recent years, incorporation of fillers into the membrane matrix by physical blending, chemical grafting and surface modifications have been investigated to enhance membrane separation performance. The rapid growth of techniques

for fabricating new nanostructured materials such as nanoparticles or nanotubes has led to breakthroughs in membrane fabrication to improve mechanical, chemical and thermal properties, as well as to increase membrane filtration performance and antifouling properties compared to those of conventional polymeric membranes (Low et al. 2015). Several types of nanoparticles including alumina (Al_2O_3), titanium oxide (TiO_2), zirconium (ZrO_2), copper (II) oxide (CuO), carbon nanotubes (CNT), graphene oxide, silica (SiO_2), zeolite, iron oxide (Fe_2O_3) and silver (Ag) are commonly used in the fabrication of inorganic-polymeric nanocomposite membranes. Among these materials, multiwall carbon nanotubes (MWCNT) and silica are the most conveniently and commonly used (Low et al., 2014; Yu et al., 2015).

Due to their large surface area, functionalization ability and exceptional properties, CNT especially MWCNT enhances the membrane performance, mechanical, chemical and thermal stability by altering the structure and morphology of the membrane matrix. Moreover, the tubular shape of MWCNT nanoparticles can offer the fast transport way to pass water molecules and facilitate mass transfer in the process of membrane formation which makes the membrane exhibit better pore structure (Sianipar et al., 2007; Al-Hobaib et al., 2017). However, because of the Van der Waals interactions among the tubes, the uniform dispersion of CNT nanoparticles in polymer matrix is very difficult, which greatly limit their application. In order to overcome the obstacles for the application of CNT, some functionalized CNT, such as carboxylic acid-functionalized CNT, sulfonated CNT and phosphonated CNT have been used as inorganic fillers (Liu et al. 2016). Silica is a widely used inorganic filler in the production of composite membranes due to its inertness, hydrophilicity, well-known chemical properties, low cost and mature preparation techniques. Integration of Silica nanoparticles into the polymeric membrane could enhance the membrane performance in terms of thermal behavior, antifouling properties owing to the low surface energy as well as mechanical stability by introducing additional pores. Previous studies confirmed that nano-SiO_2 addition to the PVC membrane presented better antifouling resistance and higher flux recovery ratio (Zargar et al., 2017; Yu et al., 2015).

In this thesis, commercial oxidized multi walled carbon nanotubes (MWCNT) were modified by introducing Silica nanoparticles to yield silica oriented carbon nanotubes (Si-MWCNT) and further use it to fabricate polyvinyl chloride (PVC) based novel

ultrafiltration membranes. In this context, there is no literature reported on the identification and application of Si-MWCNT nanoparticles as the modified fillers to PVC based UF membranes. After the characterization of synthesized Si-MWCNT nanoparticles, they were incorporated into the membrane matrix with different loadings and the properties of the new nanocomposite membranes were compared with those of pure polymeric membranes. The morphological properties such as internal structure (pore structure, pore size and porosity), surface roughness, surface composition, hydrophilicity, nanoparticle distribution on the interior and surface of the membrane as well as the filtration performance properties such as water flux, flux recovery ratio, resistances, rejection and the bulk properties such as thermal behavior, crystalline structure and mechanical properties of the developed membranes were investigated in comparison to the pristine membranes. Membrane rejection was tested using sodium alginate and humic acid model solutions to represent polysaccharide-like and humus-like substances in wastewater, respectively.

2. MEMBRANE SEPARATION TECHNOLOGY

Separation, concentration and purification of chemical components present in a solution are main issues in the industrial processes. Recently, traditional mass separation methods such as distillation, crystallization, solvent extraction and the other techniques have been replaced by membranes separation. The favored industrial application of membrane technology is the water purification, disinfection, distillation, media filtration due to the fact that they require no chemical additives, thermal inputs or regeneration of spent media. Moreover, membrane separation processes are faster, more efficient and economical than the other separation techniques. While gas separation and pervaporation membrane processes have been widely used for industrial separation, pressure driven membrane processes remain the most commonly used membrane technology especially for water purification applications since it does not involve a phase change and consume much less energy than alternate separation processes (Nunes and Peinemann, 2006; Strathmann, 1981; Strathmann, 2000; Pendergast and Hoek, 2011).

Generally, the principle of membrane separation is the result of differences in the transport rates of chemical components through the membrane matrix. This transport rate is established by the forces acting on the individual species and their mobility. The driving force might be a gradient of pressure, electrical potential, temperature or concentration (Strathmann, 1981; Mulder, 1996). Usually, pressure driven membrane processes are classified according to the characteristic of the size of the pores or their planned application. Currently, the pressure driven membranes processes are microfiltration (MF), ultrafiltration (UF), nanofiltration (NF) and reverse osmosis (RO) (Bruggen et al., 2003; Liu 2014; Pendergast and Hoek, 2011).

Synthetic membranes can be fabricated from a various materials such as polymeric or inorganic or mixture of both (hybrid) (Ulbricht, 2006). In the recent years, the rapid development of nanotechnology induced to novel membrane materials that enable enhanced functionality, such as high permeability, high selectivity and high fouling resistance compared to those of plain polymeric membrane (Low et al., 2014)

2.1. Historical Development of Membrane

In the eighteenth century, a French scientist Abbe Nollet highlighted the methodological studies of membrane phenomena. In the 19th and early 20th centuries, membranes were used as laboratory tools for the development of physical theories but were not applied at the industrial level. In 1855, Fick fabricated the first synthetic membrane from nitrocellulose. In 1986, Graham reported the first dialysis experiments with synthetic membranes. The term of "ultrafiltration" was first used by Bechold and later .in 1906 it was developed by Michaels by fabricating it from cellophane or regenerated cellulose.

After the First World War, Sartorius ran the first commercial membrane separation in the application of drinking water testing. Millipore was the world's first membrane producer, who developed filters sponsored by the US military. The search still continues for new and better membranes, not only for membranes that reach the marketing stage, but also for membranes that already exist (Mulder, 1996; Baker, 2012; Singh, 2015). Table 2.1 summarizes development of membrane in the small scale and the industrial scale in the past.

Table 2.1. *Development of membrane process (Mulder, 1996)*

Membrane processes	Country	Year	Applications
Microfiltration (s)	Germany	1920	Laboratory use
Ultrafiltration(s)	Germany	1930	Laboratory use
Hemodialysis (s)	Netherlands	1950	Artificial kidney
Electrodialysis (i)	USA	1955	Desalination
Reverse osmosis (i)	USA	1960	Sea water desalination
Ultrafiltration (i)	USA	1960	Concentration of macromolecules
Gas separation (i)	USA	1979	Hydrogen recovery
Membrane distillation (s)	Germany	1981	Concentration of aqueous solutions
Pervaporation (i)	Germany/Netherlands	1979-1982	Dehydration of organic solvents

s: small scale, i: industrial scale

2.2. Status of Membrane Technology in the World

Recently membrane separation is used as an alternative processes to the conventional water and wastewater purification techniques such as chemical processes, physical filtration and biological treatment. It has gained rapid acceptance worldwide as the most efficient and economical water treatment method (Hamingerova, Borunsky, and Beckmann, 2015). It offers the best options for drought resistance to humanity on an increasingly thirsty planet by purifying sea water or wastewater (Fane, Wang, and Hu, 2015).

Due to the intensive regulatory activity and the recent outbreak of microbes, low pressure membrane technologies are recognized by the water industry as highly attractive to drinking water production. Low pressure membranes are currently considered the most widely used technologies in the production of drinking water; where approximately 2 million m^3/day of potable water is produced in the world using this technique, including MF and UF (La, Vial and Moulat, 2000).

Europe has traditionally occupied a strong position in the membrane market in terms of scientific and technical excellence, which is expected to remain so in the upcoming years. Because of a wide range of water-based reclamation purposes, membrane systems have gained international recognition as a reliable and consistent technique (Hamingerova, Borunsky and Beckmann, 2015). Figure 2.1 demonstrates membrane-based water and wastewater treatment market in terms of revenue forecast for different types of pressure driven membranes in Europe between 2012 to 2020.

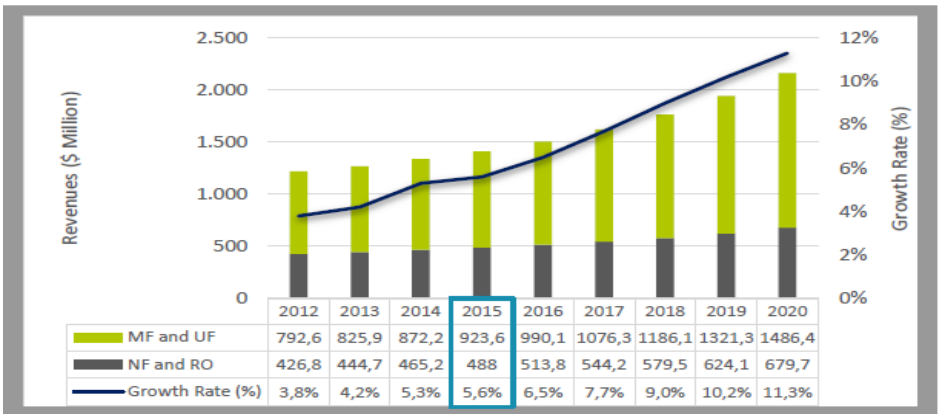

	2012	2013	2014	2015	2016	2017	2018	2019	2020
MF and UF	792,6	825,9	872,2	923,6	990,1	1076,3	1186,1	1321,3	1486,4
NF and RO	426,8	444,7	465,2	488	513,8	544,2	579,5	624,1	679,7
Growth Rate (%)	3,8%	4,2%	5,3%	5,6%	6,5%	7,7%	9,0%	10,2%	11,3%

Figure 2.1. *Membrane-based water and wastewater treatment market (Hamingerova, Borunsky and Beckmann, 2015)*

2.3. Definition of Membrane

Membrane is a semi-permeable, selective barrier that permits separation of species in a fluid medium (gas or liquid) established on sieving, diffusive and adsorptive mechanisms (Khulbe, Feng and Matsuura, 2008; Strathman, 1998).

The membrane allows selectively the passage of some components more rapidly than others; thus, if all species present in the feed could move through the membrane at the same rate, no separation would occur. Concerning this definition there are two important points. First, a membrane is defined based on what it does, not what it is. Secondly, a membrane separation is a rate process; it means the separation is accomplished by a driving force, not by equilibrium between phases. Such driving force might be gradients in pressure (ΔP), concentration (ΔC), temperature (ΔT) or electrical potential (ΔE) variation (Mulder, 1996; Noble, 1987; Singh, 2015). In the membrane separation processes, a feed or mixture is passed through a membrane barrier as illustrated in Figure 2.2. The solute (retentate) are rejected while the solvent (permeate) passes through (Stanojevi, Lazarevi and Radi, 2003).

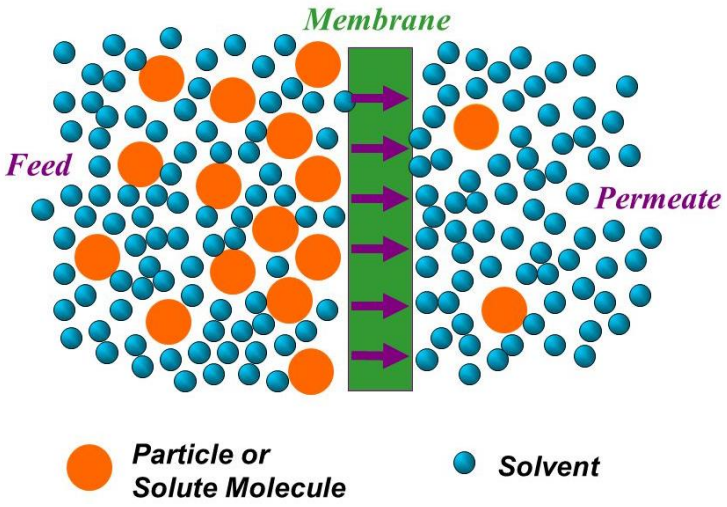

Figure 2.2. *Schematic representation of a two-phase system separated by a membrane*

2.4. Membrane classification

Membranes might be classified depending on a number of several characteristics including separation mechanisms, driving force, morphology and composition (materials) of the membrane and membrane module configuration. Figure 2.3 demonstrates classification of membranes in terms of different categories (Lonsdale, 1985).

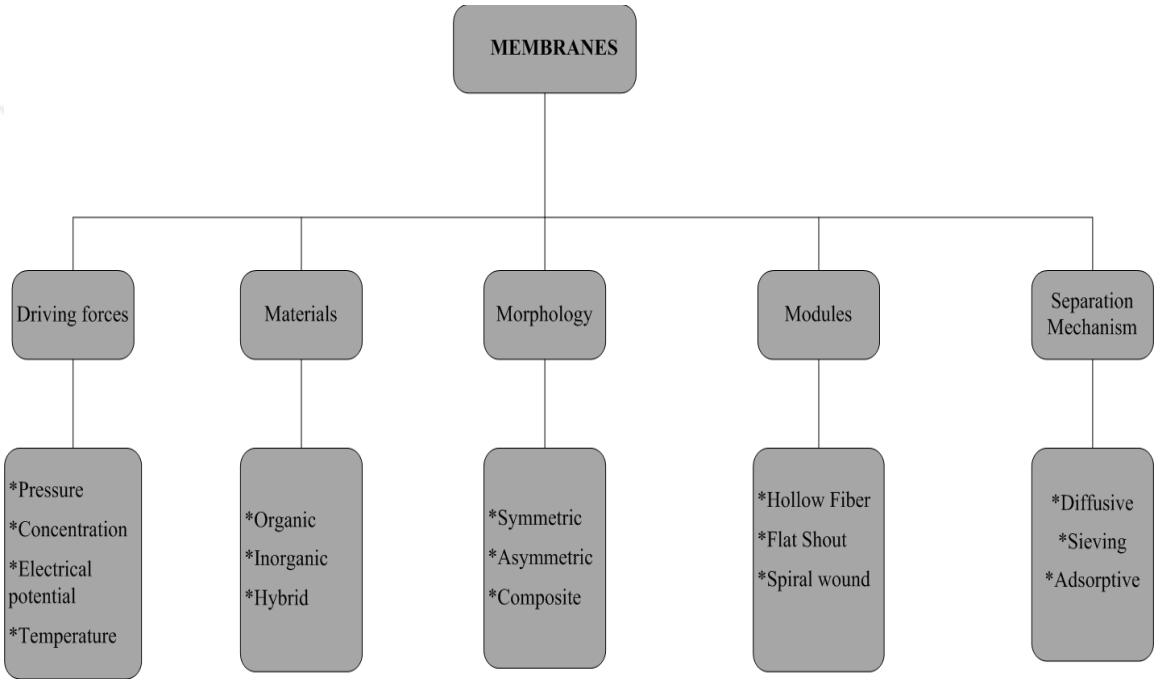

Figure 2.3. *Membrane classification*

Generally, synthetic membranes show a variety of their physical structure and depending on the type of pore structure; membranes can be classified as symmetric and asymmetric (Strathmann, 2012). Symmetric membranes can be categorized as non-porous symmetric and porous symmetric membranes. Asymmetric membranes are categorized as integrally skinned, coated and composite membranes. Their corresponding schematic shapes are given in Figure 2.4 (Scott and Hugbes, 1996, Chen et al., 2010).

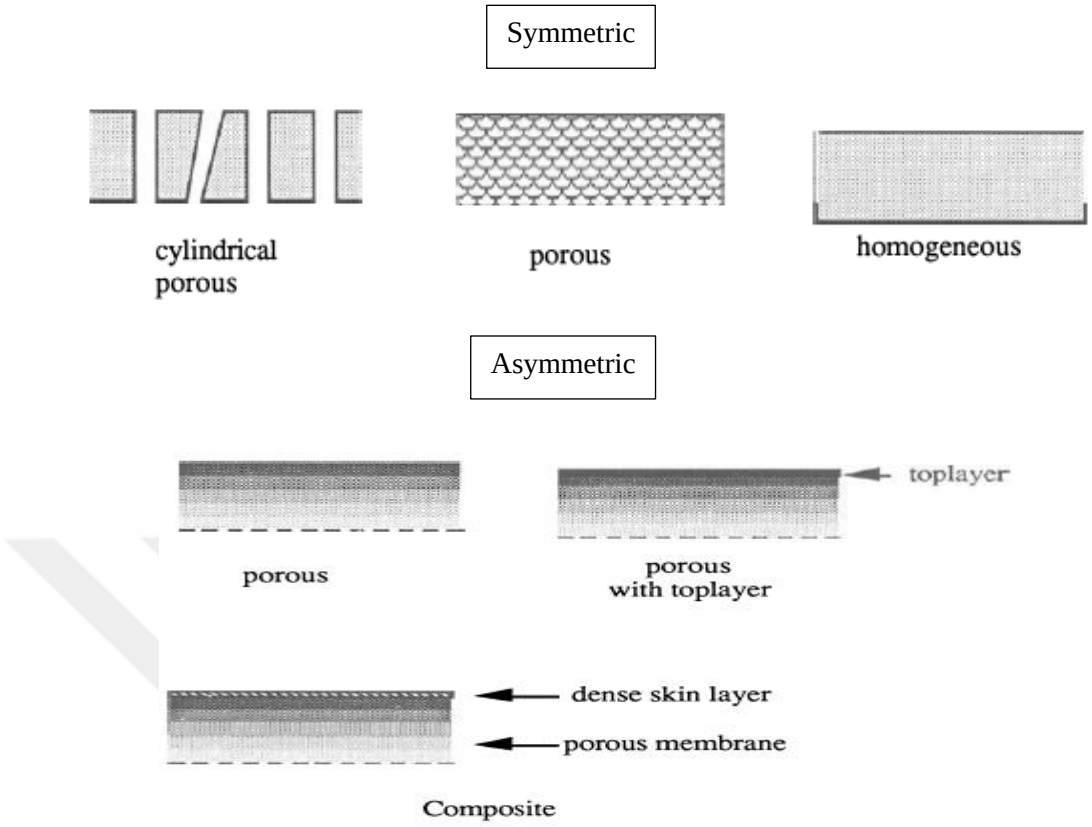

Figure 2.4. *Schematic representation of various membrane cross-sections (Mulder, 1996)*

In addition, membrane separation processes might be classified based on different driving forces, which could be pressure, concentration, temperature or electrical potential. The pressure-driven membrane processes can be distinguished by several criteria such as pore size, charge and size of the maintained molecules or particles and pressure exerted on the membrane (Scott and Hugbes, 1996).

2.5. Membrane Processes

Many membrane processes have succeeded in the field of separating molecular mixtures. The major difference between these processes lies in the driving forces used in separation. These driving forces are hydrostatic pressure, concentration, temperature, and electrical potential differences. However, the overall driving force for the transport of chemical components through a membrane is the gradient in its chemical potential, which consists of additive terms of the gradients in the hydrostatic pressure, in the concentration, temperature and in the electrical potential (Strathmann, 1980). Classification of membrane processes based on the driving force is summarized in Table 2.2.

Table 2.2. *Characteristics of membrane processes (Strathmann, 1980)*

Driving force	Membrane Process	Permeate	Retentate
Pressure difference	Reverse osmosis	Water, small polar solvents, salts	All solutes, water
	Nanofiltration	Monovalent ions, water	Small molecules, divalent salt
	Ultrafiltration	Small molecules, water	Polymers, proteins, micelles, colloids, particulates
	Microfiltration	Dissolved solute	Suspended particles
Concentration difference	Gas separation	Water, gases (≤1 nm) and polar vapors.	Water, gases
	Pervaporation	Volatile small molecules, water	Low volatility species
	Dialysis membrane	Small molecules, water gases	Large molecules
Electrical potential difference	Electro dialysis	Ionized solutes	Nonionic solutes
Temperature difference	Membrane distillation	Molecules > 1nm	Molecules<1 nm non-volatile dissolved substances

2.5.1. Pressure-driven membrane processes

Pressure-driven membrane processes depend on the application of pressure differentials between the feed side and the permeate side as a driving force to transport the solvent (often water) through the membrane (Bruggen, 2003). Pore size and pore size distribution are determined by particle or molecular size and chemical properties of the soluble component (Mulder, 1996).

Pressure driven membrane processes are characterized by multiple criteria such as membrane properties (size of pores), size and charge of particles or trapped molecules, and pressure exerted on the membrane. Through these criteria it can be distinguished into four

different processes: microfiltration, ultrafiltration, nanofiltration and reverse osmosis, which are summarized in Figure 2.5.

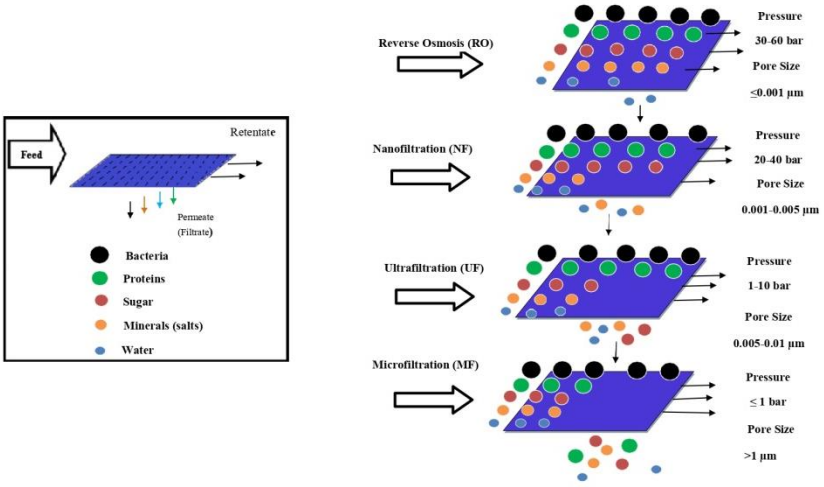

Figure 2.5. *Comparison of various pressure driven membrane processes*

2.5.1.1. *Microfiltration (MF)*

MF membrane has a pore size ranging between 0.1 and 10 µm, it has the highest permeability and its adequate water flux is obtained at lowest pressure among the other pressure driven membrane processes (Bruggen, 2003; Ismail et al., 2019). Separation of different chemical components is obtained by a sieving mechanism with the pores and relative size of the particles. MF membranes can be manufactured using polymer-based materials or inorganic materials, such as ceramic or stainless steel. MF is used in various applications, such as wastewater treatment, juice clarification, separation of proteins and bacteria (Ismail et al., 2019, Strathmann, 1981).

2.5.1.2. *Ultrafiltration (UF)*

UF is a pressure driven membrane process whose nature lies between nanofiltration and microfiltration. An ultrafiltration membrane has a pore size range of 0.001–0.05 µm and its structure is asymmetric in nature with smaller pore size and lower surface porosity that produces higher hydrodynamic resistance. The UF top layer has a thickness of 1.0 µm.

Ultrafiltration membrane has been widely used to remove materials with high molecular weight, gluten and organic materials (Figure 2.6) (Singh, 2015; Mulder, 1996).

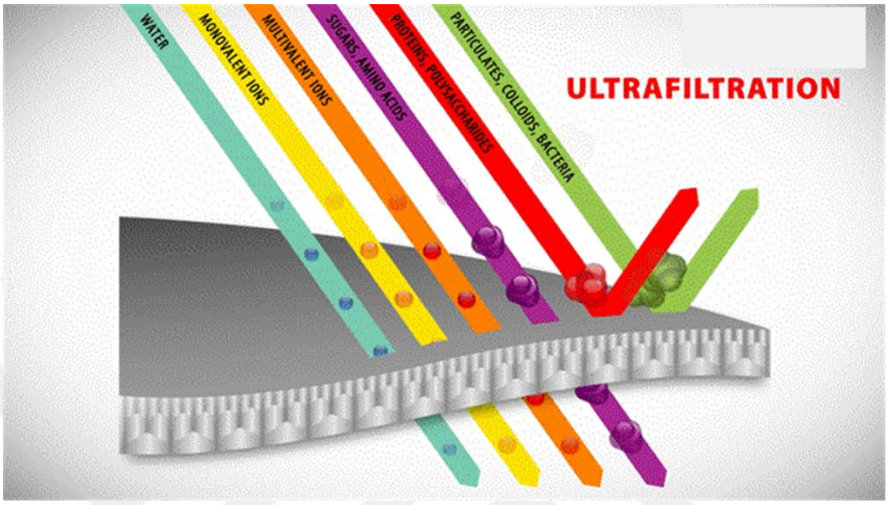

Figure 2. 6. *Schematic diagram of an ultrafiltration membrane system*

UF has been recognized as a leading separation technology with a strong history of different applications such as concentration, purification and fragmentation of several products in the food, pharmaceutical, biotechnology and petroleum industries. Moreover, UF process is also employed for drinking water purification and treatment. As with all types of membrane technology, a superior UF membrane must be constructed with the desirable characteristics of high flux, antifouling resistance and rejection rate over a continuous period of time and under mechanical pressure (Goh et al., 2015; Singh, 2015).

Due to increased demand, all efforts have been devoted to improving UF performance to meet current needs and expectations, including primary membrane processing, membrane materials, unit design and process improvement. In most cases, the key to optimizing process still depends on the structure and properties of the membrane material. Selection of membrane material must be carefully made to provide the required separation properties (Goh et al., 2015; Low et al., 2015).

2.5.1.3. *Nanofiltration (NF)*

NF is one of the pressure driven membrane process, also called low reverse osmosis or membrane softening, with pore sizes smaller than UF membrane has, typically around 1 nm, which lies between reverse osmosis and super filtration in terms of selective membrane designed to remove multiple calcium ions (calcium and magnesium) in softening processes. Recently, NF has been employed to remove relatively small organics, such as organic micropollutants and color from surface water or groundwater, and degradation products from the effluent of biologically-treated wastewater (Bruggen, 2003; Wiesner et al., 1996).

2.5.1.4. *Reverse osmosis (RO)*

RO is a pressure driven process for removing solutes which have a smaller size such as dissolved ions from using a dense membrane under high pressure. In the RO membrane process, the water diffuses through the dense membrane from the dilute phase to the concentrated phase because of the osmosis effect. Water continues to flow until sufficient osmotic pressure builds up on the concentrated solution side to prevent further flow of water up the concentration gradient. As long as the operating pressure is greater than the osmotic pressure of the feed solution, water will flow from the more concentrated solution to the more dilute solution through the membrane (Singh, 2015; Chen et al., 2010).

2.5.2. Concentration driven membrane processes

Usually, in the natural processes, the materials are automatically diffuse from high to low chemical potential. The same phenomenon happens in concentration driven membrane processes; the concentration difference between two phases separated by a membrane lead to a separation of different chemical components when their diffusivity and the concentration in the membrane are different for different components. The concentration driven membrane processes are dialysis, gas separation, pervaporation, and liquid membrane processes. The main differences between these processes are the membrane structure and the intended applications (Mulder, 1996; Strathmann, 1980). Although pressure driven processes are characterized as more or less similar processes, concentration driven membrane processes vary greatly from one to another (Mulder, 1996).

2.5.3. Temperature driven membrane processes

In temperature driven membrane processes, the separation is carried out by the transport of the heat from the high temperature side to the low temperature side.

Temperature driven membrane processes, i.e., the membrane distillation combines thermal and membrane-based techniques. In this process, porous membrane separates two liquids which do not wet it; lets the passage of only vapor molecules through the hydrophobic membrane pores. The separation of the mixture is achieved due to the temperature difference caused by the pressure difference (Mulder, 1996; Zare, and Kargari, 2018).

2.5.4. Electrical potential driven membrane processes

The electrical potential driven membrane processes use the capacity of the charged ions or particles to conduct an electric current. When an electrical potential difference is applied to a saline solution, the positive ions (cation) migrate to the negative electrode (cathode) while the negative ions pass to (anion) to the positive electrode (anode) (Mulder, 1996). The function of electrical potential driven membrane is to control the transport of ions and particles, which are electrically conductive. In this process two types of membranes can be distinguished; cation-exchange membranes, which allow the passage of the positively charged cations and anion-exchange membranes, which allow the passage of the negatively charged anions (Mulder, 1996).

2.6. Application Area of Membranes

Recently, membrane separation processes have been developed and optimized from simple applications at the laboratory level to be used in highly important industrial processes with significant technical and commercial impact. Based on the statistics, 50% of the industrial application of membranes is related to water treatment, 21% accounts for food and beverage processes and 9% contributes to pharmaceutical and medical industry (AMTA, 2014).

Among the pressure driven membrane processes, microfiltration and ultrafiltration are applied in the purification of aqueous streams and concentration and recovery of

valuable products, while reverse osmosis is used for the production of demineralized or potable water and desalination. Electrodialysis, which is another industrially common membrane process, is applied for the concentration or removal of dissolved ions and gas separation is utilized for separating gas streams, removal or recovery of specific gases, while pervaporation is applied for separation and concentration of liquid mixtures, especially for separating azeotropes (Bruschke, 1995, Strathmann, 1981).

The applications area that currently take benefit of membranes is impressive and continue to develop. Some of these are illustrated below (Figure 2.7) (AMTA, 2014).

- Food and Beverage:
  - ✓ Bottled Water
  - ✓ Fruit juices and maple syrup
  - ✓ Dairy applications
- Industrial Processes
  - ✓ Clarification of biochemical processes
  - ✓ Petroleum refining
  - ✓ Paint, adhesive, and solvent recovery
- Water treatment
  - ✓ Waste water purification
  - ✓ Desalination
- Some other applications include:
  - ✓ Pigments and paints
  - ✓ Generation of energy (electrical energy)
  - ✓ Fabrication of medical and pharmaceutical products

Figure 2.7. *Applications area of membrane technology*

3. MEMBRANE MATERIALS, PREPARATION AND CHARACTERIZATION

Membrane fabrication requires a number of methods that enable the membrane to be fabricated from a particular material. The type of method used is chosen according to the materials and the structure of the desired membrane. Based on the principles of structure, and separation, three basic types of membrane can be distinguished, which are porous membranes (microfiltration, ultrafiltration), nonporous membranes (gas separation, pervaporation and liquid membranes (carrier-mediated transport),

All kinds of synthetic materials can be used in order to prepare these types of membranes. The synthetic material might be organic including polymers, inorganic or a mixture of two. Acquisition of the membrane structure with the appropriate shape of a specific class depends on the modification of the material in an appropriate manner. The selection of materials limits the preparation techniques used in membrane morphology obtained and the principle of permissible separation. In other words, each separation problem can be achieved with each type of material (Mulder, 1996).

3.1. Membrane Materials

Membranes can be manufactured from several materials. The most important membrane materials could be distinguished as organic, inorganic and a mixture of two (composite).

3.1.1. Organic membranes

Generally all of the organic membranes explored so far have been made from different kind of polymeric materials, which offer a wide range of structures and properties. There are polymers called thermoplastics composed of linear-chain, which tend to soften with an increase in temperature and are soluble in organic solvents.

However, the decomposition of polymers, which include highly cross-linked chains was carried out at high temperature and their solubility in organic solvents is low. These polymers are called as thermosetting polymers (Luis, 2018; Lee et al., 2015). In addition, membranes can be either manufactured from rubbery or glassy polymers. When a polymer is heated to a temperature above the rubbery transition temperature, the polymer transforms

from the glassy state to the rubbery state and this critical temperature is called the glass transition temperature, T_g, which defines the state of the polymer at the synthesis conditions. Usually, rubbery polymers have high permeability for gases but a relatively low selectivity, while glassy polymers have high selectivity and a lower permeability (Jose, Kappen and Alagar, 2018).

Polymeric membranes have been a successful tool for a large range of industrial applications including water treatment and purification applications because of their superior mechanical, chemical and thermal properties and also reasonable cost in comparison with the ceramic membranes. Despite of its advantages, these membranes are characterized by their low surface energy and hydrophobic properties, which in turn causes a nonspecific adsorption of organic particles and foulant materials on membrane surface, as well as within the pores (Qin and Subianto, 2017; Kumar et al., 2018).

The most commonly used commercial polymeric membranes are polysulfone (PS), polyethersulfone (PES), polyvinylidenefluoride (PVDF), poyacrylonitrile (PAN), polyether imide (PEI), polypropylene (PP) and polyvinyl chloride (PVC) (Jose, Kappen and Alagar, 2018; Goh et al, 2015). Among all these polymers, PVC exhibits higher resistance to pH, chemical, temperature, and microbial corrosion, excellent physical and chemical properties, as well as good mechanical properties and is relatively cheaper compared to the other polymers. In addition, membranes fabricated from PVC have been considered as a promising material used for drinking water production due to its simplicity in operation with good separation performance. Therefore, the use of PVC as a polymeric material for the fabrication of high performance ultrafiltration membranes is of particular interest, which encourages its growth of production in industrial-scale (Aryanti and Wenten, 2015; Alsalhy et al., 2011).

3.1.2. Inorganic membranes

In recent years, inorganic membranes have gained considerable attention because of their relative thermal, chemical and mechanical strength. However, there are possible methods for inorganic membrane degradation, including the possibility of chemical attack (very limited and mainly by fluoric acid), and thermal shock of the membrane matrix. In

addition, their high mass and considerable production cost make them not wide enough in the industrial-scale (Lee et al., 2015; AMTA, 2018). Inorganic membranes can be classified into four categories, which are ceramic membranes, glass membranes, metallic membranes (including carbon) and zeolitic membranes. The performance of the inorganic membranes is affected by their structure and morphology. Inorganic membranes can be distinguished as porous and non-porous membranes based on their corresponding structure and morphology.

3.1.3. Composite/nanocomposite membranes

Composite membrane is a synthetic membrane, which consists of combination of polymeric and inorganic material to improve permeability and selectivity, as well as introducing new functional groups to further improve mechanical and thermal stability.

Generally, composite membranes show an asymmetric structure, generated by the deposition of a thin to top layer on a porous sublayer of a different material. The advantage of this type of membrane over the integrally skinned ones is that each layer can be optimized independently in order to achieve the desired membrane selectivity, permeability, chemical and thermal stability. Composite membranes might consist of a single-layer or multi-layer (Figure 3.1) (Duarte and Bordado, 2016).

A single-layer composite membrane has a selective membrane material deposited as a thin layer atop a microporous sublayer, which serves as support to provide only mechanical strength, whereas the separation is performed by the thin top-layer (Pinnau, 2000).

A multi-layer composite membrane consists of a porous support and several layers of different materials, each performing a specific function. Composite membranes are applied in different membrane processes such as nanofiltration, reverse osmosis, gas separation, and pervaporation applications. The biggest advantage of the composite membranes are the independent selection of materials and preparation technique, which make it possible to optimize the overall material to achieve the desired membrane properties as well as performance (Peeva, Sairam and Livingston, 2010; Pinnau, 2000).

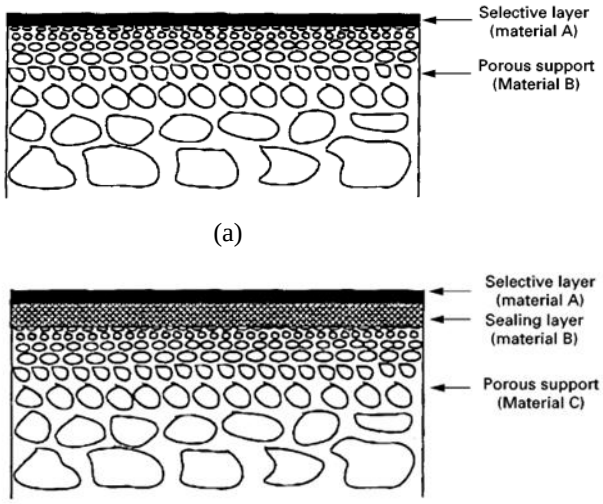

Figure 3.1. *Schematic diagram of (a) single-layer and (b) multi-layer thin-film composite membranes (Mulder, 1996)*

The most representative example of introducing inorganic material in a polymeric matrix (composite membrane) for separation purposes are nanocomposite membranes. The incorporation of inorganic materials into polymeric membrane matrix has become one of the most common trends in modern research of membranes area (Zhu and Wang, 2017, Yong et al., 2015). Recently, many inorganic metals/metal oxides or carbon-based nanoparticles have been incorporated into polymeric membranes because of their properties such as hydrophilicity, anti-fouling, self-cleaning, large specific surface area, pore channels, etc. Different membranes can be designed with some or all of these properties (Jainesh, Jhaveri and Murthy, 2015, Wang et al., 2012).

With the development of nanotechnology, the problems associated with macrocomposites can be overcome by taking the advantage of nano-scale inorganic fillers. Nanotechnology has offered a synergistic approach to the development of membrane science and technology for various applications including water purification by incorporating nanomaterials into polymeric membranes matrices. Nanocomposite membranes were characterized by different characteristics than other polymeric membranes, including resistance to target degradation, enhanced flow and selectivity, reduced tendency to contaminate, increased thermal and mechanical stability, and ease of

manufacturing (Theresa, Pendergast and Hoek, 2010). The fabrication of nanocomposite materials consists of two or more methods via mixing the inorganic phase into or on the surface of organic phase at nano-scale to develop new materials with superior performance (Bhatnagar, Kumar and Sillanpaa, 2009).

Based on membrane structure and location of nanomaterials, nanocomposite membranes can be classified into four categories, whose schematic structures are depicted in Figure 3.2.

1. Conventional nanocomposite membrane
2. Thin-film nanocomposite (TFN)
3. Thin-film composite (TFC) with nanocomposite substrate
4. Surface located nanocomposite

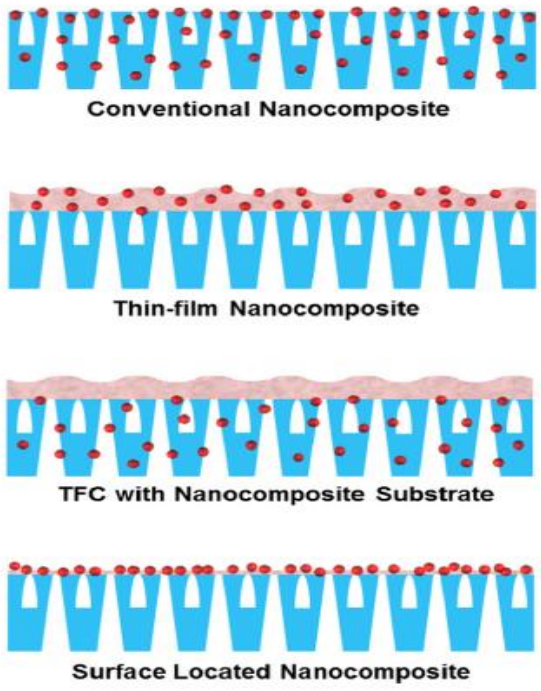

Figure 3.2. . *Typical types of nanocomposite membranes (Yin, and Deng, 2015)*

There are two basic methods of incorporating inorganic nanoparticles into a polymer matrix, which are blending and coating.

Blending:

In the blending technique, the nanoparticles are dispersed into the membrane matrices by ex-situ: melt and solvent mixing, and in-situ: sol-gel mixing (Figure 3.3). However, achieving a uniform composite structure is a major challenge when using the blending approach (Nagavarma et al., 2012).

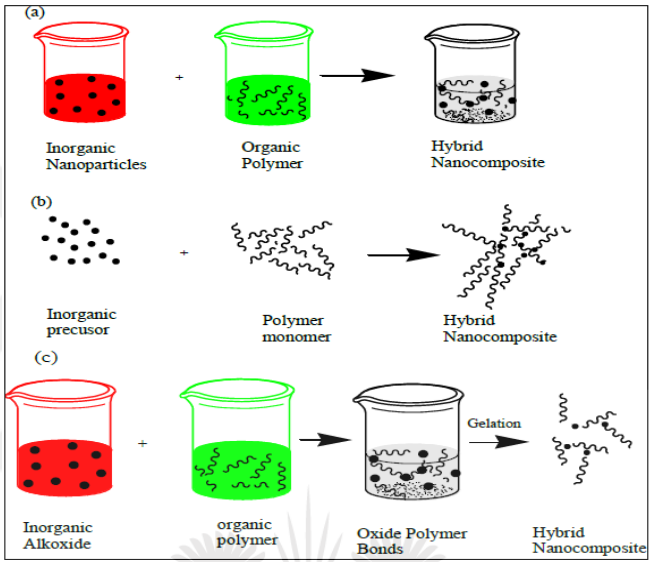

Figure 3.3. *Methods for nanocomposites preparation: ex-situ process (a) solvent mixing and (b) melt mixing; in-situ process (c) sol-gel (Nagavarma et al., 2012)*

Solvent mixing

Solvent mixing technique is the common method used for the fabrication of nanocomposites for the polymeric materials which are difficult to melt. In the solvent mixing technique, the polymer is first dissolved in a solvent and then the nanoparticles are added to the mixture by using ultrasonication, to ensure a homogenous solution. (Hossieny, 2009). After homogenizing the mixture, the solution is normally cast on a glass plate and immersed in a coagulation bath. This process is referred to as phase inversion technique. Because of the solvent and non-solvent diffusion, phase inversion of the casting solution is induced to form a polymer rich phase and polymer-poor phase, and the membrane is thereby obtained (Khulbe, Feng and Matsuura, 2008; Strathman, 1998).

Melt mixing

The melt mixing technique is the most widely used method in the preparation of nanocomposite membranes since no organic solvents are used, which makes it environmentally friendly. In this method, nanoparticles are directly mixed with the molten polymer. If the nanoparticle surfaces are sufficiently compatible with the selected polymer, a uniform nanocomposite can be achieved. This approach suffers from the drawback of particle agglomeration since nanoparticles are so reactive and tend to aggregate. However, the problem of agglomeration can be overcome by modifying the surface of the particles (Raman, Sudharsan and Pothiraj, 2012).

Coating

The coating technology is a common method which has been widely used for different applications. There are several coating techniques available such as chemical vapor deposition (CVD), physical vapor deposition (PVD), chemical (solution adsorption and sol gel) and plasma spraying coatings. CVD, PVD and plasma spraying have some drawbacks which limit their application in polymeric membrane fabrication. They are expensive as they need a high vacuum, high energy usage, need to work at high temperature and pressure, and are limited in the geometry of support to a flat substrate (Yun and Oyama, 2011).

In chemical coating route, the commercial or preformed nanoparticles are dispersed in a solvent and then deposited on the surface of the membrane through different coating approaches which include vacuum filtration, dip-coating and spin coating (Das, and Maiti, 2009; Mittal, Jana and Mohanty, 2011).

3.1.3.1. *Nanoparticles used in the fabrication of membranes*

Integration of nanoparticles in polymeric membrane matrix enhances membrane properties by altering the physical, mechanical, thermal, antibacterial, antimicrobial, the pore size and surface morphology (Low et al., 2015). In recent years, various types of nanoparticles such as Al_2O_3, ZrO_2, SiO_2, Ag, ZnO, Fe_2O_3, CuO, zeolite and carbon nanotubes (CNT) are commonly used in the polymer matrix to fabricate ultrafiltration or

reverse osmosis membranes with improved performance. The integration of nanoparticles into polymeric membranes may produce interesting results that differ from those found in conventional dense inorganic materials, as well as may enhance the filler-polymer bonding. The porous nature of the filler gives great affinity to water, which may facilitate the transfer of water through the modified membrane (Low et al., 2015). Some deposited nanoparticles in the membrane matrix are classified in Figure 3.4.

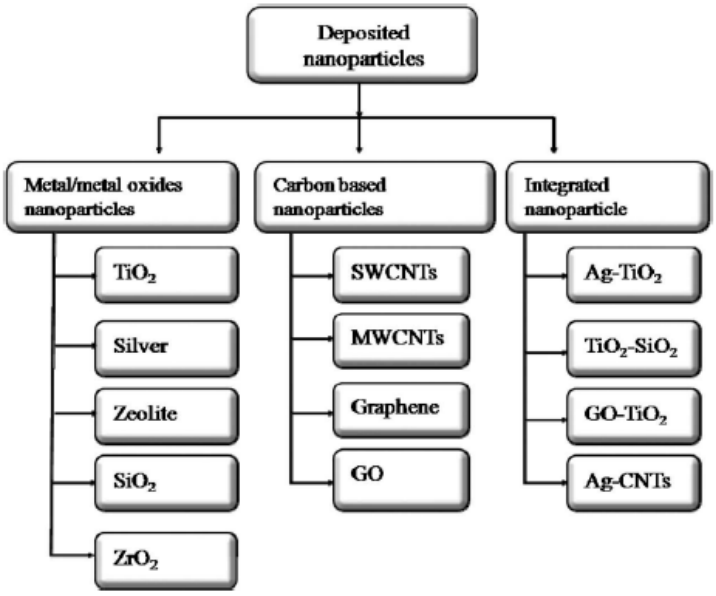

Figure 3.4. *List of different deposited nanoparticles on the nanocomposite membranes (Low et al., 2015)*

Carbon nanotubes

A short time ago, CNT has been widely explored in various fields because of its enormous mechanical, electrical, and thermal properties, especially for separation technology (Goh et al., 2016).

Carbon nanotubes are found in structures with single-walled or multi-walled (Figure 3.5). Single-walled carbon nanotubes (SWCNT) are non-welded cylinders made up of a layer of graphene that are formed by wrapping one graphene sheet seamlessly to form a 1 nm diameter cylinder and a centimeter length (Liew et al., 2014). Multi-wall carbon nanotubes (MWCNT) are homogeneous particles made up of cylindrical carbon and centrally separated from 0.35 nm with diameters ranging from 2 to 100 nm and tens of

microns. Its name is derived from its structure and the walls are made of multiple thick sheets of one atom of carbon (Liew et al., 2014).

Recently, there has been growing interest by the researchers in using CNT to develop novel membrane separation technology, in terms of permeability and fouling resistance (Kar, Bindal and Tewari, 2012). In addition, CNT can be added to the polymeric membranes to improve mechanical strength as well as to enhance membrane selectivity, which is the key parameter influencing significantly separation performance such as porosity, pore size, surface roughness, hydrophilicity and surface charge of the membrane (Kim et al., 2011). It has been suggested that the rates of the passage of liquid particles through CNT nanocomposite membrane were exceptionally fast. Many studies have been conducted in order to discover the reasons for the high permeability of CNT based nanocomposite membranes. The smooth nature of the internal walls of the CNT is an important factor, which leads to the low levels of friction with neighboring water molecules as well as the narrow diameter of the nanotubes (Rashid and Ralph, 2017; Goh et al., 2016).

Generally, the research on the CNT nanocomposite membrane focuses on the modification of pressure driven membranes by the addition of CNT nanoparticles into the polymeric membrane matrix in order to enhance permeate flux, rejection and fouling resistance (Wu et al., 2010; Rahimpour at al., 2012; Bai et al., 2015; Wei et al., 2015). However, the major problem that affects and may decrease the membrane performance other than enhancing is the possible serious aggregation of CNT nanoparticles in the matrix due to having strong Van der Waals interaction they have (Lee, Jeong and Liu, 2016).

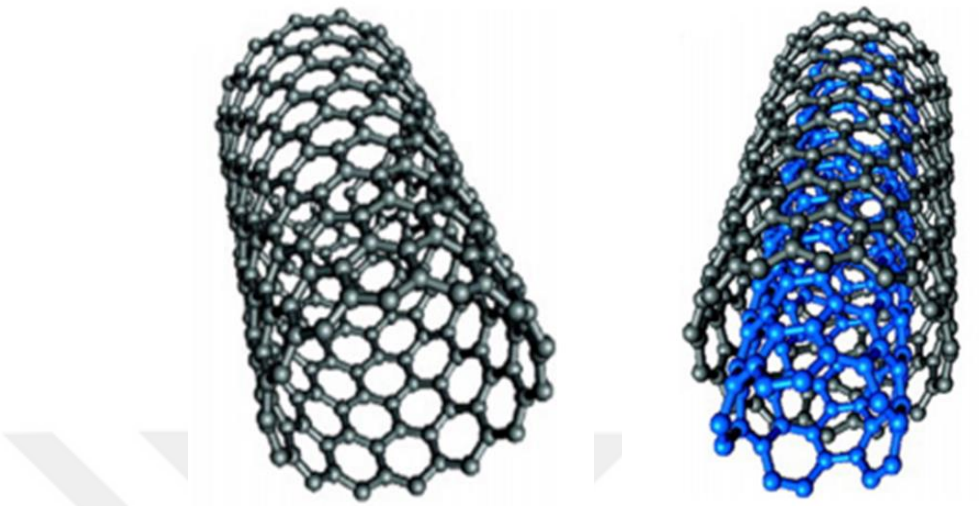

Figure 3.5. *The chemical structure of (a) single walled (b) multi walled carbon nanotubes (Lee, Jeong and Liu, 2016)*

Silica oriented carbon nanotubes

Silica nanoparticles have been widely used in numerous areas such as ceramics, chromatography, chemical catalysis etc. In addition, the application has been extended to include separation processes where properties provide attractive possibilities for the preparation of a UF membrane that is combined with silica nanoparticles. The incorporation of silica nanoparticles enhances the water flow by providing an internal water channel to allow the passage of the water molecule, which can be considered an important factor in enhancing the water flux (Goh, 2015).

To implement CNT in some applications, especially in separation processes, much work was done to activate the CNT surfaces with another phase to enhance the properties and compatibility of solution, in this context the silica was chosen for CNT coating. The silica oriented multi walled carbon nanotube materials have several unique features, including a stable mesoporous structure, a large surface area, and tunable pore size (Hsu et al., 2017).

Currently, there is no dedicated study of ultrafiltration Si-MWCNT based nanocomposite membrane. However, studies have demonstrated the significant role of CNT and silica in improving the membrane performance (Gohet et al., 2015; Tai et al., 2014; Hsu et al., 2017; Rahimpour et al., 2012), especially mechanical properties.

Sol-gel is a commonly used method to manufacture silica-oriented MWCNT by producing silica nanoparticles on a MWCNT surface. This synthetically modulated method involves mechanically modified MWCNT that are dispersed in a tetraethoxysilane solution through ultrasonic processing at room temperature. N,N-dimethylformamide is then used to remove free silica particles (Hsu et al., 2017; Cui et al., 2006).

3.2. Membrane Preparation Techniques

Synthetic membranes are fabricated using different methods which allow to forging a material in order to give it the desired characteristics. Selection of the suitable and best method for the fabrication of all types of membranes depends on two important factors, which are the characteristics of material and the morphology of the membrane. There are a several techniques available to fabricate synthetic membranes. Some of these techniques are applied in the preparation of organic membranes and some of them in the fabrication of inorganic membranes. The most common techniques are sintering, stretching, track-etching, phase inversion and coating (Tasselli, 2014).

3.2.1. Sintering

Sintering technique is a simple method which allows the preparation of porous membranes using organic and inorganic materials. This technique involves application of pressure on a powder consisting of particles of a certain size and heating it at or just below the melting temperature. The required temperature is chosen based on the materials used (Bottino et al., 2009; Mulder, 1996).

The principle of sintering is shown in Figure 3.6. Generally, the pore size and membrane porosity are affected by the particle size, sintering profile, temperature, heating or cooling rates and dwelling time. Membrane obtained by sintering technique can be converted into disks, cartridges or fine-bore tubes (Strathman, Giorno, and Driolo, 2010, Wu et al., 2013).

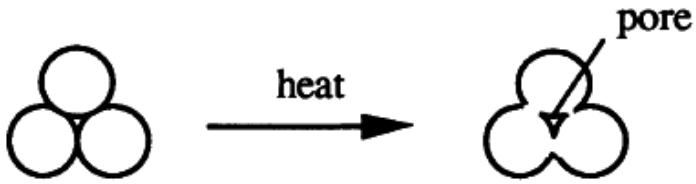

Figure 3.6. *Schematic drawing of the sintering process (Mulder, 1996)*

3.2.2. Stretching

Stretching method is used to fabricate porous membranes starting from extruded dense films of a partially crystalline polymeric material such as polytetrafluoroethylene, polypropylene and polyethylene. The pore formation is achieved by the film perpendicularly to the direction of extrusion. The porous structure obtained by applying a mechanical stress the size of these pores in the range of 0.1-3 mm. Only (semi) crystalline polymeric materials can be used for this technique. The porosity of the resultant membranes may reach 90% (Tasselli, 2014; Mulder, 1996).

3.2.3. Track-etching

Track-etching technique can be used in order to obtain the simplest geometry of the pores on the surface of the membrane with a set of parallel pores in cylindrical shape having a uniform dimension. In track drilling technology, the film or foil is exposed to high energy molecular radiation applied vertically to the film. The tracks are obtained by the effect of particles on the membrane. The film is immersed in an acidic bath after the polymeric material is drilled along these paths to form a uniform cylindrical pore with a narrow distribution of pore size (Mulder, 1996).

3.2.4. Coating

The coating method permits the preparation of composite membranes. Usually, this method is used when the separation is controlled by diffusion of the species through the membrane rather than their pore size. Membranes fabricated with this method consist of two different materials, with highly selective membrane deposition as a thin layer on more or less porous substrates as shown in Figure 3.7. The dense layer confirmed the transport

rate of the particles, however the porous layer ensure the mechanical properties of the membrane. Coating technique includes several different methods such as dip coating, spray coating, spin coating and plasma polymerization (Tasselli, 2014; Mulder, 1996).

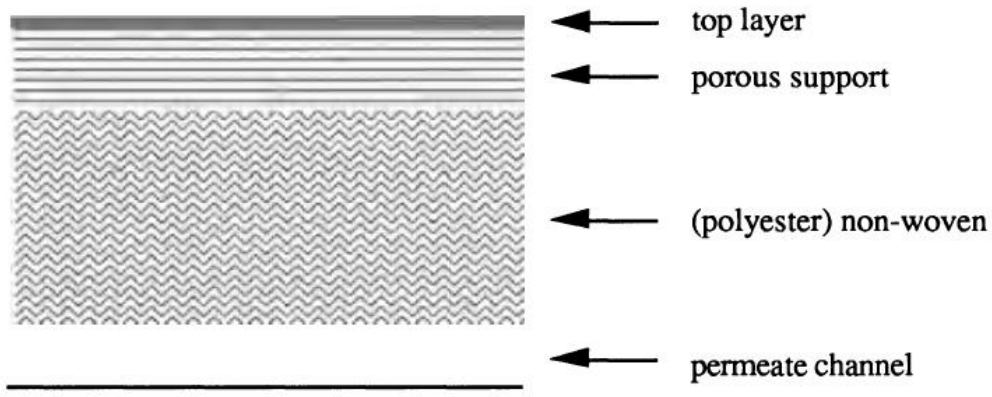

Figure 3.7. *Schematic drawing of a composite membrane (Mulder, 1996)*

3.2.5. Phase Inversion

Phase inversion is the most common technique in the fabrication of polymeric membranes. Through this process, the polymer is converted in a controlled manner from the state of the solution to the solid state. The phase inversion includes different techniques for the membrane fabrication such as immersion precipitation, precipitation by controlled evaporation and thermal precipitation from the vapor phase and. Among these techniques, the most commonly used technique is the immersion precipitation technique (Mulder, 1996).

3.2.5.1. *Immersion precipitation*

Phase inversion via immersion precipitation is the most widely used membrane preparation method. According to this technique, a polymer solution (polymer and solvent) is poured on a proper support followed by immersing into a non-solvent coagulation bath under controlled conditions. Immersion precipitation is performed by the solvent-nonsolvent exchange. Eventually the structure of the membrane is achieved by combination of mass transfer and phase separation (Figure 3.8). The main steps that determine the

membrane morphology are the non-solvent coagulation bath and rate of removal of the solvent (Rozelle et al., 1977; Tasselli, 2014).

The solidification begins once the solvent and nonsolvent diffuse countercurrently into and from the thin film. Then, at a certain point during the demixing, one of the liquid phases (high polymer concentration phase) will be solidified into a solid matrix. By controlling the initial phase of the transition, membrane morphology can be controlled, i.e., both porous membranes and nonporous membranes can be prepared (Mulder, 1996).

During the phase inversion process, there are various parameters effecting the solvent-non-solvent exchange or the demixing processes so the membrane morphology. Depending on the type of formation mechanism, two different kinds of membranes with a different structure may be produced, which are porous membranes such as microfiltration and ultrafiltration or the nonporous membrane such as pervaporation and gas separation (Mulder, 1996). The main parameters that influence the morphology of membrane are;

- The selection of solvent/non-solvent system
- The polymer concentration
- The composition of the coagulation bath
- The composition of the polymer solution

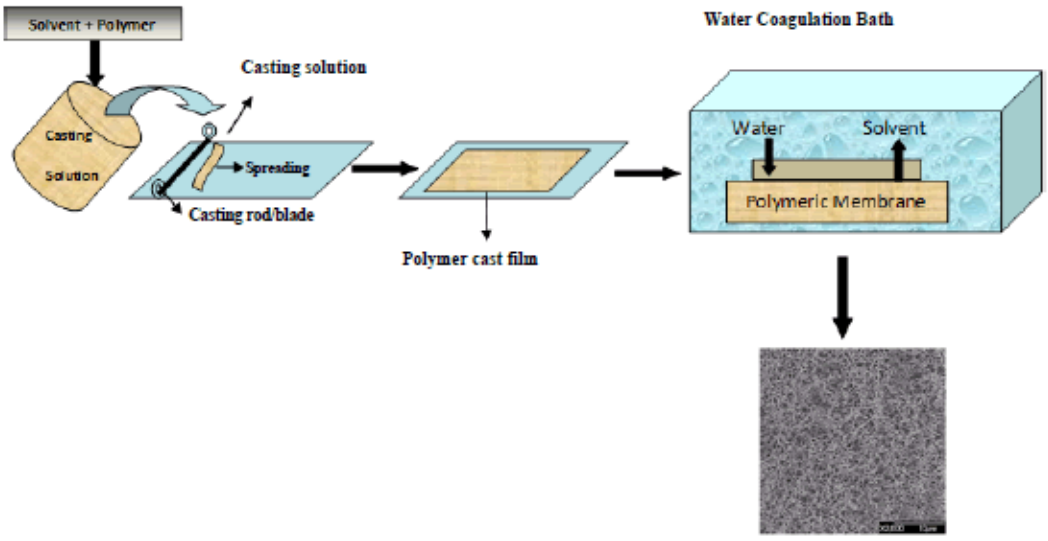

Figure 3.8. *Schematic representation of phase inversion technique with an immersion precipitation (Zahid et al., 2018)*

3.2.5.2. *Thermal precipitation*

This method is based on the decrease of the polymer solution temperature in a mixed or single solvent to allow the phase separation to occur. Solvent evaporation often allows the creation of a membrane with a skin layer. The thermal precipitation method is often used to fabricate accurate filtration membranes (Rozelle et al., 1977; Mulder, 1996).

3.2.5.3. *Evaporation-induced phase separation*

This technique is based on the dissolution of the polymer solution (polymer and solvent) in solvent and non-solvent mixture where the solvent is more volatile than non-solvent. During evaporation, the composition shifts to a higher non-solvent and polymer content. This immediately induces to the precipitation of the polymer resulting in the construction of the skin membrane (Mulder, 1996).

3.2.5.4. Vapor-induced phase separation

This method is applied by placing the casting solution into a vapor atmosphere where the steam phase consists of a non-solvent that is saturated with solvent. The high solvent concentration in the vapor phase inhibits the evaporation of solvent from the casting solution. The formation of the membrane occurs due to non-solvent penetration (diffusion) in the cast film (Rozelle et al., 1977; Mulder, 1996).

3.3. Membrane Characterization Techniques

The characterization of membranes are performed in order to define the morphology and the structure to better understand the pore size, pore size distribution, free volume and crystallinity, etc. of the membrane matrix. The characterization of the membrane becomes more difficult gradually with reduced pore size. Different classes of pore size have their own methods of characterization methods. In this section, the most important techniques implemented to characterize porous membranes are summarized.

3.3.1. Scanning electron microscopy (SEM)

Scanning Electron Microscopy (SEM) is one of the most important techniques that to ascertain the membrane morphology. SEM is used to illustrate the clear view of the overall membrane structure, the top surface, cross-sectional and bottom surface morphological structures of membranes (Demirel et al., 2017; Mulder, 1996)

The membrane sample is exposed to a narrow beam of electrons with kinetic energies between 1-25 kV. The incident electrons are called primary electrons, which have high energy, and the reflected electrons are called secondary electrons, which are not reflected but released from atoms in the surface and determine the imaging. The polymer might be charged due to the high voltage applied so in order to avoid it, membrane sample is coated with a thin layer of gold. The schematic representation of SEM instrument is illustrated in Figure 3.9 (Mulder, 1996).

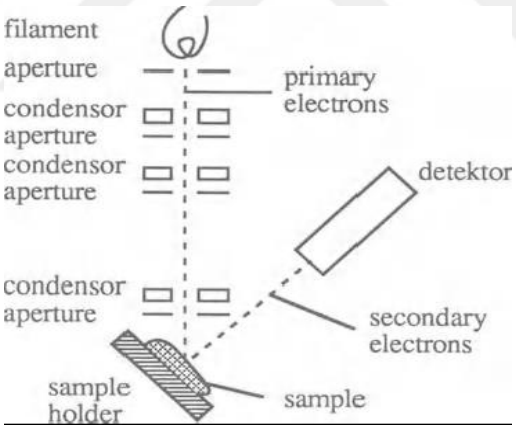

Figure 3.9. *Schematic representation of SEM instrument (Mulder, 1996)*

3.3.2. Atomic force microscopy (AFM)

This technique is used to get topographic images for the surface of the material by scanning a microscopic tip at the end of a cantilever. AFM technique is highly accurate for producing images of many materials and can be accurate to the atomic dimensions of flat surfaces.

Particularly, this technic can be used in the air or in liquid i.e. without any preparation for the sample AFM has been applied in the field of membranes that provide information

on surface morphology, porosity of the surface, and the dimensions of absorbed aggregates (Mohammed et al., 2011).

3.3.3. X-ray powder diffraction (XRD)

X-ray diffraction analysis (XRD) is a method of microscopic analysis used to determine crystallinity of materials, identification of crystalline phases and tests the degree of crystallinity of membranes. The diffractometer is used to examine polycrystalline specimens using an X-ray beam of a single wavelength. It can determine the nature of crystal by analyzing and then comparing the spectrum with a database (Bai et al., 2012).

3.3.4. Fourier transforms infrared spectroscopy (FTIR)

Infrared spectroscopy (mid-infrared, IR), in particular, is a very powerful technique to obtain an infrared spectrum from absorption, emission, optical conductivity, or Raman dispersion to a solid, liquid or gaseous substance (Adato et al., 2015). The FTIR spectrometer collects spectral data simultaneously in a wide spectral range. This provides a significant advantage over the dispersion spectrometer that measures density over a narrow range of wavelengths simultaneously. Understanding of positions of IR absorption bands in the spectrum as wave numbers could be used for determination of different chemical spices onto the membrane surface (Dwivedi et al., 2017; Mohamed et al., 2017).

3.3.5. Thermogravimetric analysis (TGA)

TGA is a very important technique used to measure the amount and rate of material weight change as a function of temperature in the galvanized atmosphere. TGA thermograms are obtained using an automatic thermal analyzer system, which explores the change in material weight as a function of time or temperature (Dwivedi et al., 2017). The weight change profile is recorded when the sample is subjected to a controlled heating or cooling environment. If weight change is recorded as a function of time, it is called isothermalmode (Loganathan et al., 2017).

3.3.6. Contact angle goniometer

This technique used to measure the hydrophilicity of the membrane surface. It is one of the easiest and reliable methods to determine the properties of a solid surface when it is possible to separate intrinsic differences from obvious differences. These obvious differences occur through surface porosity and roughness, and morphological surface changes during measurement, surface heterogeneity and contaminations of the solution(s) and/or solid surface (Rosa and Pinho, 1997).

In most cases, contact angle measurements are performed either to characterize hydrophobic membranes used for pervaporation or gas permeation and porous hydrophilic or hydrophobic membranes used in microfiltration or ultrafiltration (Rosa and Pinho, 1997).

3.3.7. Total organic carbon analyzer (TOC)

TOC analysis is specific measurement of organic compounds and theoretically measures all the covalently bonded carbon in an aqueous system. It is a very sensitive method with detection capabilities in the range of parts per billion so it has been accepted as a valid way of detecting the residue of contaminants (Albert 2015).

In general, TOC is measured by oxidation of organic compounds found in quantifiable forms (CO_2). Carbon is found in two forms: inorganic and organic carbon (IC and OC, respectively). This analysis was carried out as a specific indicator of water purity or cleanliness of permeate, which in turn determine the selectivity of the fabricated membrane (Bisutti et al., 2004).

3.3.8. Mechanical properties

Mechanical behaviors of materials require measuring of material's respond to an applied load. Mechanical behavior of a material can be realized from the measurement of the applying load as well as the displacement according to the specimen cross section area and the applying force mode. It is difficult to apply directly the conventional test to study the mechanical characteristics of membranes due to their small thickness (Wang et al., 2015; Hilal, Vinci and Vlassak, 1996).

The most commonly used techniques to study the mechanical strength of membranes and the reported mechanical behaviors such as elastic, stiffness, plastic, viscoelastic, hardness, uniaxial tensile test, bending test, dynamic mechanical analysis and nanoindentation (Wang et al., 2015; Hilal, Ismail and Wright, 2015).

3.3.8.1. Dynamic mechanical analysis (DMA)

Dynamic mechanical analysis (DMA) is the most widely used methods for the investigation of viscoelasticity and thermal properties of materials under the action of a periodic force. In most cases, DMA strain is the controlled input, while the resulting stress is measured (Chartoff, Menczel and Dillman, 2008; Wang et al., 2015).

DMA measures the stiffness, elastic properties, damping and viscoelastic properties of membranes as function of temperature or frequencies. In addition, DMA technique is also used to determine the glass transition temperature at which the membrane passes from the rigid glassy state to rubbery state (Wang et al., 2015). Dynamic properties measured by DMA are the storage modulus (E'), loss modulus (E'') and loss factor (tan δ) or damping factor (Yadav, 2009).

*The storage modulus (E') is the energy stored in a materials and presents the elastic behavior.

*The loss modulus (E'') is the loss energy of a material and is a measure of viscous behavior.

*Tan delta (tan δ) is related to the mechanical damping. A high tan delta value indicates that the material has a high nonelastic property whereas a low value indicates that the material is more elastic.

$$tan\delta = (E''/E') \tag{3.1}$$

3.3.8.2. ***Nanoindentation***

Nanoindentation is a technique developed to determine the Young's modulus (elasticity) and the hardness of a material. Because of its high accuracy, nanoindentation technique is used for the nanomechanical characterization of small size materials. In this method, a hard pyramidal indenter is pushed into the surface of a material, where the

applied force and the corresponded indenter displacement (Figure 3.10) are recorded (Wang et al., 2015).

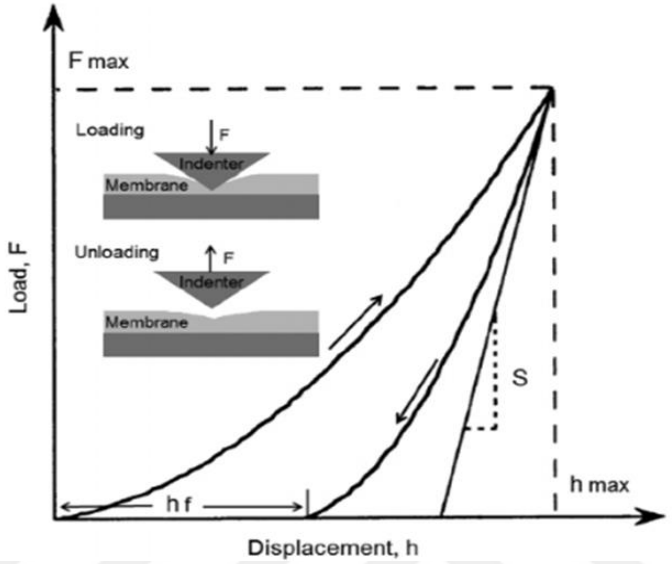

Figure 3.10. *Typical indentation load-displacement curve (Wang et al., 2015)*

3.4. Membrane filtration performance

Membrane performance could be summarized in terms of pure water flux, rejection (selectivity), anti-fouling properties such as flux recovery ratio. Membrane performance is highly affected by membrane composition and the specific features of porous structure and the membrane surface.

3.4.1. Flux

Flux is an important parameter which is defined as the volume of liquid flowing through the membrane per unit area and per unit time at constant transmembrane pressure and is generally expressed in terms of L/m^2h (Peeva, Sairam and Livingston, 2010). It is affected by a number of different parameters including the membrane material, pore size, pore interconnection, skin thickness, hydrophilicity of membrane and porosity (Erkan et al., 2018). In the other hand, Permeability P is also an important parameter in the study of membranes, which is defined as the transport flux of material through the membrane per unit driving force. The permeability values must be experimentally determined to

characterize the membranes and understand the action of the driven force (Dao et al., 2013).

In most cases, selectivity and flow permeability determine membrane applications. Typically, the higher selective membrane appearance tends to reduce flux. For example, the larger pore size may increase flux but reduces selectivity. The best way to enhance both of these two parameters is the modification of the membrane matrix by the addition of nanomaterial, which can positively alter both selectivity and flux (Bhadra and Mitra, 2013).

The incorporation of constituent nanoparticles always gives better performance to membranes. Specifically, hydrophilic nanoparticles give a significantly higher flow, pore size, and porosity, and reinforce the structure (Murugesan, 2017).

The flux is calculated by the following equation:

$$J = \frac{Q}{A \times \Delta t} \tag{3.2}$$

where J is the pure water flux (L/m^2h), Q is the volume of the permeate (L), A is the membrane area (m^2), and Δt is the time interval for the measurement (h).

There are two major competing types of filtration technologies used in industrial processes, which are cross flow filtration and dead-end filtration.

In cross-flow filtration, there is a constant flow across tangentially the surface of the membrane (Figure 3.11a) which prevents the accumulation of the fouling material onto the surface of the membrane and keeps the flux constant. Generally, the membranes used in this process are commonly tubes with a membrane layer on the inside wall of the tube. The process is referred to as cross flow because the feed flow and the filtration flow direction are perpendicular (Calabrò and Basile, 2010).

In dead-end filtration (Figure 3.11b), the fluid flow is applied perpendicular to the membrane surface. In order to reduce concentration polarization, stirring is typically applied. In dead-end mode, the retained particles are collected on the membrane surface forming a filtration cake which influences the course of the separation. Flux may decrease due to the additional resistance of the accumulated particles. This type of filtration is also called batch filtration (Nagy, 2019; Bruggen, 2018).

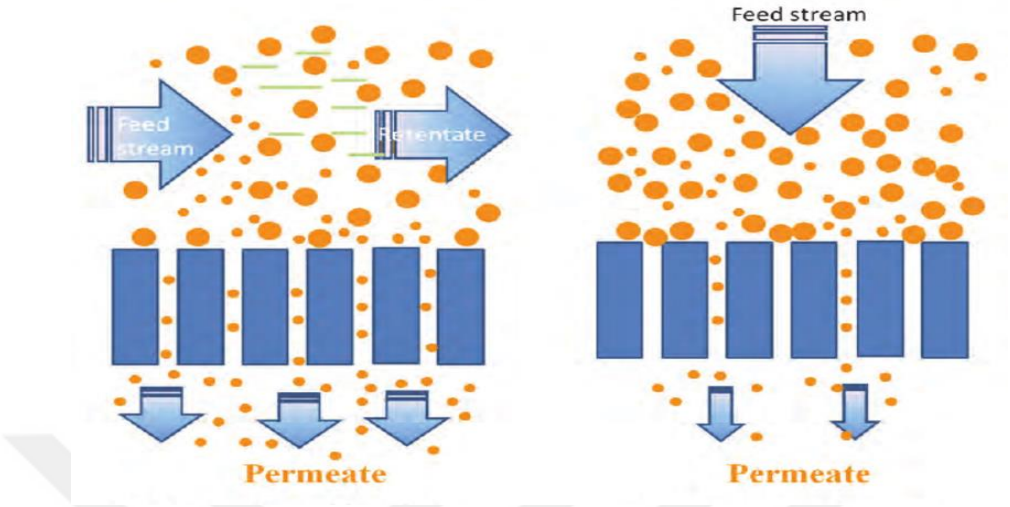

(a) (b)

Figure 3.11. *Schematic diagram of (a) tangential (cross) flow filtration and (b) dead–end filtration (El–Saft, and Hoa, 2012)*

3.4.2. Rejection

Molecular weight cut-off (MWCO) is defined as the lowest molecular weight (in Daltons) at which greater than 90% of a solute with a known molecular weight is retained by the membrane. It is used as a reference for the evaluation of the performance and describes retention capabilities of membrane (Bruggen, 2018)**.** The method based on measuring the permeability of the selected solutes of different molecular sizes under controlled conditions. Dissolved solvents should cover the expected size range of rejection from 0% to 100% and do not interact with membranes (Scott, 1995). The nominal molecular weight cut-off rating of the membrane selected should be an order that is less than the average size of the dissolved substance to be rejected or retained (Singh, 2015).

Studies have differed on the addition of nanoparticles in the polymer matrix. Some have demonstrated that the addition of nanoparticles in the polymer matrix has small effect on the rejection properties of the resulting UF membrane, other studies showed that the addition of nanoparticles in the polymer matrix significantly improve the structure of the pores which become more uniform so that the rejection is enhanced. The nanocomposite membrane differs in size and thickness of the surface pores compared to pure polymer membrane, the behavior of rejection in the nanotubes explained by the hydrophilic effect

detected by the inorganic nanoparticles on the surface and within the cross-section of the membrane (Goh, 2016).

Rejection coefficient, R, is a reliable indicator of the separating ability of a membrane process, which is expressed by:

$$R(\%) = \frac{permeate\ concentration}{feed\ concentration} \times 100 \quad (3.3)$$

3.4.3. Anti-fouling properties

Fouling is a global issue that leads to a gradual decrease in permeable flux because of the deposition and the adsorption of certain constituents on the membrane surface and in the membrane matrix. This issue is called membrane fouling (Purkait et al., 2018).

Most of the commercially available membranes have a considerable satisfactory rejection and flux, while their anti-fouling properties are inferior. In a broad view, high anti-fouling resistance of UF membranes must appear on smooth surfaces and high hydrophilicity. This is available in nanocomposites membranes. Studies have confirmed that the integration of nanoparticles into a polymer membrane is useful to significantly reduce membrane contamination (Goh, 2016).

3.4.3.1. *Flux recovery ratio (FRR)*

The percentage of feed that is transferred to the permeability is called recovery (water or liquid) of the membrane system. For NF and RO, recovery is critical, as not all fluids pass through the surface of the membrane. In the case of MF and UF, the liquid stream applied to the membrane surface will go through (Press, 2006).

The related studies have indicated that the incorporation of nanoparticles on the membrane matrix is very useful in improving the flux recovery ratio (Goh, 2016).

The flux recovery ratio (FRR) is calculated using the following equation:

$$FRR(\%) = \frac{Jw,2}{Jw,1} \times 100 \quad (3.4)$$

where $J_{w,1}$ is the pure water flux and $J_{w,2}$ denote the water flux after fouling of membrane.

4. LITERATURE SURVEY

Sianipar et al. modified MWCNT nanoparticles with polydopamine (Pdop-MWCNT) and incorporate them into polysulfone (PSf) using different concentrations (0.1–0.5 wt%) to fabricate ultrafiltration membranes. The obtained Pdop-MWCNT/Psf nanocomposite membranes were characterized using several techniques to distinguish membrane morphology, casting solution viscosity, hydrophilicity, and other physical properties. The optimum Pdop-MWCNT dose was determined to be 0.1 wt.%, in which the membrane exhibit maximum flux with 99.88% BSA rejection and better antifouling properties. It was concluded that nanocomposite Pdop-MWCNT/PSf membranes showed lower permeability and higher mechanical strength than pristine PSf membranes (Sianipar et al., 2007).

Choi et al. fabricated multi-walled carbon nanotube (MCWNT)/polysulfone (PSf) nanocomposite membranes using the phase inversion method. The prepared MWCNT/PSf nanocomposite membranes were characterized using various techniques such as SEM and FTIR Spectroscopy, a contact angle goniometer, and permeation tests. Addition of MWCNT nanoparticles enhanced the morphology of the PSf membranes and controlled the hydrophilicity of the membrane surface. It was also found that the amount of the MWCNT nanoparticles affected the performance properties of the MWCNT/PSf nanocomposite membranes (Choi, Jegal, and Kim, 2006).

Al-Hobaib et al. reported that the integration of MWCNT in the polyamide membrane enhanced the surface hydrophilicity and permeability of the fabricated membrane. In addition, the presence of the MWCNT nanoparticles increased the porosity as well as improved the pore size of the nanocomposite membranes. It was also reported that the membrane the salt rejection value increased with the addition of MWCNT nanoparticles (Al-Hobaib1 et al., 2017).

Vatanpour et al. synthesized polypyrrole (PPy) coated raw and oxidized MWCNT nanoparticles and used them for the fabrication of polyvinylidene fluoride (PVDF) ultrafiltration membranes by phase inversion method. The prepared nanocomposite membranes were characterized to recognize membrane morphology, water contact angle and crystallinity structure. The performance results showed that PPy:ox-MWCNT hybrid membranes exhibited the highest flux value of 399.3 L/m^2h (with the addition of 1% by wt.

of oxidized MWCNT) with and improvement of anti-fouling properties and bovine serum albumin (BSA) rejection (Vatanpour et al., 2018).

Wu et al. reported that introduction of MWCNT nanoparticles into brominated polyphenylene oxide (BPPO) polymeric membrane improved the surface hydrophilicity and permeability properties of the bare membrane. The membrane morphologies were also significantly affected by the presence of MWCNT nanoparticles in terms of porosity and roughness (Wu, Tang and Wu, 2010).

Yu et al. synthesized functionalized multi-walled carbon nanotubes (f-MWCNTs) by grafting 3-aminopropyltriethoxysilane (APTS). A novel PVDF membrane was fabricated by incorporation of different loading of APTS modified MWCNT nanoparticles (A-MWCNTs) via the phase-inversion method. The surface morphology studies showed that A-MWCNTs/PVDF nanocomposite membranes exhibited superior surface morphology and pore structure. The pure water flux, BSA rejection and antifouling properties increased with the addition of 2% by wt. of the modified nanoparticle (Yu et al., 2015).

Zhang et al. added oxidized-multi-walled carbon nanotubes (o-MWCNT) into PVDF/perfluorosulfonic to prepare new nanocomposite membrane with high performance properties. The results confirmed that the structure parameters of o-MWCNT nanoparticles significantly influenced the surface morphologies, hydrophilicity and permeability of the prepared hollow fiber membranes. The mechanical properties of the nanocomposite membrane were also affected by the structural parameters of o-MWCNT and the mechanical strength decreased as the o-MWCNT diameter increased from 10-20, 20-40 and 40-60 nm (Zhang et al., 2015).

Yu et al. fabricated a new SiO_2/PVC nanocomposite membrane with different SiO_2 loading via phase-inversion process. With appropriate nano-SiO_2 addition, the hydrophilicity, mechanical property, pure water flux, rejection and antifouling properties of PVC-based membrane were significantly improved. However, the casting solutions having more than 3 wt.% of nano-SiO_2 exhibited increased viscosity, unfavorable degassed effect and film-formation performance (Yu et al., 2014).

Zargar et al. synthesized novel nanoparticles by modifying the silica particle with polyethylenimine (PEI). The fabricated nanoparticles were used to synthesize PSf based SN-PEI nanocomposite membranes. The results confirmed that the presence of nano-SiO_2

in the skin layer could enhance the thermal stability, hydrophobicity, performance properties of the membrane and controlling its rejection rate (Zargar et al; 2017).

5. MATERIALS AND METHODS

5.1. Materials

Functionalized multi-walled carbon nanotubes (MWCNT-COOH) with a purity of 96% and an inner diameter of 5-15 nm and a length of 1-3 μm were supplied from Nanografi, Germany and were used in the synthesis of silica oriented multi-walled carbon nanotubes (Si-MWCNT) and in the fabrication of PVC/MWCNT-COOH nanocomposite membrane. Polyvinyl chloride (PVC, high molecular weight) and polyvinylprolidone (PVP, MW=40,000 Da) were used as main membrane polymer and pore forming agent, respectively. N,N-dimethylacetamide (DMAc, Acros Organics, MW= 87.12 g/mol) was used as a solvent in the fabrication of membranes. Sodium alginate (SA) (Sigma-Aldrich) and humic acid (HA) (Aldrich) were used as model foulant solutions to represent polysaccharide-like and humus-like substances in wastewater, respectively.

5.2. Other Chemicals

Ammonium hydroxide	Sigma-Aldrich
Tetraethyl orthosilicate (TEOS)	Aldrich
Ethanol	J.T. Baker
Sodium chloride	Millipore
Deionized water	Milli-Q
Nitric acid	Sigma-Aldrich
NaOH	Emsure
N,N-dimethylformamide (DMF)	Carlo Erba

5.3. Equipments

Magnetic Stirrer	Thermo Scientific
Analytical Balance	Mettler Toledo
Doctor blade (Universal Blade Applicator)	Paul N. Gardner
Digital Micrometer	Mitutoyo
Ultrafiltration System	Millipore/Amicon Stirred Cells
Ultrasonic Water Bath	Bandelin Sonorex

Total Organic Carbon Analyzer	Shimadzu, Japan
Scanning Electron Microscopy	Hitachi Regulus 8230
Fourier Transform Infrared Spectroscopy	Thermofisher Science, Nicolet iS10
Contact Angle Goniometer	Dataphysics, OCA
Centrifuge	Hitachi
Vacuum Oven	Memmert
X-ray diffraction Analyzer	Rigaku Miniflex600
Atomic Force Microscopy Analyzer	Park Systems, XE-100E
Dynamic Mechanical Analyzer	Perkin Elmer, DMA8000
Nanoindentation Analyzer	Hysitron, Triboindenter TI 950
Thermogravimetric analyzer	PerkinElmer (STA) 6000

5.4. Synthesis of Silica Oriented Multi-Walled Carbon Nanotubes

Si-MWCNT nanoparticles were fabricated through a sol-gel process using commercial functionalized MWCNT-COOH (Cui et al., 2010; Yang , Qiu and Cui, 2009). First, 500 mg of MWCNT COOH were dispersed in a mixture of ethanol (250 mL) and NH_4OH (8 mL) by using the ultrasonic bath for 3 hours to obtain a stable and homogeneous suspension. Immediately afterwards, TEOS (12 mL) was added to the mixture very rapidly followed by keeping the solution for 15 hours in the magnetic stirrer at room temperature. The resulting mixture was centrifuged at a speed of 5000 rpm for 6 hours. In order to eliminate the free silica particles, the mixture was redispersed in 100 mL of N,N-dimethylformamide (DMF) in an ultrasonic water bath for 15 min (Cui et al., 2006) and then vacuum-filtered through a 0.45 μm nylon membrane. After air drying, the resultant product was kept in vacuum oven under 50 mbar at 80°C for 8 h remove the remaining humidity. Finally, the synthesized Si-MWCNT nanoparticles were grinded using a mortar to be able to obtain a fine powder. A schematic view of the experimental method, the pictures of the route and the reaction scheme are given in Figure 5.1 and 5.2, respectively.

(a)

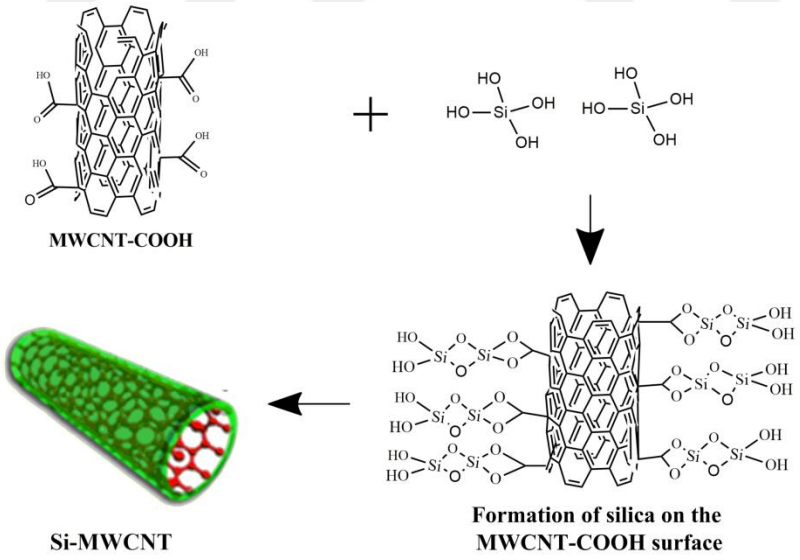

(b)

Figure 5.1. *(a) Sol-gel process steps for the preparation of Si-MWCNT (b) reaction scheme of conversion of MWCNT-COOH to Si-MWCNT*

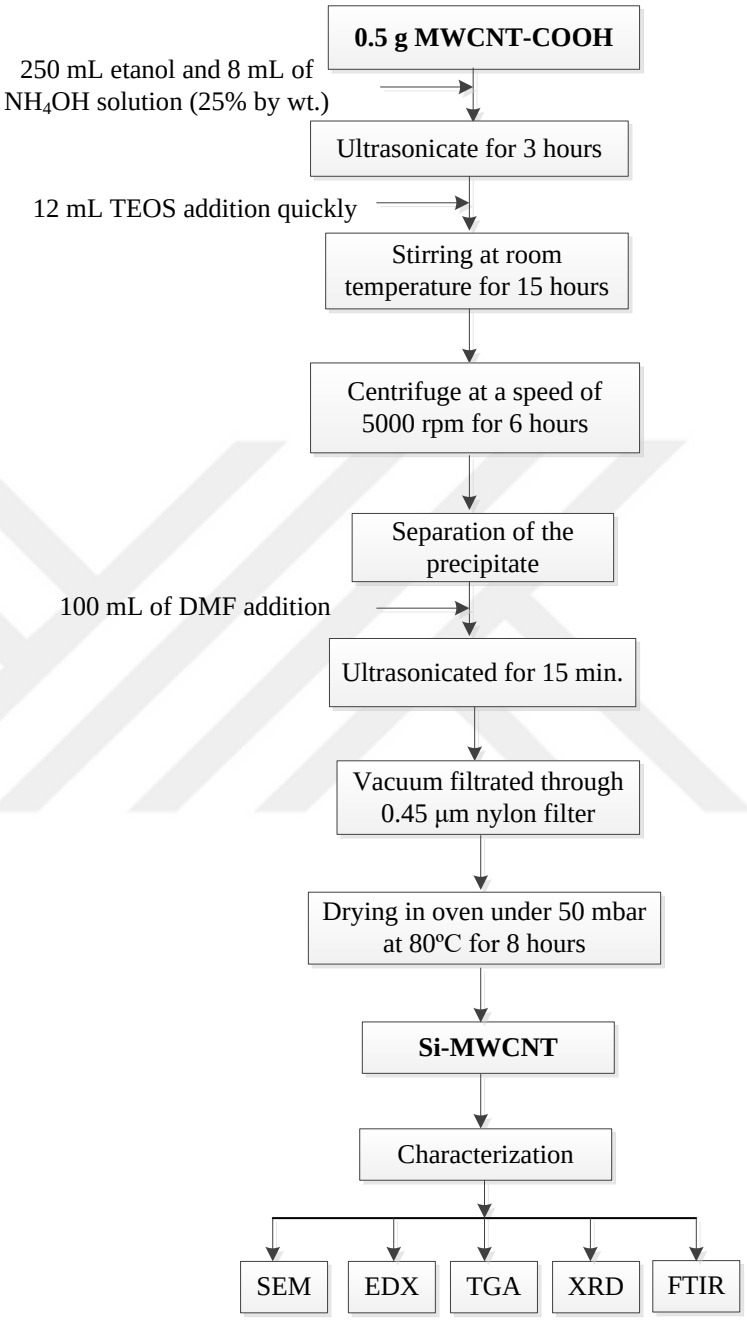

Figure 5.2. *Experimental steps of convertion of MWCNT-COOH to Si-MWCNT*

5.5. Preparation of Pristine PVC and PVC/Si-MWCNT Ultrafiltration Membranes

For the preparation of the pristine PVC and PVC/Si-MWCNT UF nanocomposite membranes, phase inversion with immersion precipitation technique was applied (Zhao et al., 2015). Membranes were fabricated using casting solutions containing PVC, PVP, Si-MWCNT nanoparticles and DMAc according to the compositions listed in Table 5.1. In order to prepare casting solutions, Si-MWCNT with varying amounts (0%, 0.25%, 0.5%, 1%, 1.5% and 2.0% by weight of the PVC) were added to DMAc solvent. In order to get a good dispersion, the mixture was ultrasonicated approximately for 2 hours. For higher percentages of Si-MWCNT nanoparticles (more than 0.5%), the mixture was ultrasonicated more than 3 hours to get a homogenous solution. After that, PVP and PVC were added; the mixture was stirred at 60°C and 500rpm for 24 hours prior to formation of a homogenous solution. The resultant casting solution was kept static at room temperature for at least 4 h before using; in order to get rid of bubbles hence avoid any defects in the membrane. Then, the casting solution was poured on a glass plate and cast into a thin film of 200 μm thickness using an adjustable casting blade (Figure 5.3). After 15 s evaporation time in air, the cast thin film was immediately immersed in a coagulation bath containing deionized water at room temperature, 25±1^{o}C to initiate phase inversion process, and subsequently was transferred into another fresh deionized water bath and left for 24 h to remove the remaining solvent (Zhao et al., 2015, Demirel et al., 2017). The membrane was kept in deionized water until performing filtration tests and further air dried for 24 hours before use for characterization.

Table 5.1. *Compositions of the casting solutions for all the fabricated membranes*

Membrane ID	PVC (g)	PVP (g)	DMAc (g)	Si-MWCNT (g)	Si-MWCNT/PVC (wt/wt%)
Pristine PVC	6.4	1.6	42.00	0	0
PVC/0.25 Si-MWCNT	6.4	1.6	41.81	0.016	0.25
PVC/0.5 Si-MWCNT	6.4	1.6	41.90	0.032	0.5
PVC/1.0 Si-MWCNT	6.4	1.6	42.00	0.064	1.0
PVC/1.5 Si-MWCNT	6.4	1.6	42.00	0.096	1.5
PVC/2.0 Si-MWCNT	6.4	1.6	42.00	0.128	2.0

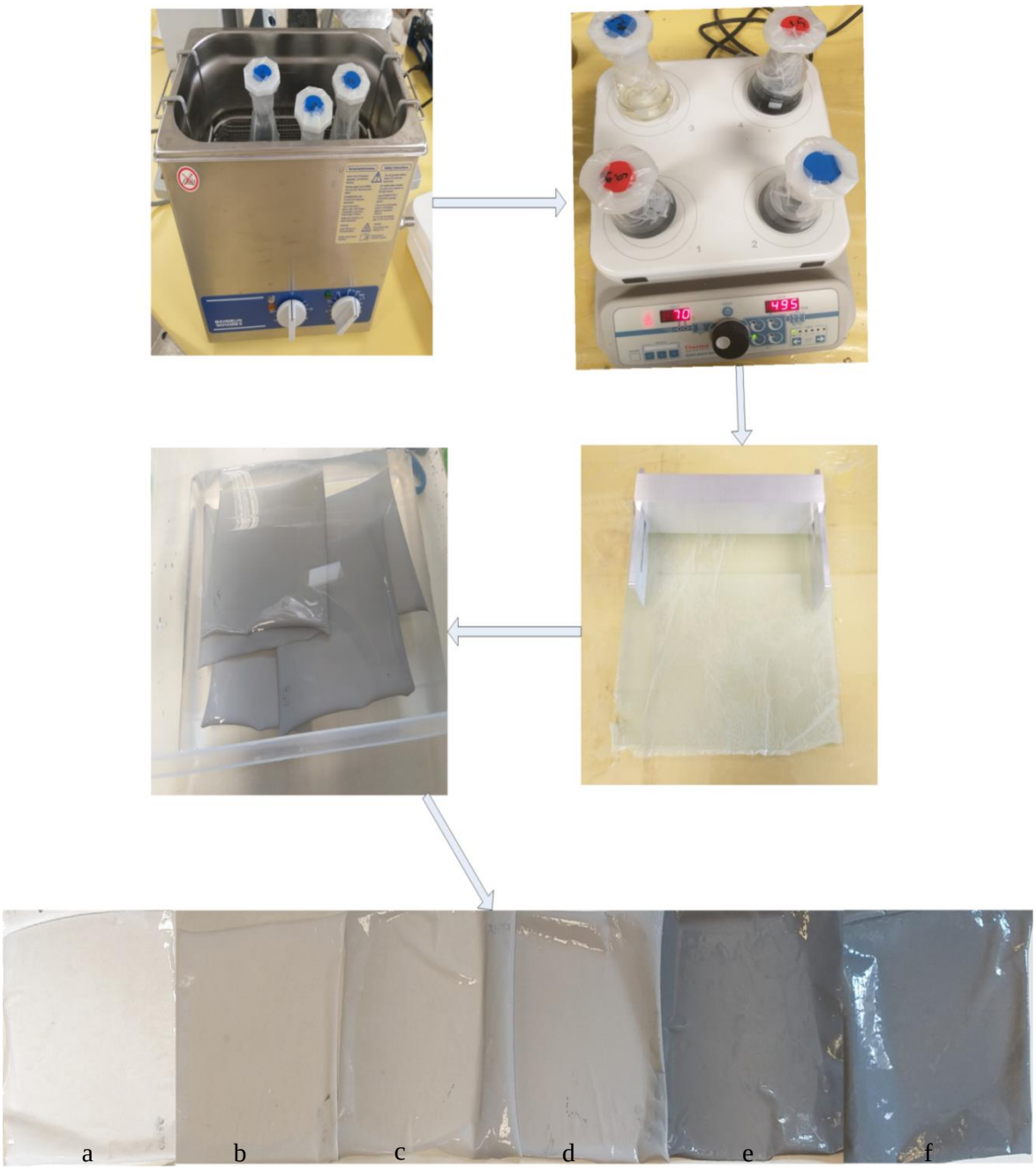

Figure 5.3. *Basic membrane fabrication steps of the PVC and PVC/Si-MWCNT nanocomposite membranes: (a) Pristine PVC, (b) PVC/0.25 Si-MWCNT, (c) PVC/0.5 Si-MWCNT, (d) PVC/1.0 Si-MWCNT, (e) PVC/1.5 Si-MWCNT and (f) PVC/2.0 Si-MWCNT*

5.6. Filtration Performance

5.6.1. Flux performance and rejection

Pure water flux analysis was carried out in a dead-end filtration system (Figure 5.4). A membrane sample was placed in a stirred cell (Millipore, USA), which had an effective filtration area of 28.7 cm^2 and a capacity of 200 L. The feed solution was poured into a 5.0 L dispensing vessel connected to the filtration cell and the flow of the solution was provided using a nitrogen gas cylinder, which was connected to the vessel. A constant agitation speed of 500 rpm was maintained to minimize concentration polarization effect. Before each flux test, membrane samples were compacted at a pressure of 0.69 bar using compressed nitrogen gas and the mass of the permeate was measured in every minute using a balance and the data was saved using Ohaus SPDC Data Collection V2.03 Software.

The pure water flux was calculated using the equation 5.1

$$J_{w,1} = \frac{\Delta V}{A \times \Delta t} \tag{5.1}$$

where $J_{w,1}$ is the pure water flux (L/m^2h), ΔV is volume change of the permeate (L) in one minute interval, A is the membrane filtration area (m^2), and Δt is the permeation time (h). In addition, the flux values of the fabricated membranes were determined at different transmembrane pressures (TMP) (0.07–0.27 MPa) to investigate the compaction behavior and stability of membranes. Permeability coefficient of each membrane was calculated from the slope of the curve of variation of flux as a function of TMP. Membrane flux tests were performed at least three times in order to minimize experimental errors.

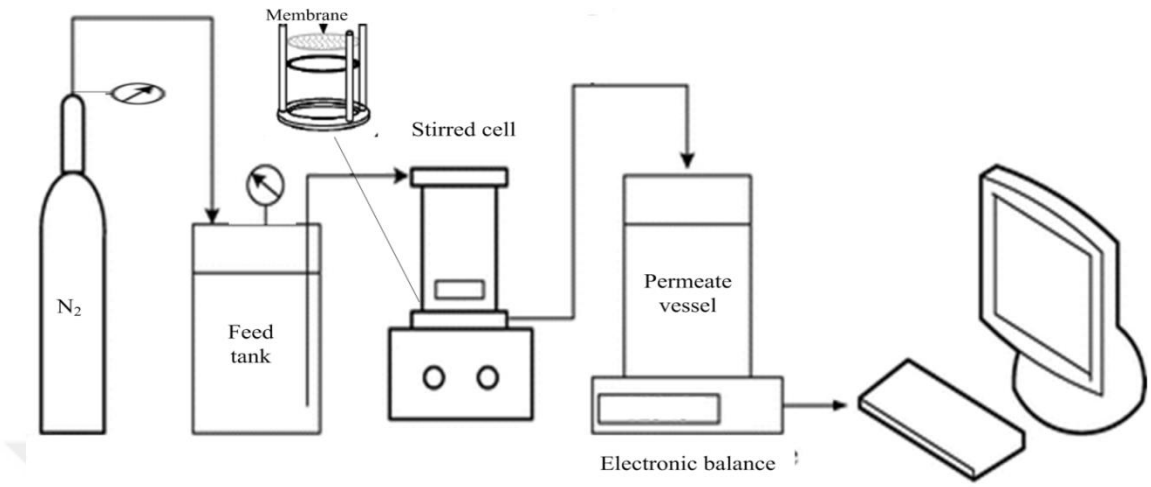

Figure 5.4. *Schematic view of dead-end UF system*

Rejection performance of the prepared membranes were performed using sodium alginate (SA) and humic acid (HA) as model fouling solutions at a constant TMP of 0.69 bar. Before the rejection test, the membrane samples were subjected to 2 L of NaCl solution with an ionic strength of 10 mM. Then a solution consisting of 20 mg/L SA and 10 mM NaCl were filtered eight hours until the flux was almost constant. The concentration of HA foulant solution used was 20 mg/L and its pH was adjusted to 10 using 0.1 M NaOH solution. 10 min. after initiating the fouling test, a permeate sample was collected in a graduated tube to calculate the rejection. Total organic carbon contents of permeate and feed were determined quantitatively using a TOC-L Analyzer (Shimadzu, Japan) (Figure 5.5) (Teow et al., 2012). Before the calculation of TOC content of each sample, the device was calibrated and the calibration curves were drawn.

The rejection (R%) was determined using the following equation.

$$R\,(\%) = \left(1 - \frac{C_p}{C_f}\right) \times 100 \qquad (5.2)$$

where C_p is the concentration of the permeate and C_f is the concentration of the feed solution.

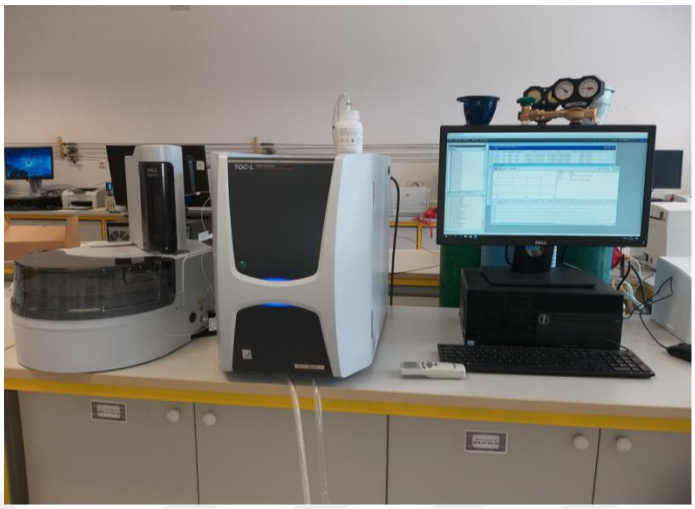

Figure 5.5. *TOC-L Analyzer*

5.6.2. Anti-fouling performance

Fouling experiments was conducted using SA foulant solution at a constant TMP of 0.69 bar for eight hours to investigate the antifouling behavior of the fabricated membranes. After each fouling experiment, the membranes were physically cleaned with water and the flux of water was measured once again in order calculate flux recovery ratio (FRR) using the following equation.

$$FRR\ (\%) = \frac{J_{w,2}}{J_{w,1}} \times 100 \tag{5.3}$$

where $J_{w,1}$ is the pure water flux and $J_{w,2}$ is water flux after the SA fouling test.

During SA filtration, foulant molecules are adsorbed on the surface and inside fingerlike pores of the membrane structure that in turn leads to a flux decline. To better understand the fouling resistances of the prepared membranes, the resistance-in-series model was used to ascertain fouling behavior (Bai et al., 2015; Zhao et al., 2014), as shown in the following equation

$$R_t = R_m + R_r + R_{ir} = \frac{\Delta P}{\mu \times J_{w,2}} \tag{5.4}$$

where (R_t) denote the total filtration resistance of the membrane (m^{-1}), (R_m) is the intrinsic membrane resistance (m^{-1}), (R_{ir}) is the irreversible fouling resistance (m^{-1}), (R_r) is the

reversible fouling resistance (m^{-1}), $J_{w,2}$ is the water flux after the SA fouling test ($m^3/m^2.s$), ΔP is the corresponding transmembrane pressure in (Pa) and μ is the dynamic viscosity of water at room temperature (Pa.s) (Bai et al., 2015; Arumugham et al., 2019; Zhao et al., 2014).

Each resistance against flow was computed using the following equations.

$$R_m = \frac{\Delta P}{\mu \times J_{w,1}} \tag{5.5}$$

$$R_r = \frac{\Delta P}{\mu \times J_{w,3}} - R_m \tag{5.6}$$

$$R_{ir} = R_t - R_m - R_r \tag{5.7}$$

In order to calculate each resistance term, after SA fouling test, backwashing of the membrane was performed by placing the reverse side of the membrane upwards and filtering pure water for 30 min. Then pure water flux, which represented by $J_{w,3}$ (Bai et al., 2015).

5.7. Characterization

Characterization of oxidized MWCNT and Si-MWCNT nanoparticles were performed using Thermogravimetric Analysis (TGA), Energy Dispersive X-ray Spectroscopy (EDX), Scanning Electron Microscopy (SEM), Fourier Transform Infrared (FTIR) Spectroscopy and X-ray diffraction (XRD) diffraction analysis. Pristine PVC and PVC/Si-MWCNT nanocomposite membranes were characterized using various techniques such as FTIR, SEM, EDX, AFM, XRD, TGA, DMA, nanoindentation, contact angle goniometer, and porosity and mean pore diameter measurement.

5.7.1. SEM and EDX analysis

SEM (Hitachi Regulus 8230) (Figure 5.6) was used for imaging the morphology and structure of MWCNT and Si-MWCNT nanoparticles as well as the cross-section and surface morphological of the fabricated membranes. Before analysis of the membrane

cross-section, the membrane sample was first immersed into propanol and immediately afterwards into liquid nitrogen (30 s) in order to freeze it so that it could be cut properly. For the surface imaging, the membranes were fixed on stubs with carbon dots and then coated with gold layer of 2-3 nm using a coating device (Leica EM ACE600). EDX coupled to SEM was used to determine elemental composition of Si-MWCNT, as well as to observe the dispersion of the nanoparticles on the surface and within the pore of the fabricated membrane matrices.

Figure 5.6. *Field Scanning electron microscopy (FE-SEM)*

5.7.2. Atomic force microscopy (AFM) analysis

AFM (Park Systems, XE-100E) (Figure 5.7) was used to map the topography and to quantify the surface roughness of the synthesized membranes. A membrane sample with a 1 cm^2 surface area was fixed on a stub and scanned with a 40×40 μm^2 scan size and a scan rate of 1 Hz. The acoustic non-contact tapping mode was used to characterize the membrane morphology. Three different positions of the membrane surface were mapped to get the reproducible results and the average values were reported.

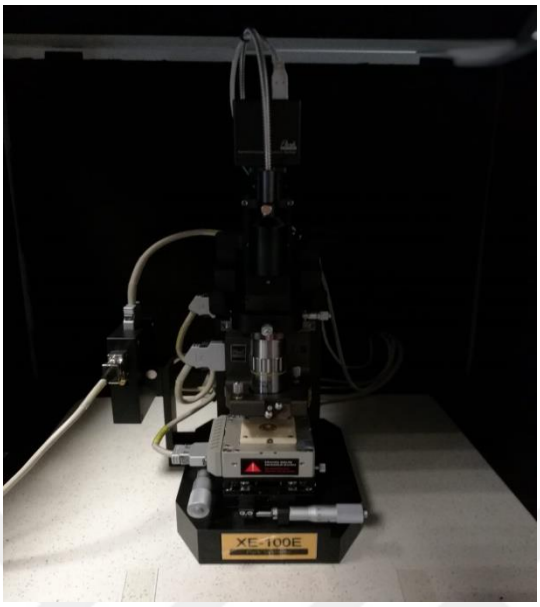

Figure 5.7. *Atomic force microscope (AFM)*

5.7.3. Porosity and mean pore diameter and water uptake determination

Membrane porosity was calculated by the ratio of pore volume to the geometrical volume of the membrane (Zhao et al., 2014). Furthermore, water uptake, which give insight about the membrane hydrophilicity, was determined using the following experimental procedure. A membrane sample with a specific area was kept in water and weighed after carefully mopping water on the surface and the backside of the membrane. Then it was dried in the vacuum oven at 60°C in order to evaporate the excess water and weighed.

Porosity and water uptake values were determined according to the following equations.

$$\varepsilon = \frac{W_w - W_d}{\rho_w(\pi r^2 l)} \times 100 \quad (5.8)$$

$$Water\ uptake = \frac{W_w - W_d}{W_w} \times 100\% \quad (5.9)$$

where W_w denote the mass (g) of the wet membrane, W_d is the mass (g) of the dry membrane, ρ_w is the water density at ± 25ºC (g/cm^3), r is the radius (cm) and l is the thickness (cm) of the membrane.

Membrane mean pore diameter was determined by the measured flux values of the fabricated membranes at constant pressure as well as other specific membrane properties using the Guerout-Elford-Ferry equation given below (Wua et al., 2008).

$$a = \sqrt{\frac{(2.9-1.75\varepsilon)\times(8\mu l Q_w)}{\varepsilon A \Delta P}} \quad (5.10)$$

where a is the mean pore diameter (m), ε is the porosity, μ is the viscosity of the water to be filtrated at room temperature (Pa.s), l is the thickness of the membrane (m), Q_w is the water flux (m^3/s), A is the surface area of the membrane sample (m^2), and ΔP is the corresponding transmembrane (TMP) pressure (Pa).

5.7.4. Contact angle and water uptake analysis

Water contact angle measurement of the synthesized membranes was performed using a contact angle goniometer (Dataphysics, OCA) (Figure 5.8). Membrane sample was dried in a vacuum oven for 24 hours before the measurements. Contact angle values were monitored at 0.276s intervals over 240 seconds as soon as the distilled water was applied onto the surface of the membrane and mean values of all six measurements were calculated and reported.

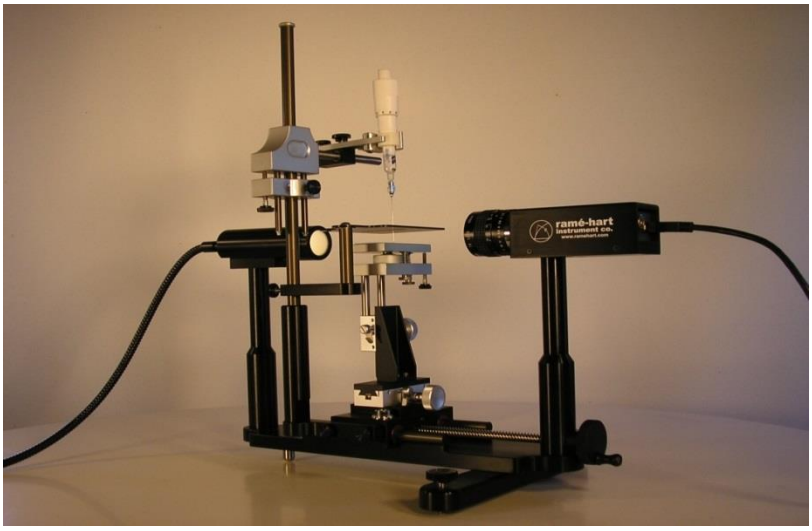

Figure 5.8. *Contact angle ganiometer*

5.7.5. FTIR analysis

FTIR (Thermofisher Science, Nicolet iS10) was recorded by the attenuated total refrection technique (Figure 5.9) in the frequency of 650-4000 cm^{-1} to characterize the presence of the silica in the MWCNT-COOH and synthesized Si-MWCNT nanoparticles. Samples were prepared by blending 1 mg of dry nanoparticles (MWCNT-COOH and Si-MWCNT) and 99 mg of KBr and pressing the mixture into a pellet of 1 mm in thickness by applying a pressure of 50 bar for 5 minutes. Furthermore, FTIR analysis was conducted to verify the functuonal groups due to the presence of Si-MWCNT nanoparticles in the fabricated membranes. Attenuated total reflection (ATR) mode was used to record the infrared spectra of the samples in the range of 650 to 4000 cm^{-1}.

Figure 5.9. *FTIR spectrometer*

5.7.6. Thermogravimetric analysis (TGA)

TGA was carried out using simultaneous (STA) 6000 thermal analyser apparatus (PerkinElmer) (Figure 5.10) to study the thermal behavior of MWCNT and Si-MWCNT nanoparticles. Moreover, TGA was performed to investigate the effect of Si-MWCNT addition to the bare PVC membrane on its thermal behavior. Approximately 10 mg of sample was placed in a platinum pan and heated up to 900°C with a heating rate of 10ºC/min using nitrogen as a sweeping gas (30 mL/min). The weight change of the sample

as a function of temperature was recorded and the amount of residue was monitored once the weight of the sample was stabilized.

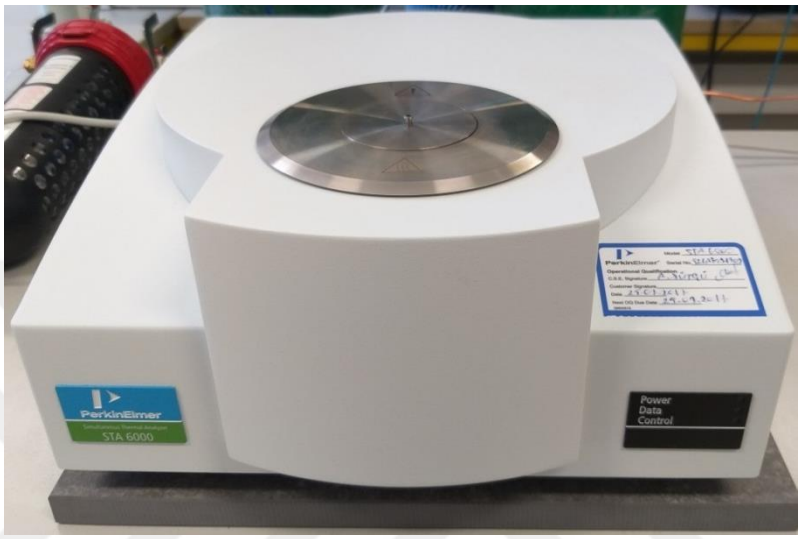

Figure 5.10. *TGA analyzer*

5.7.7. X-ray diffraction analysis (XRD)

X-ray diffraction (Rigaku, MiniFlex600) (Figure 5.11) analysis was performed in order to characterize the alteration in the chemical structure of MWCNT-COOH nanoparticles after modification with Silica and to examine the nature of the crystallinity of the pristine PVC membrane after incorporating with Si-MWCNT nanoparticles. Approximately 2 cm^2 of a membrane sample was cut and fixed on a copper stub. The angle range was kept between 5-80 2theta degrees with a scanning speed of 0.2 seconds/step. X-ray tube voltage and current voltage were set at 40 kV and 40 mA, respectively.

Figure 5.11. *X-ray diffraction analyzer*

5.7.8. Dynamic mechanical analysis (DMA)

DMA is a thermal analysis technique which is used to provide information about the mechanical properties of a metarial as a function of temperature. Viscoelastic properties of the membranes were examined using a DMA analyzer (Perkin Elmer, DMA8000) (Figure 5.12) in film tension mode. The membrane samples (10 mm×8 mm) with a thickness of 80 µm were first heated to 28°C in the DMA device and stabilized for 5 min to reach thermal equilibrium. A constant load of 2 N was applied to keep the samples straight during the test and the strain was oscillated at an excitation frequency of 1 Hz. Temperature was varied from 28°C to 150°C with a rate of 2°C/min to locate glass transition temperatures of the fabricated membranes. Furthermore, stiffness, storage modulus, loss modulus and tan delta values of the membrane samples were stored as a function of temperature.

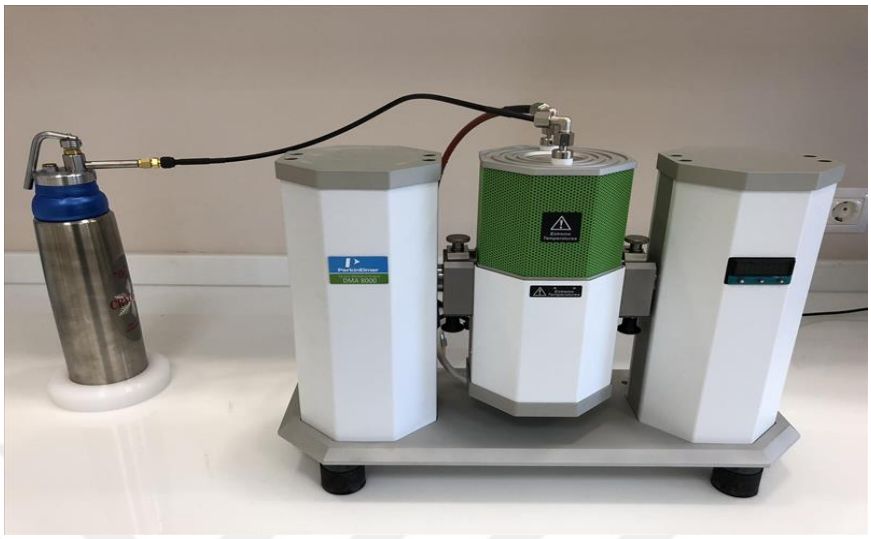

Figure 5.12. *Dynamic mechanical analyzer*

5.7.9. Nanoindentation analysis

Nanoindentation analysis was conducted to investigate the mechanical behavior of membranes in terms of elastic modulus (E) and surface hardness (H) using a nanoindenter (Hysitron, Triboindenter TI 950) (Figure 5.13)**.** A conical diamond flat punch Berkovich type indenter was used in the measurements. The analysis was carried out in a 3x3 matrix under the maximum load of 800 μN at room temperature according to the Oliver-Pharr analysis technique. In this method, a linear increase of the load was applied for 5 seconds and then kept constant for 2 seconds followed by removal of the load gradually for 5 seconds. Based on these measurements, a displacement curve for the load was drawn and mechanical properties such as hardness and elastic modulus (Young's modulus) of the membrane samples were calculated.

Figure 5.13. *Nanoindentation analyzer*

Table 5.2. and 5.3 summarize all the techniques used to characterize MWCNT-COOH and Si-MWCNT nanoparticles and pristine PVC and PVC/Si-MWCNT nanocompozite membranes, respectively.

Table 5.2. *Techniques used for the characterization of nanoparticles*

Bulk properties	TGA (Thermal Gravimetric Analysis) XRD (X-Ray Diffraction Analysis)
Surface properties	SEM (Scanning Electron Microscopy) EDX (Energy Dispersive X-ray Spectroscopy) FTIR (Fourier Transform Infrared Spectroscopy)

Table 5.3. *Techniques used for the characterization and performance determination of membranes*

Bulk properties of membrane	TGA (Thermal gravimetric analysis) XRD (X-Ray Diffraction Analysis) DMA (Dynamic Mechanichal Analysis) Nanoindentation Analysis
Surface properties of membrane	SEM (Scanning electron microscopy) EDX (Energy Dispersive X-Ray Spectroscopy) AFM (Atomic Force Microscopy) FTIR-ATR (Fourier Transform Infrared Spectroscopy) Contact angle and water uptake test Water Flux Rejection Anti-fouling test Porosity and mean pore diameter test

6. RESULTS AND DISCUSSION

This section gives the experimental results and discussion concerning the characterization of MWCNT and Si-MWCNT nanoparticles as well as the filtration performance and characterization of pristine PVC and the novel modified nanocomposite membranes after the addition of Si-MWCNT nanoparticles.

6.1. Characterization of Si-MWCNT

Characterization results of MWCNT-COOH and synthesized Si-MWCNT nanoparticles performed using FTIR, SEM, EDX, TGA and XRD analysis are given in this section.

6.1.1. SEM-EDX analysis

SEM analysis was conducted to visualise the morphology change of MWCNT-COOH after the modification of the structure with Silica. Furhermore, EDX coupled wih SEM was applied to determine the elementel composition (by weight) of Si-MWCNT nanoparticles. The results are demonstrated in Figure 6.1.

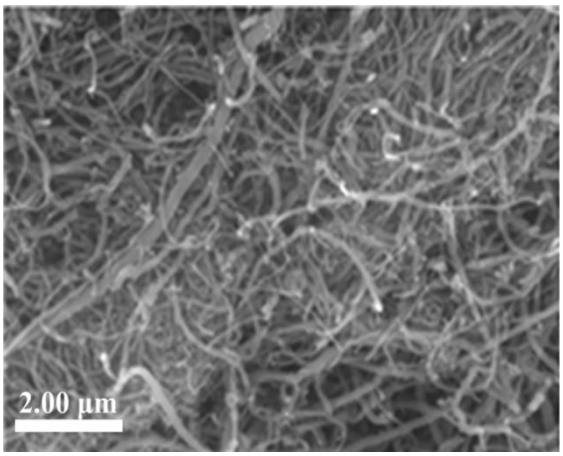

(a)

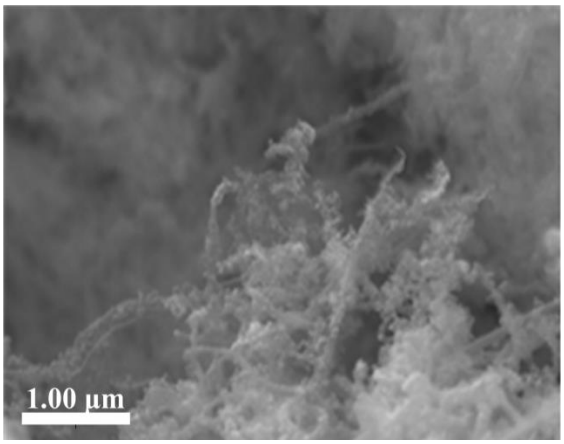

(b)

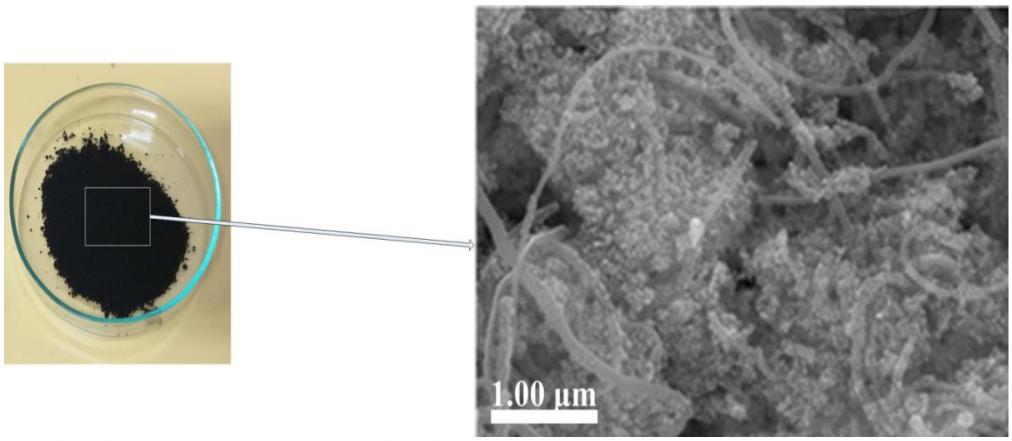

(c)

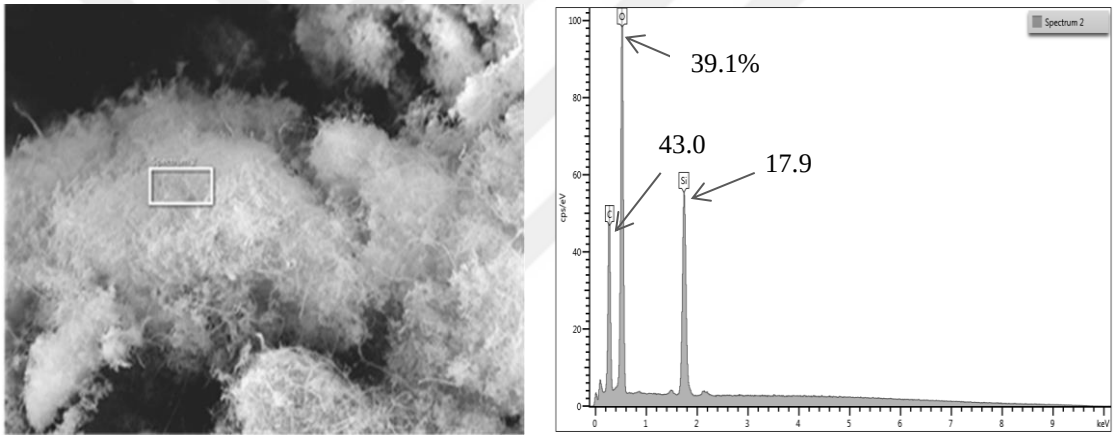

(d) (e)

Figure 6.1. *SEM images of (a) MWCNT-COOH (b-c) Si-MWCNT nanoparticles (d-e) EDX spectrum of Si-MWCNT nanoparticles*

It can be seen from Figure 6.1a that there are obvious CNT windings around each other under the strong Van der Waals force, tubular and tangled structure while smooth and clear surface can be observed. During the sol-gel process, with the addition of silica precursor, TEOS, the silica layer coverage on the MWCNT formed a sharp contrast structure that consisted of a rough and uniform coating layer, which was clearly observed along the x axis direction of the nanotubes (Figure 6.1b-c). Moreover, Figure 5.1e exhibits EDX result of Si-MWCNT, in which three distinct peaks of carbon (C) 43.0%, oxygen (O) 39.1%, silica (Si) 17.9% are observed. This result further confirmed that silica could

successfully deposit onto the CNT surface nanoparticles (Liu et al., 2015; Yang et al., 2009).

6.1.2 FTIR analysis

FTIR spectroscopy provides information about the functional groups MWCNT-COOH and Si-MWCNT nanoparticles have and their spectrums are given in Figure 6.2.

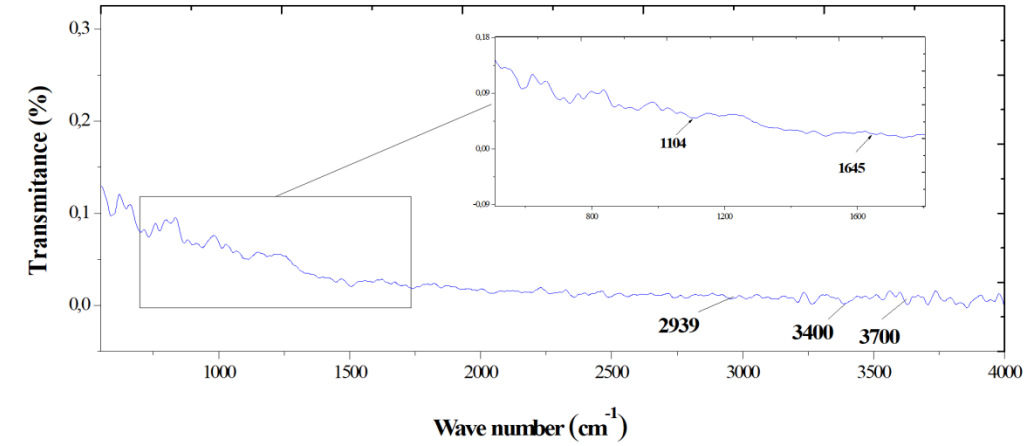

(a)

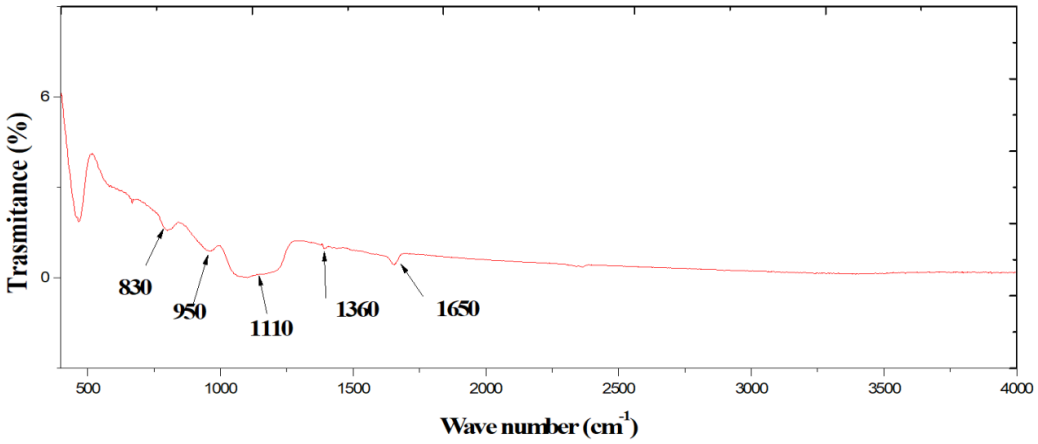

(b)

Figure 6.2. *FTIR spectra of (a) MWCNT-COOH and (b) Si-MWCNT nanoparticles*

In Figure 6.2a, the characteristic peaks at 1104, 1645, 2939, and 3400-3700 cm^{-1} correspond to C-O stretching, carbonyl stretching in carboxylic functional group (-COOH), C-H stretching and stretching mode of hydroxyl group (-OH), respectively (Nikje, Yaghoubi, 2014; Islam et al., 2006). Figure 6.2b reveals the chemical interaction between functionalized MWCNT and the TEOS solution. The resultant composite nanotubes showed new peaks of Si-O-Si asymmetric, Si-OH stretching and bending vibrations at 1100, 830 and 950 cm^{-1}, respectively. The presence of Si-O further indicated the formation of SiO_2 in the modified nanoparticle (Hsu et al., 2017; Yang et al., 2009; Tai et al., 2014). Furthermore, no Si-C bond was identified in the modified nanoparticle, which formed the crosslinking structure separately (Tai et al., 2014; Si et al., 2013).

6.1.3. XRD analysis

XRD analysis was performed to characterize and compare the structures of MWCNT-COOH and Si-MWCNT in terms of the crystallinity of their corresponding atoms, which are represented in Figure 6.3.

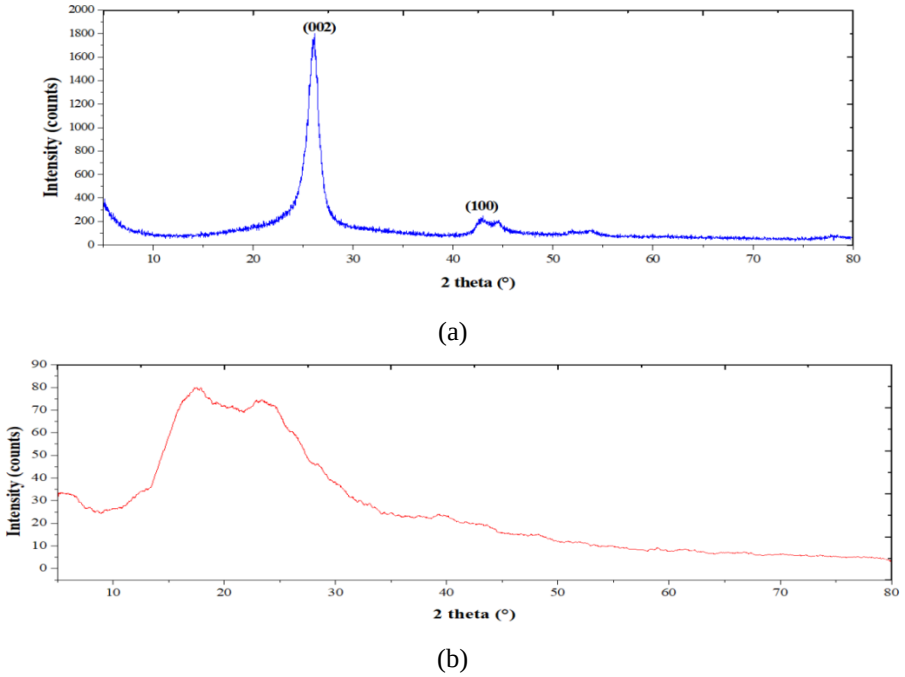

Figure 6.3. *XRD patterns of (a) MWCNT-COOH and (b) Si-MWCNT nanoparticles*

According to Figure 6.3a, the strong and sharp diffraction peak observed at 2θ=26.09^{o} and 42.7^{o} correspond to the (002) and (100) crystal planes of hexagonal graphene, respectively. This magnified view of the bifurcated (002) peak was an evidence of two distinct, compressed crystalline layers within a typical graphite shell (Kim et al., 2008; Ramoraswi, 2014; Molyanyan et al., 2016). The peak observed at 44.41^{o} was characteristic peak of the MWCNT-COOH nanoparticles so that it was observed in both patterns. However, crystallinity in the structure of MWCNT-COOH was damaged as a result of the interaction between silica and MWCNT-COOH (Figure 6.3b), i.e., the sharp peak of MWCNT-COOH at 26.09^{o} disappeared due to the fact that the amorphous silica caused the hindrance of MWCNT-COOH characteristic peak due to the interference of the X-ray, which confirmed that the MWCNT-COOH nanoparticles were perfectly coated with amorphous silica (Kim et al., 2008; Ramoraswi, 2014).

6.1.4. TG analysis

Thermal behavior of MWCNT-COOH and Si-MWCNT nanoparticles were studied by TGA and the results are given in Figure 6.4.

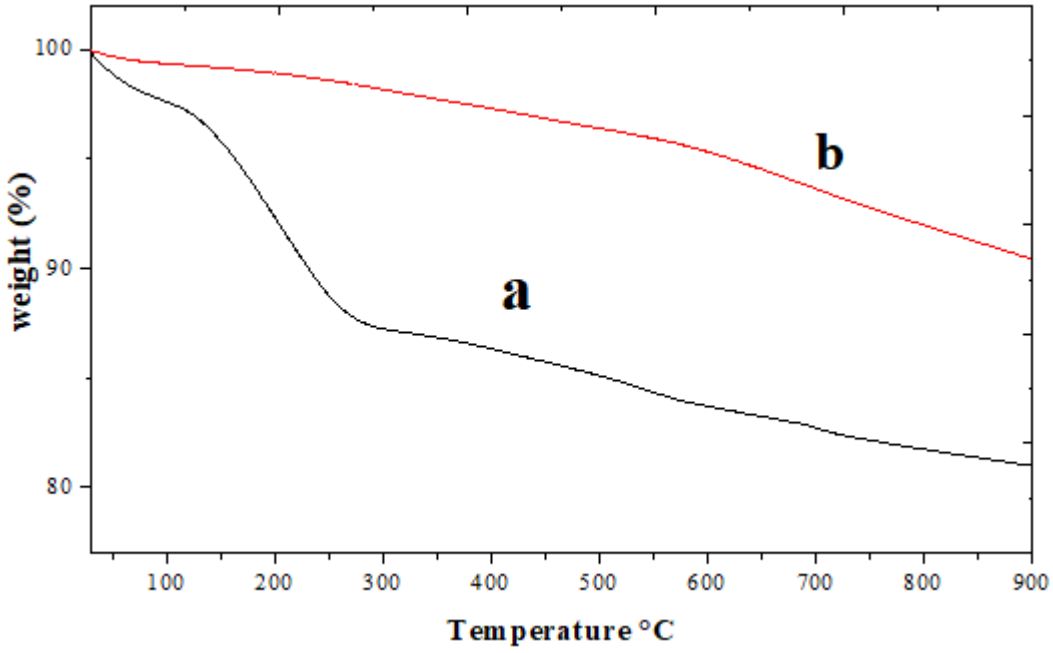

Figure 6.4. *Thermal degredation of (a) MWCNT-COOH, (b) Si-MWCNT nanoparticles*

The TGA curve of the MWCNT-COOH shows obvious weight loss (about 15%) at temperature ranges between of 100 to 300°C, which corresponded to the decomposition of hydroxyl groups (Wang et al., 2008; Zhou et al., 2011) (Figure 5.4-a) and the decomposition continued up to 900^{o}C due to the degradation of MWCNT nanoparticles It is predicted to decompose further if the temperature had been increased beyond 900^{o}C or the analysis had been carried out under the oxygen atmosphere (Kim et al., 2008). For the Si-MWCNT nanoparticles, the weight loss occurred between 300 to 900 ^{o}C owing the decomposition of MWCNT nanoparticles and the remaining material is Silica from the composite. Furthermore, it is obvious that the decomposition rate of Si-MWCNT was slower due to having a compact and stiff structure compared to MWCNT nanoparticles (Kim et al., 2008, Lavorgna et al., 2012; Hong et al., 2010).

6.2. Filtration Performance

Filtration performance of pristine PVC and Si-MWCNT embedded nanocomposite membranes were investigated in terms of pure water flux, rejection, anti-fouling characteristics such as flux recovery ratio and resistances and the results are given in this section.

6.2.1. Flux and rejection measurements

The results of flux values and HA and SA rejections of the fabricated membranes at a constant TMP of 0.69 bars as a function of Si-MWCNT loading are presented in Figure 6.5.

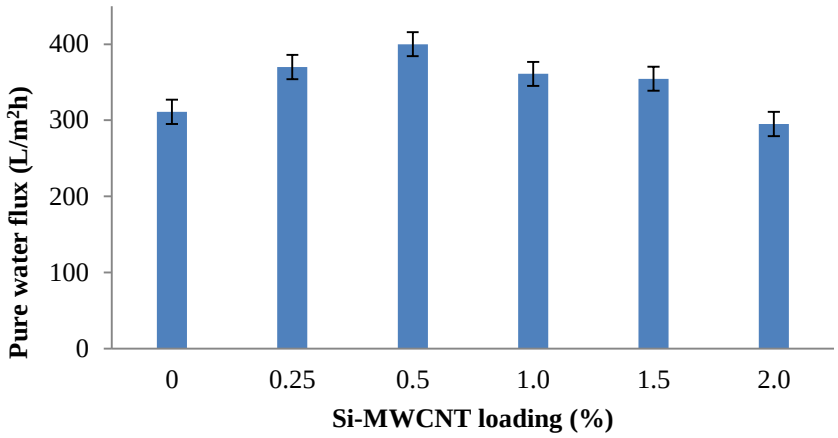

(a)

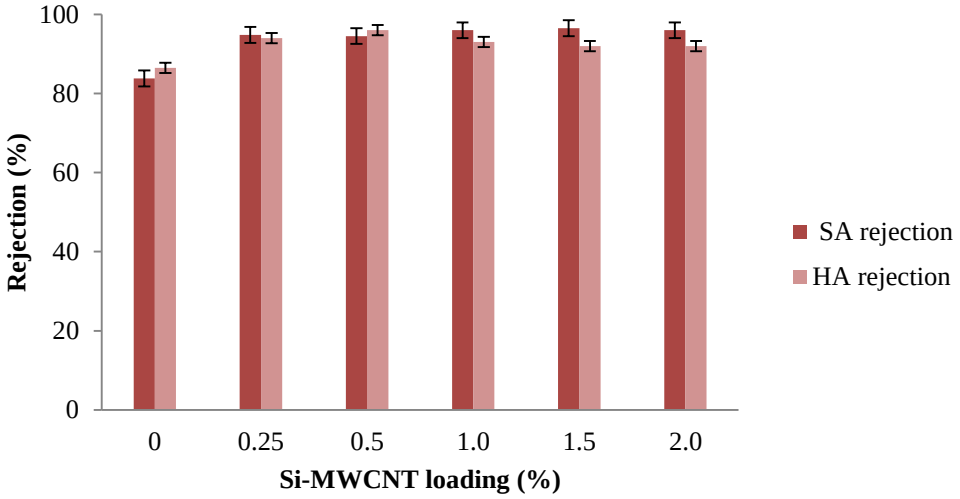

(b)

Figure 6.5. *(a) Pure water flux (b) Sodium alginate and humic acid rejections of the fabricated membranes as a function of Si-MWCNT loading (results are average of three replicates*

According to Figure 6.5a, the pure water flux of pristine PVC membrane was 311 L/m^{2}h. Addition of 0.5% of Si-MWCNT nanoparticles to the membrane matrix enhanced the pure water flux approximately by 25% (to 400 L/m^{2}h) compared to that of the pure PVC membrane with the pristine PVC membrane (Choi, Jegal and Kim, 2006; Silva et al., 2015). This improvement in the flux values was due to the enhancement of the membrane surface porosity as confirmed by SEM analysis and porosity calculation which clearly indicated the increase in the number of pores on the surface of the modified membranes, as

well as the increase of the membrane hydrophilicity (Mater et al., 2018). The uniform distribution of the hydrophilic nanoparticles onto the membrane surface as well as the into the finger-like pores enhanced the water permeability by attracting water molecules inside the membrane structure and facilitates their passage through the membrane (Mittal, Jana and Mohanty, 2011). However, further loading of Si-MWCNT nanoparticles resulted in a change in the structure and size of the finger-like pores, which led to an increase of membrane resistance and a consequent decrease in water permeability. The decrease of flux in the presence of greater amounts of nanoparticles beyond 0.5% may be attributed to the higher density as well as viscosity of the casting solution of the membrane. The increase of the density with the addition of high Si-MWCNT content suppressed the membrane pore forming during phase inversion process, because the countercurrent mass transfer between the solvent and water will slow down the precipitation of the membrane, which in turn will give a lower porous membrane (Demirel et al., 2017). On the other hand, due to the higher casting solution viscosity, solvent's outdiffusion from the casting solution was favored over non-solvent's indiffusion into the solution; a membrane with smaller pore size was formed (Krishnamoorthy and Sagadevan, 2015; Choi, Jegal and Kim, 2006).

Figure 6.5b presents SA and HA rejections of the pristine and PVC/Si-MWCNT nanocomposite membranes. The SA rejection of pure PVC membrane was the lowest (83.9%) compared to those of Si-MWCNT modified membranes. This result could be attributed to the hydrophilic effect due to the addition of Si-MWCNT, which was located at the surface and within the cross-section of the modified membranes. The addition of Si-MWCNT enhanced the hydrophilicity based on the principle of the interfacial hydration layer as protective barrier, which could decrease the interaction between SA and membrane surface so as to hinder the foulant molecules to penetrate through the modified membrane during the fouling or SA filtration. The rejection values of all composite membranes varied between 94.0-96.7%. The higher SA rejection of the nanocomposite membrane which had a further loading than 0.5%Si-MWCNT could be attributed to the decline in surface porosity as well as the pore size of the modified membrane as indicated in the SEM analysis and porosity results (Zhang et al., 2013). Moreover, the HA rejection of pristine PVC membrane was found to be 86.0% and those for the PVC/Si-MWCNT nanocomposite membranes ranged between 92.0-96.0%, which were higher than that of pristine PVC

membrane. This improvement of the rejection might be attributed to the increase of the pore numbers onto the membrane surface and a greater hydrophilic effect disclosed by the Si-MWCNT addition (Saraswathi et al., 2018; Ng et al., 2013).

The variation of flux with TMP for the pristine PVC and Si-MWCNT modified PVC membranes are presented in Figure 6.6.

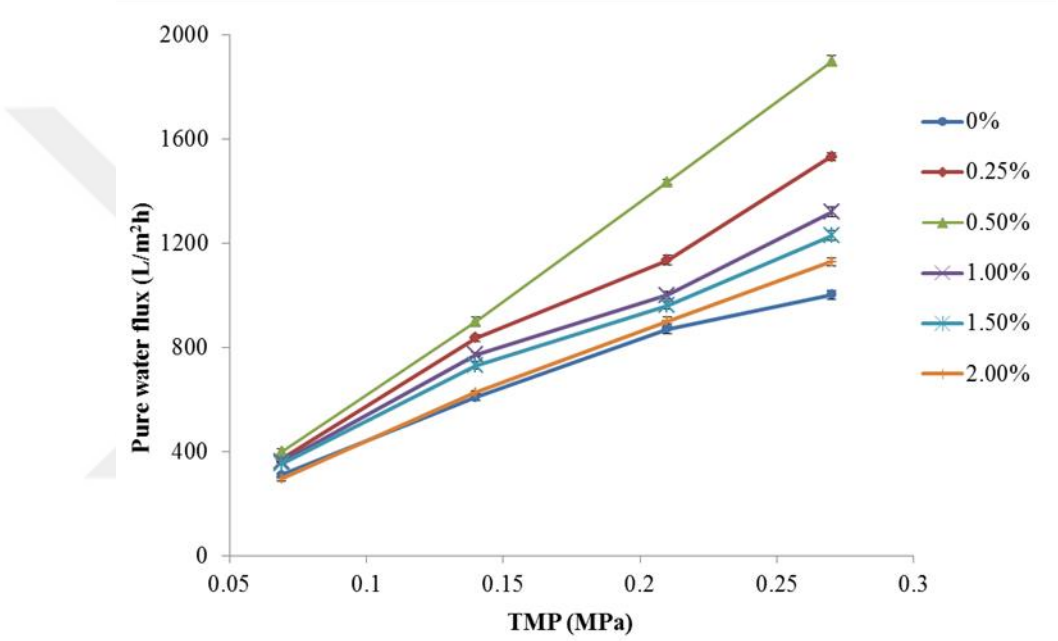

Figure 6.6. *Pure water flux vs. TMP as a function of Si-MWCNT loading*

According to Figure 6.6, pure water flux of all the fabricated membranes increased with applied transmembrane pressure. However, for the Si-MWCNT modified nanocomposite membranes, the variation of flux with TMP continued to be linear up to the highest pressure applied, while in the case of PVC membrane, the linear pattern started to deviate once a pressure around 0.2 MPa was exceeded, which confirmed that the pore integrity degree as well as the mechanical property of the pristine PVC membrane was enhanced due to the addition of Si-MWCNT nanoparticles.

6.2.1.1. *Anti-fouling properties*

Fouling is a significant issue in membrane processes, which influences the permeability and shortens the membrane life (Yang et al., 2007; Celik and Choi, 2011). It is well known that membrane fouling can be influenced by hydrodynamic conditions (such as permeation drag and back transport), as well as affinity between the foulants and membrane material such as the sorption and aggradation of foulants on membrane surface or in the finger like pores (Yang et al., 2007; Zhang et al., 2013).

The anti-fouling performance of the pure PVC and the modified PVC/Si-MWCNT membranes were analyzed in terms of water flux recovery ratio (FRR), total fouling resistance or total fouling ratio (R_t), intrinsic or hydraulic membrane resistance (R_m), reversible (R_r) and irreversible (R_{ir}) fouling resistances, which were quantified during filtration experiments using SA fouling solution (Khalid et al., 2015; Yang et al., 2007; Martín et al., 2014). R_m, R_r and R_{ir} are factors which are related to the membrane properties, loose attachment of foulants on the surface of the membrane or formation of a cake layer (which could be removed by simple hydraulic cleaning), and the adsorption of foulants on the membrane pore wall or surface or pore blockage (which lead to strong adsorption or entrapment of protein molecules on the surface or in the pores), respectively (Martínet et al., 2014; Orooji et al., 2016).

Figure 6.7 and 6.8 show FRR values and the filtration resistance of the fabricated membranes as a function of Si-MWCNT loading, respectively.

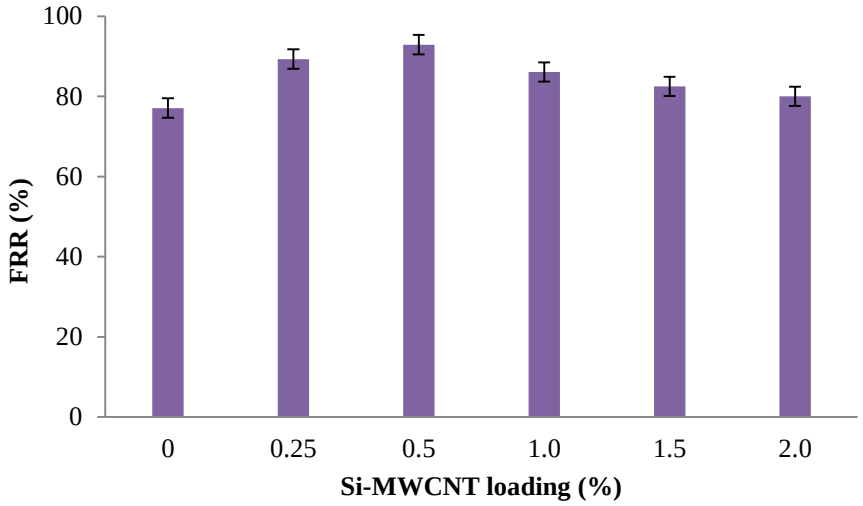

Figure 6.7. *FRR values of the fabricated membranes as a function of Si-MWCNT loading after SA fouling*

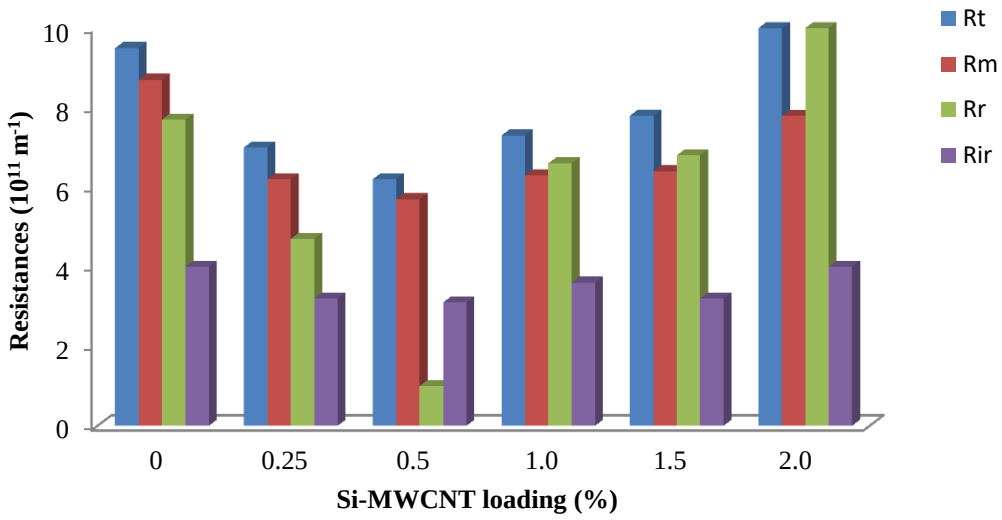

Figure 6.8. *Filtration resistances of the fabricated membranes as a function of Si-MWCNT loading during SA fouling*

FRR values depicted in Figure 6.7 can obviously present the suitable regeneration properties of the modified membranes. The higher FRR means the better antifouling property for the membrane. FRR value of the pristine PVC membrane was found to be 77.1%, which indicated a poor antifouling property and a serious membrane fouling occurred due to the irreversible adsorption of SA on the hydrophobic sites of the membrane

surface. FRR gradually increased up to 0.5% Si-MWCNT loading and reached 92.9%, which was mainly due to the hydrophilic sites of the PVC/Si-MWCNT nanocomposite membrane, inhibiting the hydrophobic touch, bond probabilities and interactions between the foulants and the membrane. Further amount of nanoparticles beyond 0.5% caused a decrease in the FRR value, which was attributed to the aggregation of the nanoparticles confirmed by SEM, EDX and AFM analysis. The agglomeration of nanoparticles led to the pore blocking, which in turn declined FRR (Demirel et al., 2017; Yang et al., 2017).

According to Figure 6.8, total fouling resistance (the sum of R_m, R_r and R_{ir}) of the membranes prepared with the incorporation of Si-MWCNT, were low compared to that of pure PVC membrane. R_{ir} value of the bare PVC membrane was 4×10^{10} m^{-1}. However, with the addition of Si-MWCNT nanoparticles up to 0.5%, the irreversible fouling value remarkably reduced to 3×10^{10} m^{-1}, as well as the reversible fouling resistance decrease from 7.7×10^{10} m^{-1} to 1.5×10^{10} $m^{-1}$and the intrinsic membrane resistance (R_m) declined from 8.7×10^{11} m^{-1} to 5.7×10^{11} m^{-1}. This result indicated that the enhancement of PVC membrane in terms of its hydrophilicity decreased the touch and interactions between SA and membrane, accordingly weakened the sorption and conglomeration of SA easily causing to membrane fouling, and improved the anti-fouling ability (Rana, Matsuura, 2010; Yang et al., 2017). However, further loading of Si-MWCNT nanoparticles decrease the antifouling performance, due to their aggregation during the casting and phase inversion process and allocation of the nanoparticles mainly in the polymer body rather than on the surface of the membrane, which in turn cause pore plugging and provides extra hydraulic resistance leading to a noticeable increase in the irreversible resistance values (Khalidet et al., 2015; Oroojiet et al., 2016).

6.3. Membrane Characterization

6.3.1. Membrane morphology

Membrane morphology studies provide atomic or nano-scale structure information about pore shape, pore size distribution and roughness. Analytical imaging techniques used for mapping the surface morphology of the prepared membranes were SEM, EDX and AFM. These methods provide high-spatial-resolution images that show the relative surface and cross section morphology of membrane structure.

6.3.1.1. *SEM and EDX analysis*

SEM imaging and EDX analysis were used to inspect the effect of Si-MWCNT addition on membrane morphological characteristics such as cross-section and surface morphology and the results are given through Figures 6.9-6.13.

The top surface SEM images of the fabricated membranes as a function of Si-MWCNT loading are given in Figure 6.9.

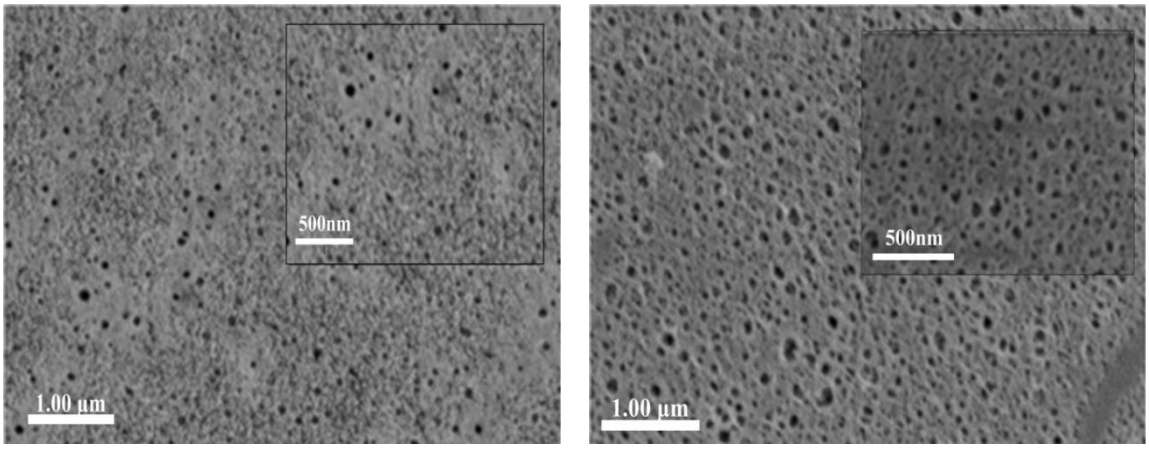

(a) (b)

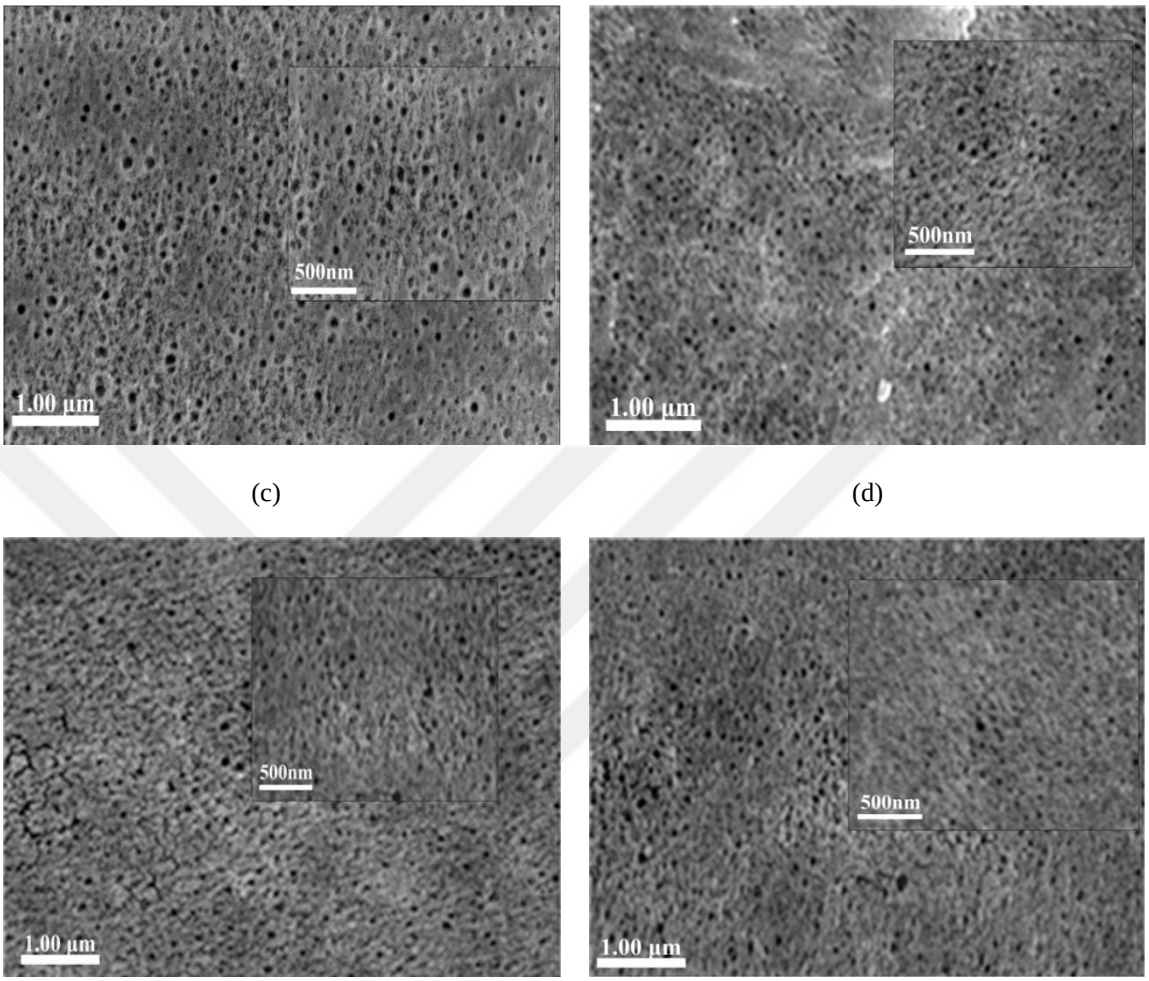

(c) (d)

(e) (f)

Figure 6.9. *Surface SEM images of the membranes as a function of Si-MWCNT loading (a) 0 wt%, (b) 0.25 wt%, (c) 0.5 wt%, (d) 1.0 wt%, (e) 1.5 wt%, and (f) 2.0 wt%*

As illustrated in Figure 6.9, the pristine PVC membrane surface contained a lower porosity as well as a nonuniform pore distribution compared to those in the PVC/Si-MWCNT nanocomposite membranes, which confirmed that, the addition of Si-MWCNT nanoparticles enhanced the size of the pores as well as the porosity of the pure PVC membrane. Among the PVC/Si-MWCNT nanocomposite membranes, PVC/0.5Si-MWCNT membrane had the largest pore diameter and also the highest surface porosity (Ding et al., 2016). The changes in the membranes surface pore size and porosity might be attributed to the stronger hydrophilic nature of Si-MWCNT nanoparticles and the high casting solution viscosity, which accelerated the exchange rate between solvent and non-solvent during the

phase inversion which, in turn, led to a higher membrane porosity and a larger porous structure (Gohari et al., 2015; Saki and Uzal, 2018; Wang et al., 2018) These results were also in accordance with the porosity and pore size data listed in Table 6.1. However, the pores of the blend membranes became irregular and the connections among layers became poor when further Si-MWCNT nanoparticles were added due the excessive viscosity, which decreased the rate of the solvent-non-solvent diffusion during the phase inversion, inducing to a lower surface porosity. Moreover, the agglomeration of nanoparticles caused blockage of some pores (Ding et al., 2016).

The surface EDX images of the PVC and composite membranes displaying the presence and distribution of Silica nanoparticles on the surface of the membranes are given in Figure 6.10.

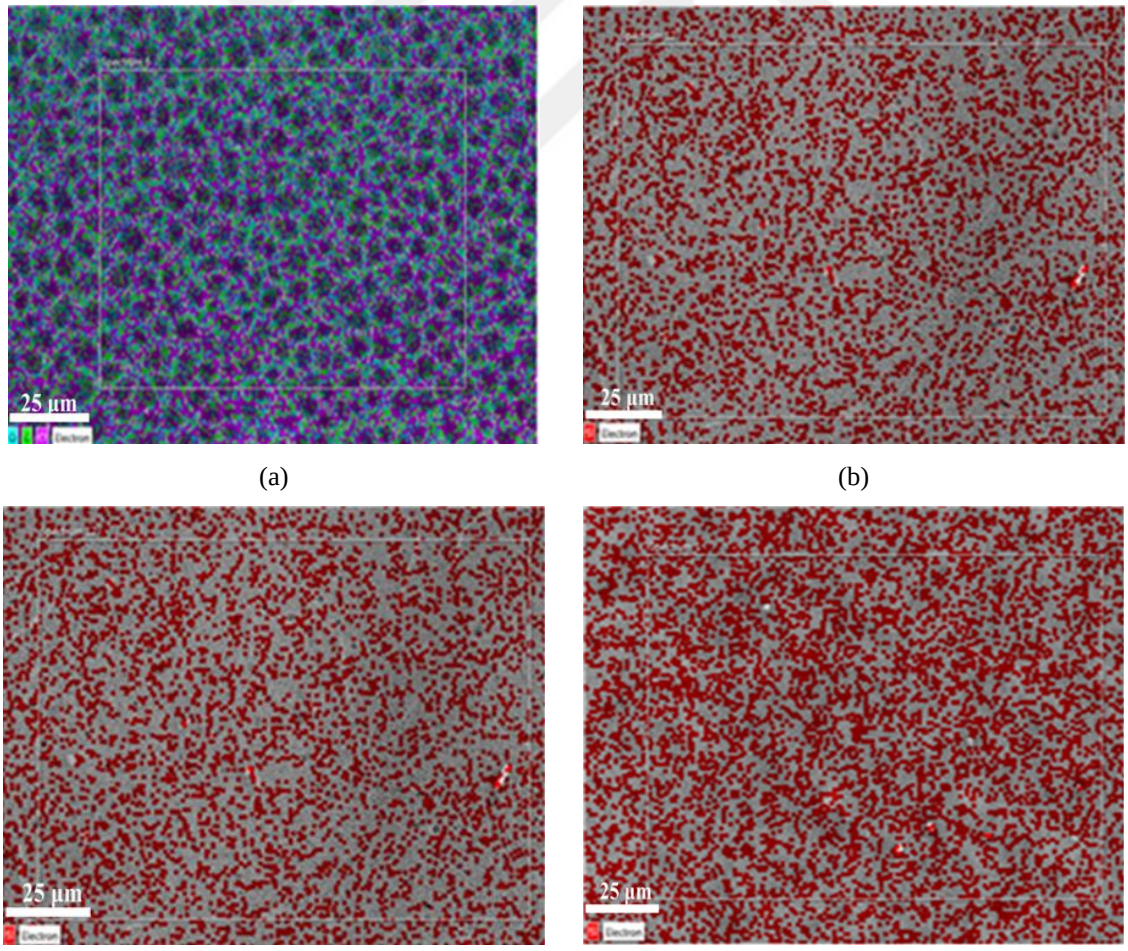

(a) (b)

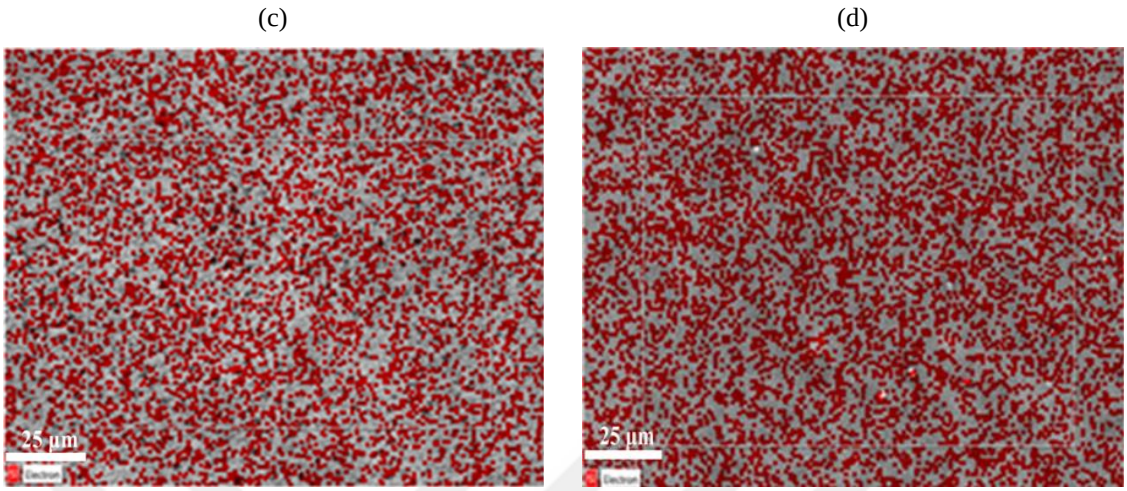

Figure 6.10. *Surface EDX images of the membranes as a function of Si-MWCNT loading (a) 0 wt%, (b) 0.25 wt%, (c) 0.5 wt%, (d) 1.0 wt%, (e) 1.5 wt%, and (f) 2.0 wt.*

In Figure 6.10, the first image (a) represents the distribution of elements (C, O and Cl) on the PVC membrane surface, which further displays that there are no Silica nanoparticles and the red dots in the rest of the images for the nanocomposite membrane represents the Silica nanoparticles. As it can be visualized from the figure that the intensity of Silica nanoparticles embedded on the membrane surface increase with the percentage of nanoparticles in the casting solution. Furthermore, there is a uniform distribution of nanoparticles on the surface of membranes having 0.25 and 0.5% of Si-MWCNT and the nanoparticles tend to gather and form unserious agglomerates for other membranes having higher nanoparticle content, which might block the surface pores avoiding the passage of water molecules through (Peyravi et al., 2014).

The cross-sectional SEM images of the fabricated membranes as a function of Si-MWCNT loading are given in Figure 6.11.

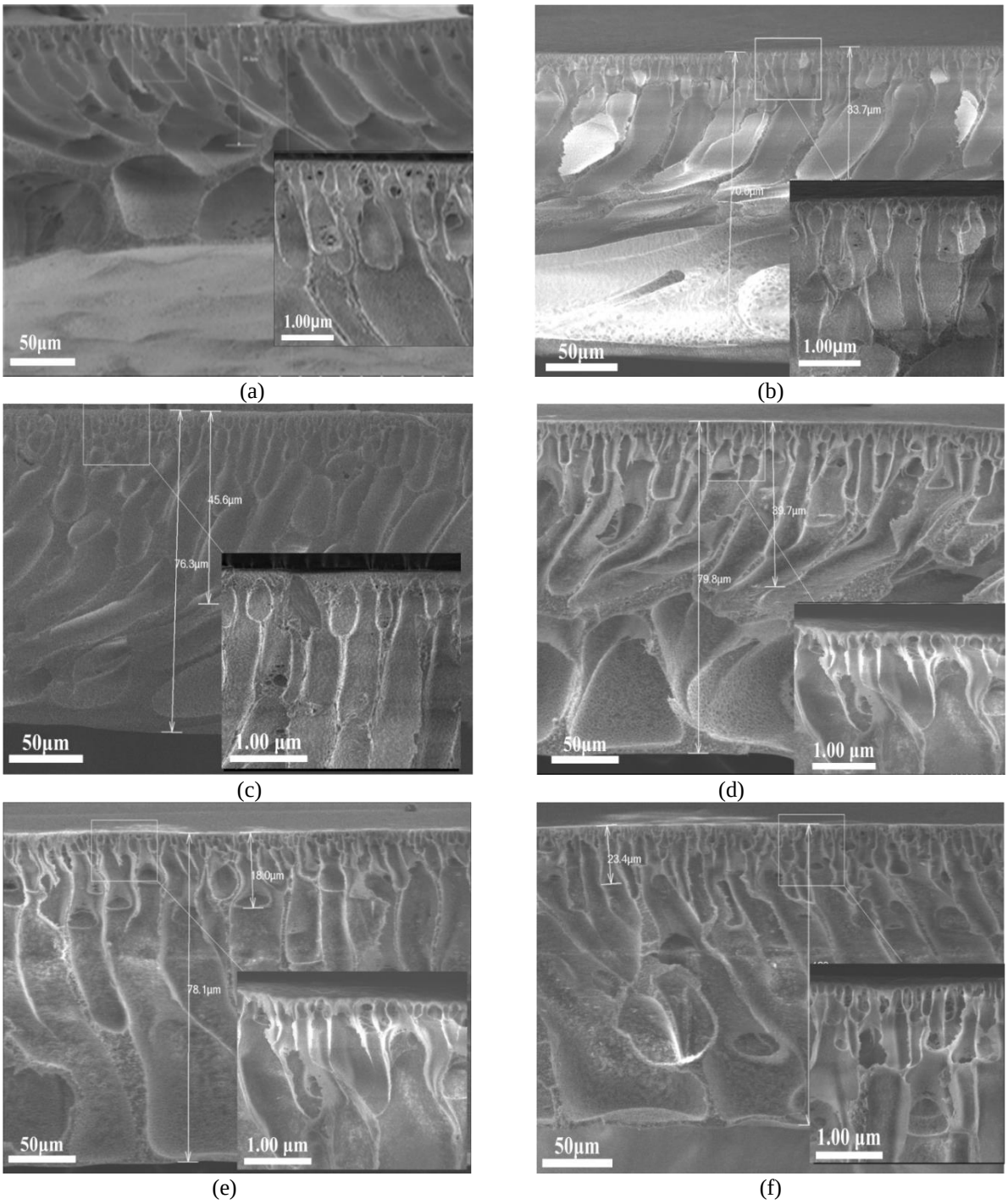

Figure 6.11. *Cross-sectional SEM images of the membranes as a function of Si-MWCNT loading (a) 0 wt%, (b) 0.25 wt%, (c) 0.5 wt%, (d) 1.0 wt%, (e) 1.5 wt% and (f) 2.0 wt%*

As illustrated in Figure 6.11, all the membranes exhibit a typically asymmetric cross-section structure, including a selective thin upper skin, finger-like and spongy-like pore

structure in the sublayer. This structure arises due to the high mutual diffusivities of water and DMAc during the phase inversion process. With the incorporation of Si-MWCNT nanoparticles into the PVC polymer matrix, the finger-like pores in the upper layer appeared larger than those seen in the cross-section of pure PVC membrane (Xu et al., 2015; Zhao et al., 2014). This could be attributed to instantaneous phase inversion during membrane formation due to the presence of hydrophilic Si-MWCNT nanoparticles. However, when the nanoparticle loading was increased beyond 0.5%, they started to aggregate in the pore walls of the blended membrane due to their strong Van der Waals interaction, which consequently result in blockage of the finger-like pores and hence, decrease the membrane permeability (Zhu and Wang, 2017).

The cross-sectional EDX images of the fabricated membranes are illustrated in Figure 6.12.

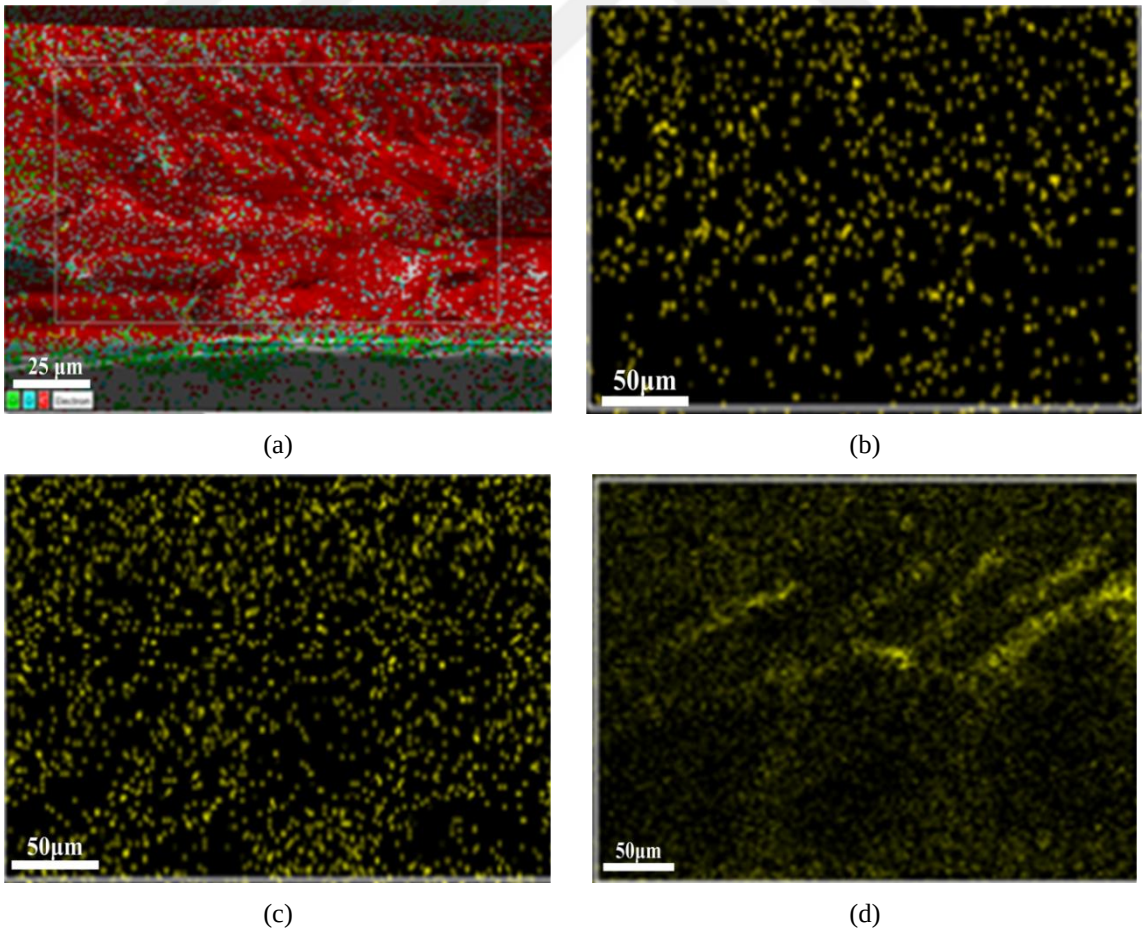

(a) (b)

(c) (d)

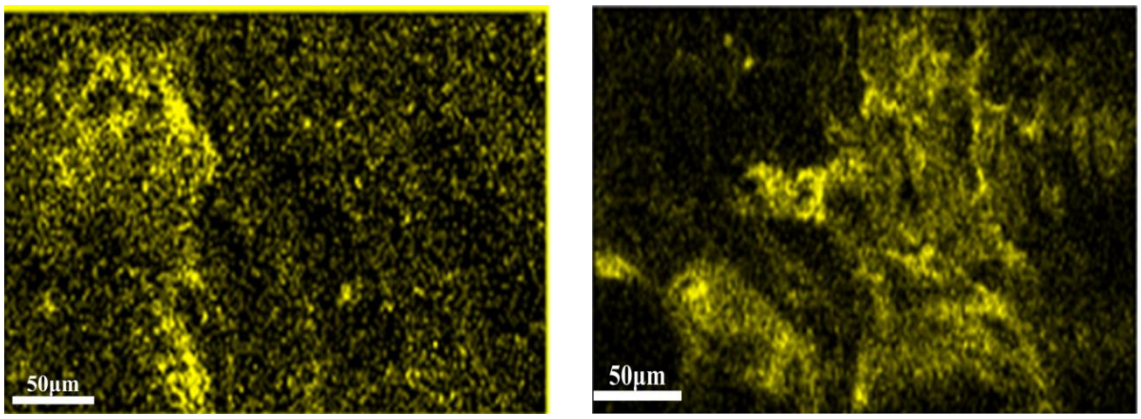

(e) (f)

Figure 6.12. *Cross-sectinal EDX images of the membranes as a function of Si-MWCNT loading (a) 0 wt%, (b) 0.25 wt%, (c) 0.5 wt%, (d) 1.0 wt%, (e) 1.5 wt%, and (f) 2.0 wt%*

According to the cross-sectional EDX mapping (Figure 6.12), the yellow dots represent Silica nanoparticles, which were dispersed in the cross-section of polymer matrices. As shown in Figure 6.12a, there are no Silica nanoparticles in the pristine PVC membrane matrix. For the PVC/0.25% Si-MWCNT and PVC/0.5% Si-MWCNT nanocomposite membranes, Silica nanoparticles were distributed homogenously along the membrane matrix both skin layer and sublayer. However, when the Silica content increased beyond 0.5%, the aggregation of nanoparticles become more clear, especially those for the 1.5 and 2.0%, it became more serious, which led to pore blockage so induced a sharp flux decline as also indicated by the flux value given in 6.5a.

Table 6.1 represents some morphological properties (porosities, thickness values and mean pore diameters) along with the permeability values calculated from the slope of the flux versus TMP curves of the fabricated membranes (Sile-Yuksel et al., 2014).

Table 6.1. *Morphological properties and permeability values of the pristine PVC and PVC/Si-MWCNT nanocomposite membranes*

Si-MWCNT loading (%)	Permeability (L/m^2hbar)	Porosity (%)	Thickness (μm)	Mean pore size (nm)
0	332	78.1 ±1.7	74±4	36.1
0.25	538	85.0 ± 2.6	73±4	40.0
0.5	716	90.0± 1.4	74±2	41.2
1.0	442	82.0 ±1.1	75±2	40.9
1.5	406	80.0 ±1.0	74±2	40.3
2.0	395	79.0±1.2	76±2	40.0

Membrane porosity is dependent on the phase inversion kinetics and solvent-nonsolvent interactions (Zhu and Wang, 2015). It can be seen from Table 6.1 that porosity values were significantly increased with the increase of Si-MWCNTs loading. The porosity of the pristine PVC membrane was found as 78.1% and increased with the addition of Si-MWCNT nanoparticles and the highest porosity was observed (90.2%) in the case of 0.5% Si-MWCNT. In addition, the mean pore diameter of the PVC membrane increased from 36.1 to 41.2 nm with the addition of 0.5% Si-MWCNT nanoparticles. However, the surface morphological properties of the nanocomposite membranes started to decrease as the nanoparticles loading increased beyond 0.5%. As more Si-MWCNT nanoparticles were added, the casting solution became more viscous which led to the change in finger-like pore structures with reduced pore connectivity (Low et al., 2014). Moreover, the permeability values of the fabricated membranes increased with the addition of Si-MWCNT nanoparticles up to 0.5% loading and then tend to decreased, which was also suggested by the flux values and were in good agreement with the morphological properties.

6.3.1.2. *Atomic force microscope (AFM) analysis*

Determining surface roughness and monitoring the topology of membranes are crucial tasks since they give insight into the membrane performance. Figure 6.13 displays the 2D and 3D topographic AFM images of the top surface of the synthesized membranes. The images cover an area of 40x 40 μm and the color intensity shows the vertical profile of the membrane surfaces, with the bright high peaks denoted the nodules and the dark regions

being the depressions and pores. The mean surface roughness (R_a) and the root mean square roughness (R_q) parameters of the fabricated membranes are presented in Table 6.2.

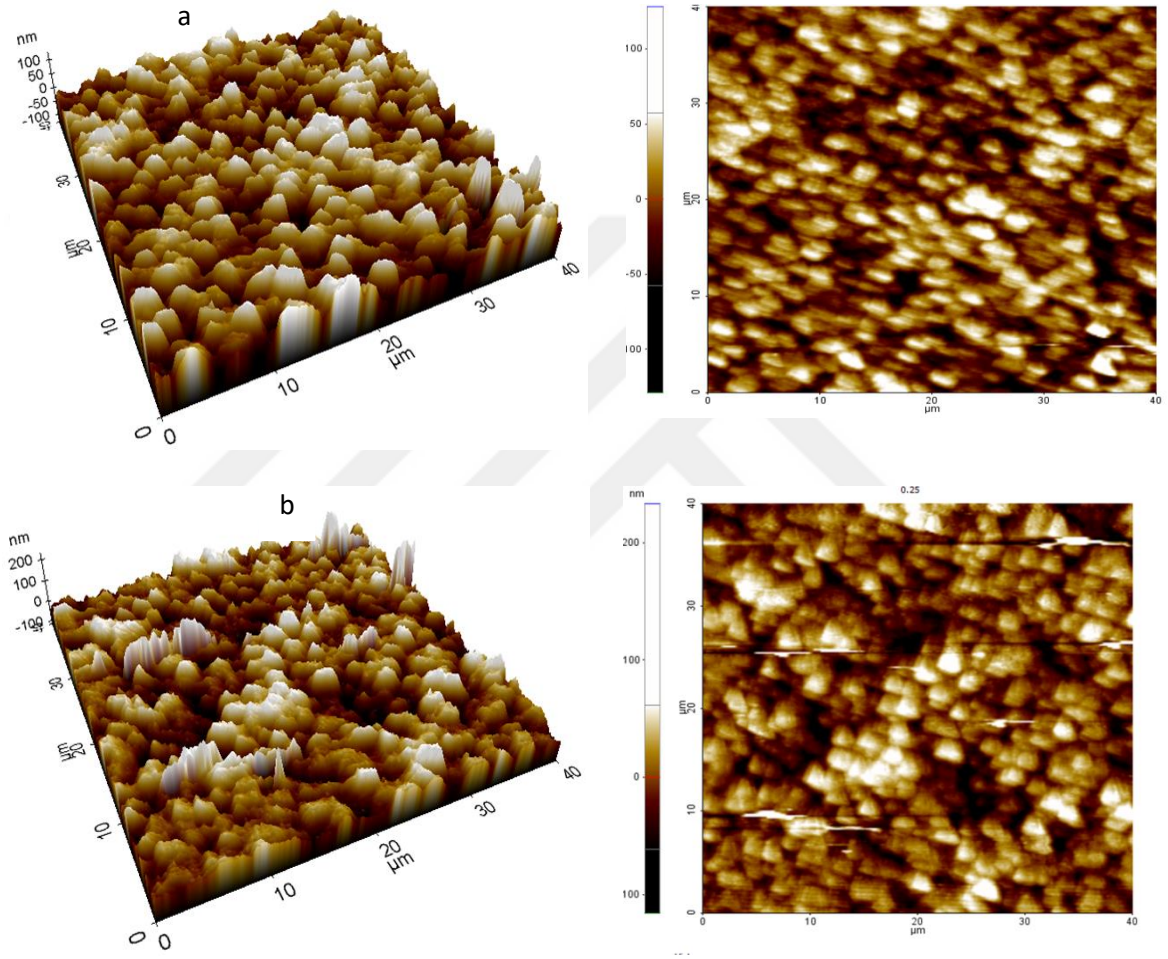

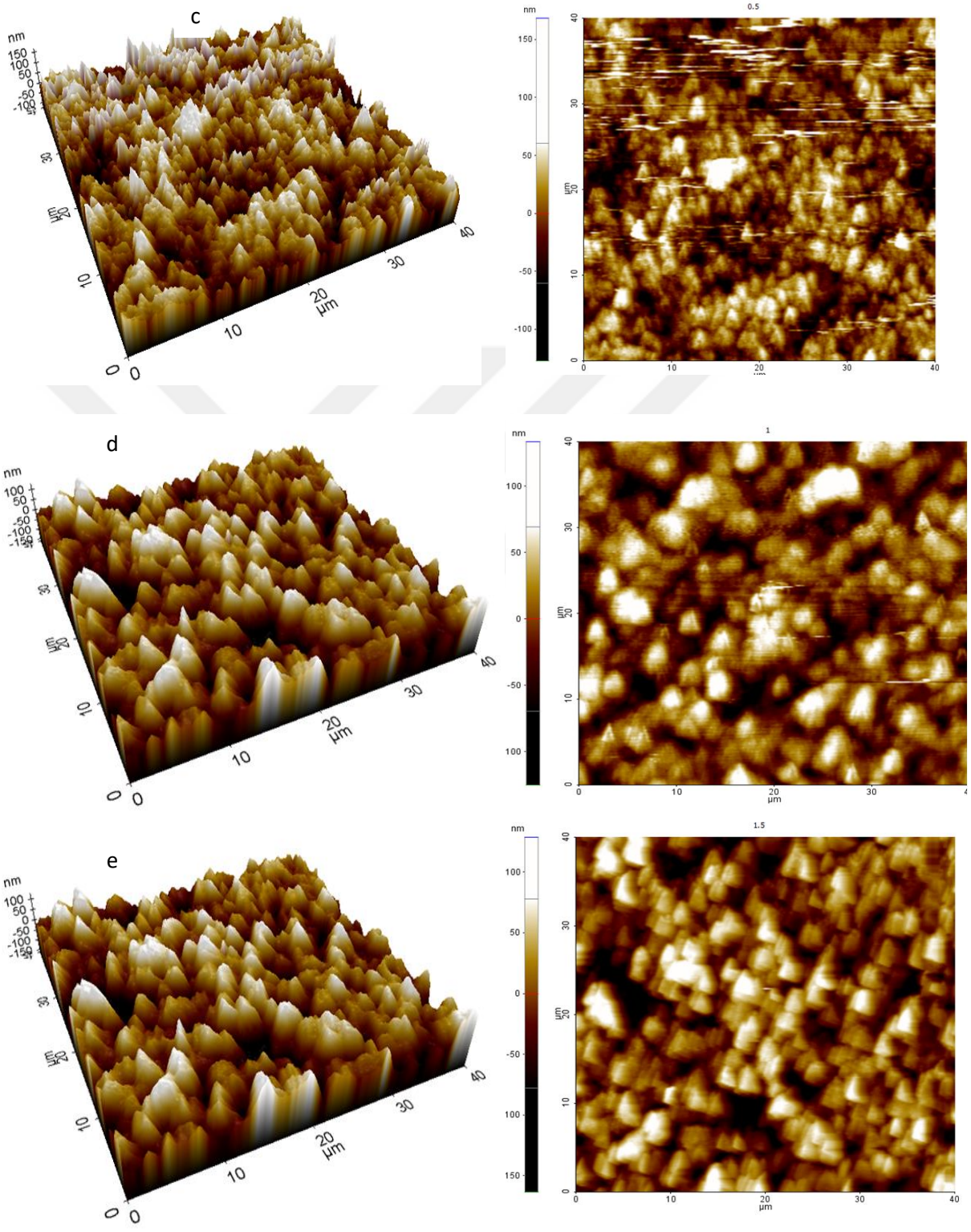
c
d
e
nm
µm
0.5
1
1.5

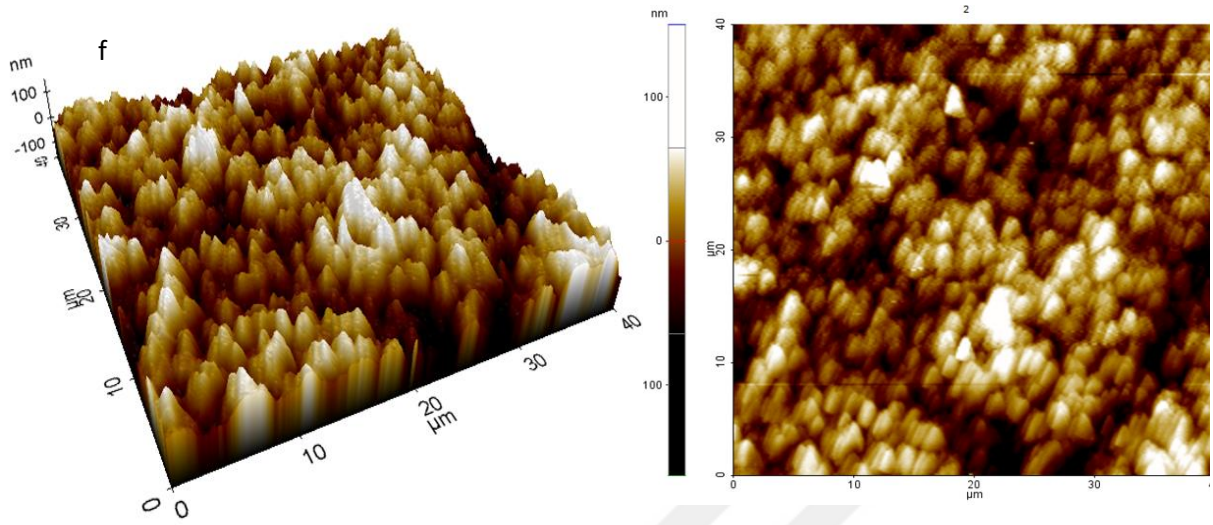

Figure 6.13. *AFM topography images of the PVC and PVC/Si-MWCNT nanocomposite membranes: (a) 0 wt%, (b) 0.25wt%, (c) 0.5wt%, (d) 1.0 wt%, (e) 1.5 wt%, and (f) 2.0 wt%*

Figure 6.13 clearly shows that the morphology of the surface of pristine PVC membrane was altered with the addition of Si-MWCNTs nanoparticles, where the nodules merged and became denser comparing to that of PVC pristine membrane (Idris, Mat Zain, and Noordin, 2007; Krishnamoorthy and Sagadevan, 2015). Merging of nodules resulted in a higher selectivity due to availability of water absorption sites and hence indicated an effective performance as already indicated by the rejection results (Idris, Mat Zain, and Noordin, 2007; Krishnamoorthy and Sagadevan, 2015; Kim, Lee, and Kim, 1999). The nodular structure was more pronounced in the case of PVC/0.5Si-MWCNT nanocomposite membrane, which may be attributed to the phase inversion mechanism in which polymer rich phase became nodules and polymer-poor phase was interstitial cavities (pores) onto membrane surface. In this case, the phase inversion may be stopped instantly resulting in the co-continuous structure because the solidification process was also very rapid due to high diffusion rate of DMAc and water (Kim, Lee, and Kim, 1999). However, with further addition of Si-MWCNT nanoparticles to the membrane casting solution, slight decoupling of nodules was observed, which was due to the increase of the casting solution's viscosity and agglomeration of the Si-MWCNT nanoparticles (Krishnamoorthy and Sagadevan, 2015).

Table 6. 2. *Roughness parameters of the PVC and PVC/Si-MWCNT nanocomposite membranes*

Membrane ID	R_a (nm)	R_q (nm)
Pristine PVC	23.5	29.3
PVC/0.25 Si-MWCNT	24.5	31.3
PVC/0.5 Si-MWCNT	24.9	30.7
PVC/1.0 Si-MWCNT	28.2	35.5
PVC/1.5 Si-MWCNT	31.3	39.7
PVC/2.0 Si-MWCNT	28.1	37.1

The surface roughness of the raw membrane was apparently lower than those of the modified PVC membranes. For lower loading levels of Si-MWCNT nanoparticles, the increase of mean surface roughness was small due to the low electrostatic interactions among the nanoparticles, which were regularly dispersed in the polymeric matrix. For higher loading levels, especially beyond 0.5%, there was a more significant increase in the mean surface roughness of the nanocomposite membrane, which might be referred to the increase in the viscosity of the casting solution. At values above 1.5% Si-MWCNT nanoparticles, there was a combined effect of increased viscosity and more serious agglomeration of the nanoparticles, which lowered the thermodynamic stability of the casting solution reducing the pore size and resulting in a smoother membrane surface (Vatanpour et al., 2011, Rahimpour et al., 2012).

6.3.2. Contact angle and water uptake

Surface hydrophilicity is one of the important parameters since it influences the water flux as well as membrane fouling (Demirel et al., 2017; Xia et al., 2014). To investigate the surface hydrophilicity of bare PVC and modified nanocomposite membranes, a dynamic contact angle test was applied at 25°C. A low contact angle represents a high tendency for water to wet the membrane, a high surface energy and high hydrophilicity. The effect of varying amounts of Si-MWCNT addition into the membrane casting solution on the static and dynamic contact angle values of the resulting membranes are depicted in Figure 6.14.

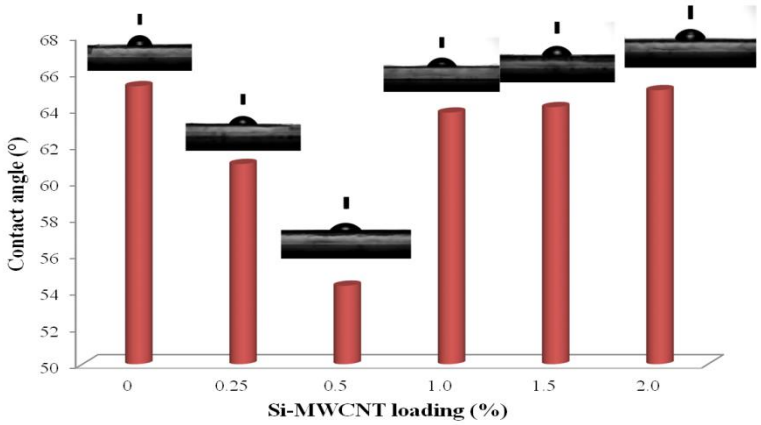

(a)

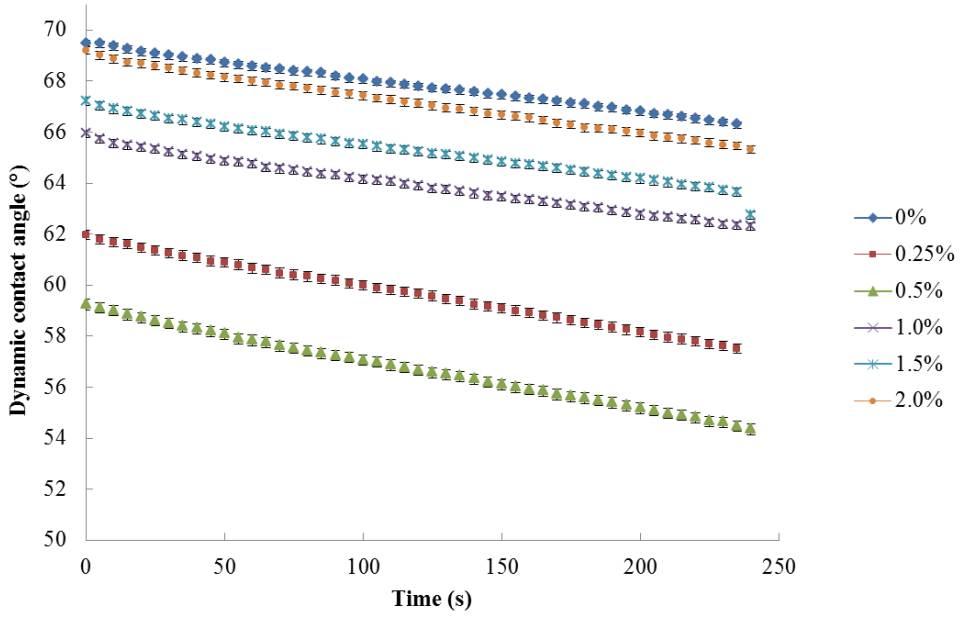

(b)

Figure 6.14. *(a) Static and (b) dynamic contact angles of the fabricatd membranes as a function of Si-MWCNT loading*

According to Figure 6.14, the contact angle values of the fabricated membranes decreased with increasing Si-MWCNT nanoparticle content, indicating increasing hydrophilicity of the nanocomposite membranes due to the hydrophilic nature of the nanoparticles. The static contact angle of the pure PVC membrane decreased from 65.2^{o} to 54.3° with the addition of 0.5% Si-MWCNT membrane because of the existence of polar

functional groups on the skin layer, which might have interact with water by hydrogen bonding. Moreover, the surface porosity also showed an effect on the contact angle, because the water drop could penetrate into the pores because of the capillary action, which decreased the contact angle and increased the water uptake (Figure 6.14). However the further addition of Si-MWCNT nanoparticles induced to an increase in contact angle, which can be referred to the increase in the viscosity of the casting solution and the resulting slight agglomeration of Si-MWCNT nanoparticles with a reduced effective area on the surface of the membrane matrix, and also decline of the membrane surface porosity.

Figure 6.15 depicts the water uptake values of the PVC and PVC/Si-MWCNT nanocomposite membranes.

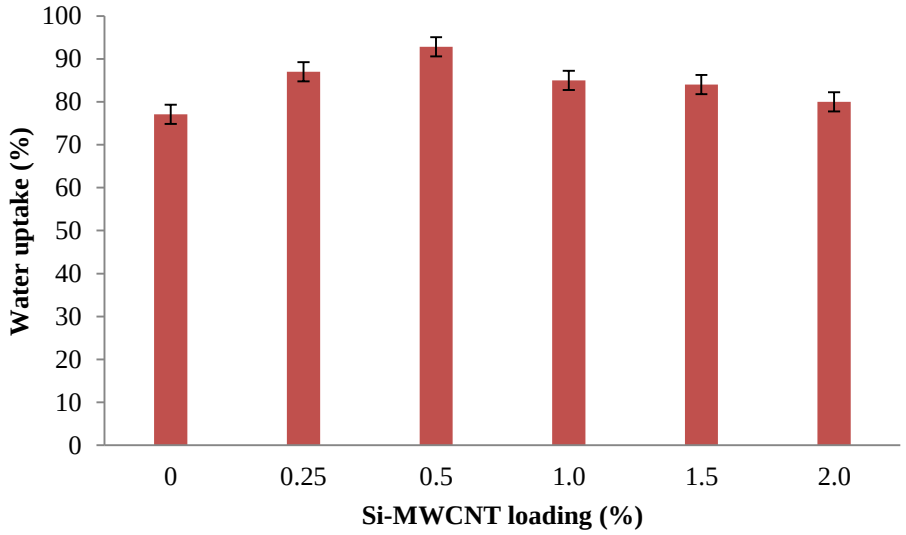

Figure 6.15. *Water uptake values of PVC and PVC/Si-MWCNT nanocomposite membranes*

As shown in Figure 6.15, the water uptake of pristine PVC membrane was 77.1% and it increased with the addition of nanoparticles into the polymeric matrix and reached its highest value of 92.8% with the addition of 0.5% Si-MWCNT nanoparticles. These results provided an evidence for the fact that the addition of Si-MWCNT nanoparticles increased the hydrophilic nature of the modified membranes. After loadings further than 0.5% Si-MWCNT nanoparticles, the water uptake tend to decrease, which may be attributed to the

agglomeration of Si-MWCNT nanoparticles with a reduced effective area in the structure of membrane (Eren et al., 2015).

6.3.3 FTIR analysis

The FTIR analysis of pristine PVC and PVC/Si-MWCNT nanocomposite membranes were carried out to confirm the membrane surface modification and the results are given in Figure 6.16.

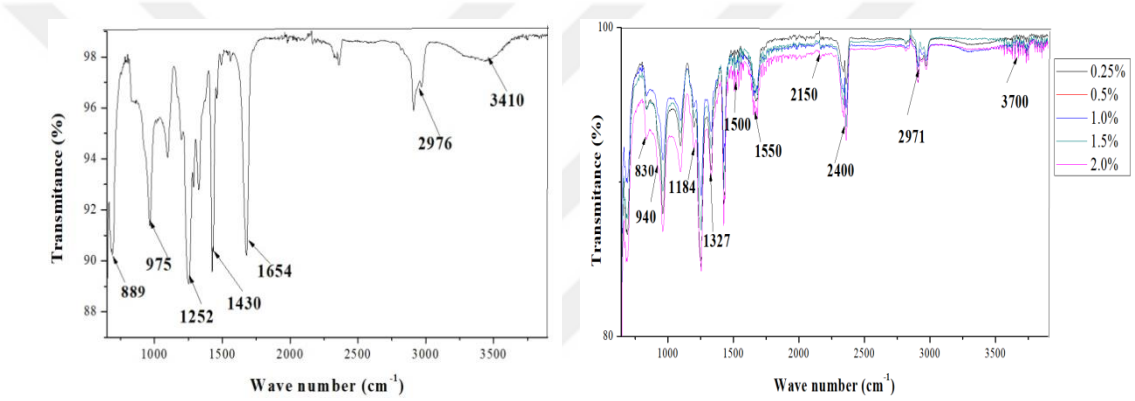

Figure 6.16. *FTIR spectra of (a) PVC and (b) PVC/Si-MWCNT nanocomposite membranes*

As illustrated in Figure 6.16, the characteristic peaks of the saturated C–H asymmetric stretching of CH_2 for PVC chains appeared at 2970 cm^{-1}, and 1430 cm^{-1} absorption, for both pure PVC and PVC/Si-MWCNT nanocomposite membranes (Bhavsar and Tripathi, 2017). The observed peaks at 1252 cm^{-1}, 689 cm^{-1} were attributed to the C–N vibration, and C–Cl bond stretching in the group CHCl, respectively (Rajendran, Prabhu and Rani, 2007; Bhavsar and Tripathi, 2017). The absorption peak at 3410 cm^{-1} were attributed to the O-H vibration from the intermolecular hydrogen bonds (Bhavsar and Tripathi, 2017; Sabir et al., 2015). Inspection of the peak intensity of the band at 1184 and 836 cm^{-1} indicated a progressive occupation of Silica of the accessible sites on the membrane surface with the addition of Si-MWCNT. At about 836 and 1184 cm^{-1}, the absorption peaks were initiated by Si–O–Si symmetric and asymmetric stretching vibration (Abdel-Baset, Elzayat and Mahrous, 2016; Marbelia et al., 2016), respectively,

demonstrating the generation of Si–O–Si in the system. In addition to that, the bands at 1654 and 1550 cm^{-1} were corresponded to the symmetric and asymmetric C=O vibration (Marbelia et al., 2016), respectively, whereas deformation vibration of Si-CH was observed at 1327 cm^{-1} (Mishra and Mukhopadhyay, 2017). Consequently, the FTIR spectra of all the nanocomposites membranes confirmed the presence of interactions between the Si-MWCNT nanoparticles and the PVC polymer.

6.3.4 . XRD analysis

XRD measurement was achieved to examine the nature of the crystallinity of the fabricated membranes. Figure 6.17 shows the diffraction patterns of the pristine PVC and PVC/Si-MWCNT nanocomposite membranes.

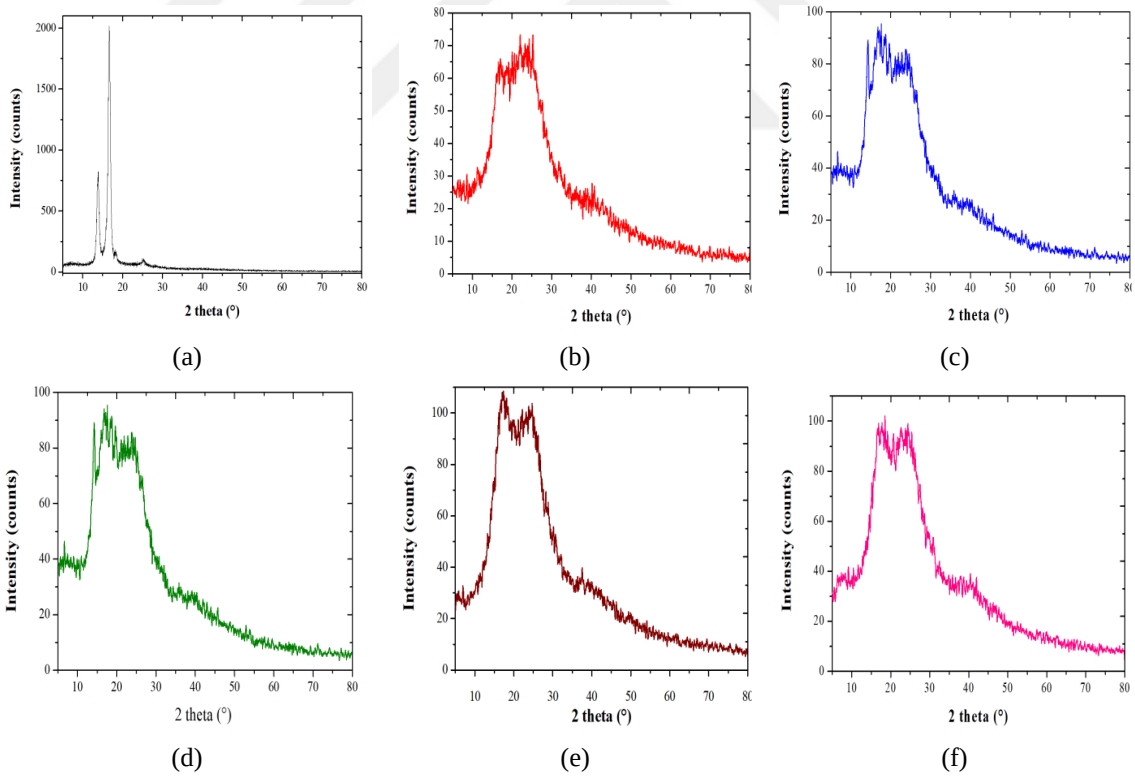

Figure 6.17. *XRD patterns of the membranes as a function of Si-MWCNT content (a) 0 wt%, (b) 0.25 wt%, (c) 0.5 wt%, (d) 1.0 wt%, (e) 1.5 wt%, and (f) 2.0 wt%.*

It can be seen from Figure 6.17 that pristine PVC membrane exhibits a semi-crystalline structure with peaks at the 2θ angles of 14^{o}, and 19^{o} and a relatively less intense peak at 25^{o} respectively. Peaks at 14° and 19° for pure PVC have slightly shifted in doped polymer films. It was clearly observed that the peak intensity of the pristine PVC membrane greatly reduced with the addition of Si-MWCNT nanoparticles. This implies that the addition of Si-MWCNT fillers into PVC membrane matrix greatly augmented the domain of amorphous region (the intensity of XRD crystal peak decreased). It can also be visualized that the degree of amorphism increased with the increase of Si-MWCNT nanoparticle content due to the disruption of the amorphous structure of Si-MWCNT nanoparticles. When Si-MWCNT nanoparticles dissolved in the polymer, the interaction between PVC and Si-MWCNT led to a decrease of the intermolecular interaction among the polymer chains which reduced the crystalline phase and hence increased the intensity of the amorphous region (Kayyarapu, 2016).

6.3.5. TG analysis

TG analysis was carried out to investigate the effect of addition of Si-MWCNT nanoparticles into PVC matrix on the thermal resistance improvement of pristine PVC membrane. TGA curves for the pure PVC and PVC/Si-MWCNT nanocomposite membranes are shown in Figure 6.18.

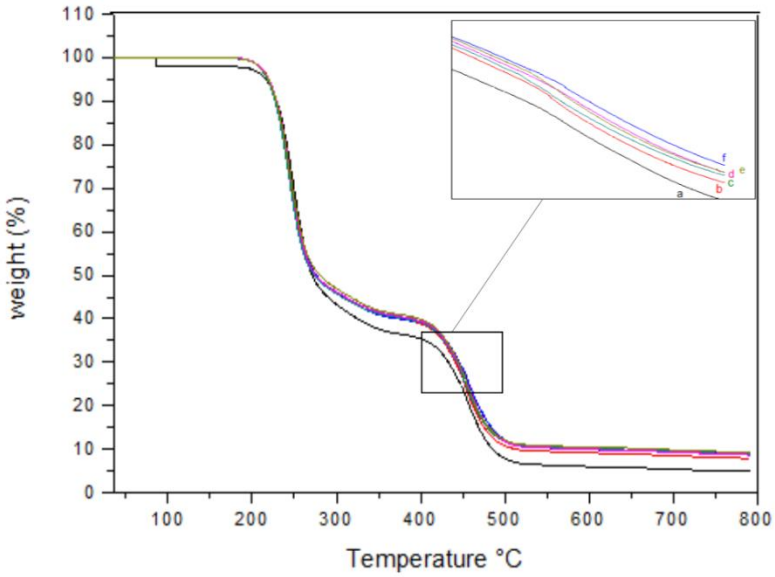

Figure 6.18. *TG thermograms of pristine PVC and PVC/Si-MWCNT nanocomposite membranes*

As shown in Figure 6.18, the thermal stability of all the membranes took place in three mass loss stages. The decomposition of pristine PVC membrane was observed at about 150-300°C up to a weight loss of 50%, however the decomposition of PVC/Si-MWCNT nanocomposite membrane was observed in the range of 230-300ºC, which may be due to chain stripping by the elimination of HCl molecule (dehydrochlorination). Second stage was observed at about 300-400°C owing to the thermal decomposition of polymer chain being the corresponding weight loss around 20%, and the third one in a higher temperature region (400-800°C) was related to crosslinking with a weight loss of 20-25% (Roy, Anjali and Sujith, 2017; Sabir et al., 2015). The decomposition of all PVC/Si-MWCNT nanocomposite membranes started from 230°C and considering the complete decomposition of the PVC control membrane, the increase of residual mass should correspond to the weight percentage of added Silica nanoparticles to the membrane matrix (Arsuaga et al., 2013).

6.3.6. Mechanical properties

Mechanical behaviors of the fabricated membranes were investigated using dynamical mechanical and nanoindentation analysis.

6.3.6.1. *DMA analysis*

DMA was employed to obtain dynamic mechanical responses of the pristine PVC and fabricated Si-MWCNT modified nanocomposite membranes as a function of temperature. Furthermore, DMA test was also applied on the PVC based MWCNT-COOH membrane fabricated in order to signify the enhancement of the mechanical properties of the membrane due to the orientation of MWCNT-COOH nanoparticles with Silica. The results are given in terms of storage modulus, loss modulus and stiffness for a temperature range of 28-140^{o}C (Figure 6.19).

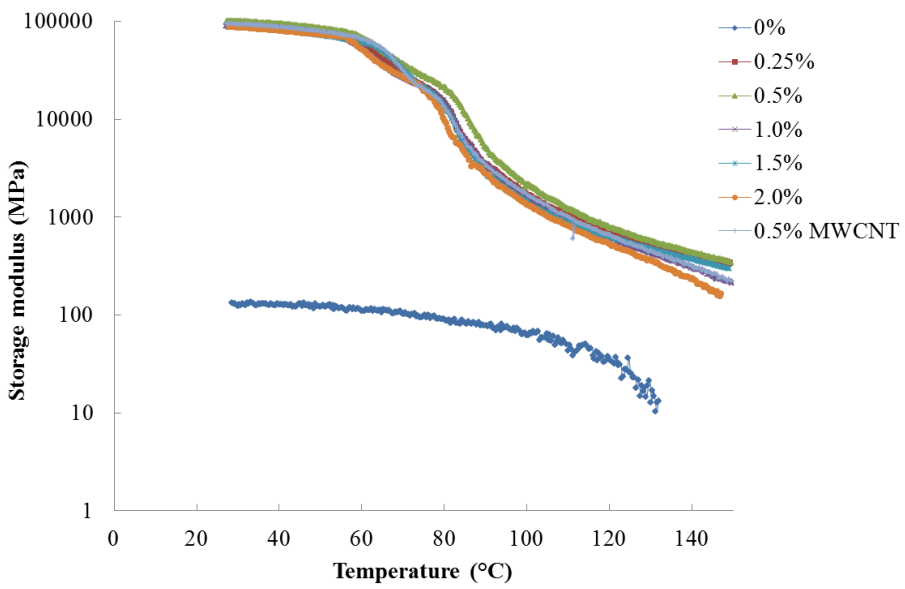

(a)

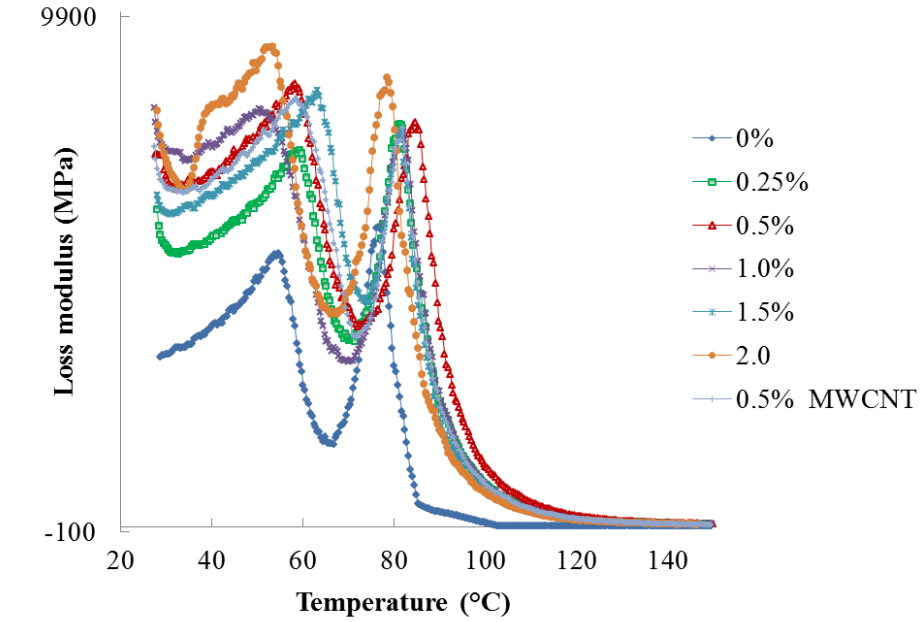

(b)

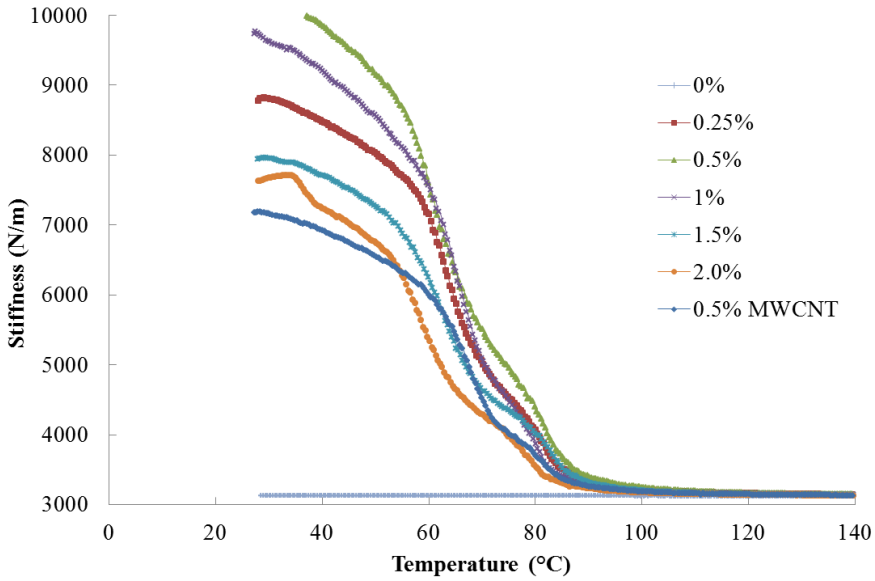

(c)

Figure 6.19. *Dynamic mechanical properties of pristine PVC and PVC/Si-MWCNT and PVC/0.5%MWCNT-COOH nanocomposite membranes as a function of temperature (a) storage modulus (b) loss modulus (c) stiffness*

As demonstrated in the Figure 6.19a, the initial storage modulus values of all the nanocomposite membranes have been enormously enhanced compared to that (0.134 GPa)

of the pristine PVC membrane. The storage modulus increased with the addition of Si-MWCNT nanoparticles up to 0.5% with a value of 100 GPa. The enhancement of the storage modulus might be due the strong interfacial bonds between the PVC polymer and Si-MWCNT nanoparticles which are uniformly distributed on the membrane matrix (Saha et al., 1999; Young and Mauritz, 2001). However, with the addition of more Si-MWCNT nanoparticles than 0.5% led to a decrease in the storage modulus values, which was attributed to the increase of the viscous nature of the membrane casting solution inhibiting the interaction between the polymer and the Si-MWCNT nanoparticles and the resulting agglomeration of the nanoparticles creating interfacial voids, which could reduce the storage modulus values (Saha et al., 1999). Furthermore, the storage modulus of the PVC/0.5% MWCNT-COOH nanocomposite membrane showed lower value (93 GPa) compared to the PVC/0.5% Si-MWCNT modified membrane, which confirmed that the orientation of MWCNT-COOH with Silica particles greatly enhanced the elastic behavior of the MWCNT-COOH.

Figure 6.19b shows the loss modulus versus of the pristine PVC, PVC/Si-MWCNT and PVC/0.5MWCNT-COOH membranes as a function of temperature. The loss modulus curve represents the viscoelastic behavior of a material or the ability of a material to disperse mechanical energy through internal molecular motion. Besides, glass transition temperature of a material could be determined from the maximum loss modulus value after which the membrane polymer transfers from the glassy to rubbery phase (Sgreccia et al., 2010; Saha et al., 1999). So according to the figure, pristine PVC membrane showed the lowest the loss modulus peak temperature (T_g =74ºC) so the lowest glass transition membrane compared to those of PVC/Si-MWCNT nanocomposite membranes. The glass transition temperature increased with the addition of Si-MWCNT nanoparticles up to 0.5% (T_g =90ºC). The increase of the glass transition membrane temperature might be due to the increase of the rigidity of the PVC/Si-MWCNT nanocomposite membrane matrix due to the improved interaction between PVC polymer and Si-MWCNT nanoparticles or the adsorption of polymer chain on the surface of nanoparticles, which caused restrictions against molecular motion of polymer chains resulting in more elastic response of the nanocomposite membrane (Saha et al., 1999; Young and Mauritz, 2001). With the addition of further of Si-MWCNT nanoparticles, the glass transition membrane temperature tended

to decrease because of the high casting solution viscosity which inhibited the PVC- Si-MWCNT bounds and also because of the agglomeration of Si-MWCNT in the membrane structure which caused weak points in the membrane structure (Saha et al., 1999). Moreover, it can been observed from the figure that the PVC/0.5% MWCNT-COOH nanocomposite membrane presented a lower glass transition temperature (82ºC) compared to that of PVC/0.5Si-MWCNT membrane which confirmed that the orientation of MWCNT-COOH with Silica particles enhanced the mechanical property of the nanocomposite membrane.

Figure 6.19c illustrates the change of stiffness values as a function of the applied temperature for all the fabricated membranes. The stiffness curves represented the load-bearing capability of the fabricated membranes. As shown in the figure, the initial stiffness value of the pristine PCV membrane was negligible (≈ 3123 N/m) compared to those of PVC/Si-MWCNT and PVC/0.5MWCNT-COOH nanocomposite membranes. The membrane stiffness increase with Si-MWCNT content up to 0.5% (≈ 10371 N/m) due to the uniform distribution of the Si-MWCNT in the membrane matrix resulting in a strong interaction between PVC and Si-MWCNT nanoparticles (Saha et al., 1999). However, with the addition of Si-MWCNT beyond 0.5%, the stiffness values started to decrease due to the voids creation by the effect of the nanoparticles agglomeration and the weak interaction between the PVC polymers and Si-MWCNT nanoparticles resulting a lower stiffness and strength. In addition, the stiffness showed a lower value for the PVC/0.5MWCNT-COOH nanocomposite membrane compared to that of PVC/0.5Si-MWCNT modified membrane, which revealed a better reinforcing effect of Si-MWCNT nanoparticles than the unmodified MWCNT-COOH.

6.3.6.2. *Nanoindentation analysis*

Nanoindentation test was applied for the investigation of surface damage of the fabricated membranes by applying force vertically on the surface of the membranes and the results are recorded in terms of the applied force and the corresponding indenter displacement as well as Young's modulus and hardness of the fabricated membranes (Figure 6.20). Moreover, in order to investigate the enhancement of membrane mechanical

strength after the modification of MWCNT-COOH nanoparticles by Silica, the mechanical properties of a PVC based membrane fabricated with 0.5% by wt. of MWCNT-COOH were measured and the results are given below.

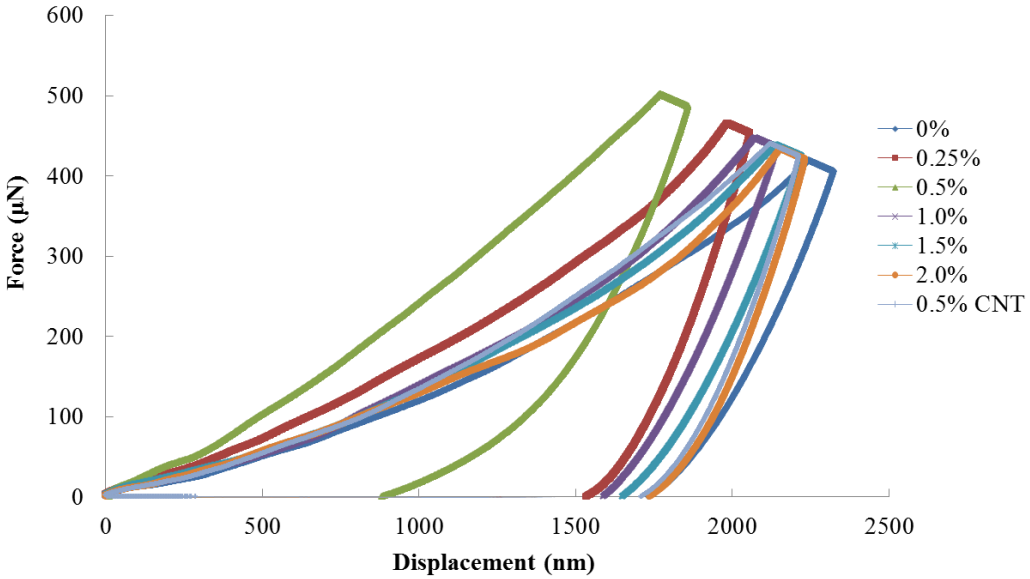

(a)

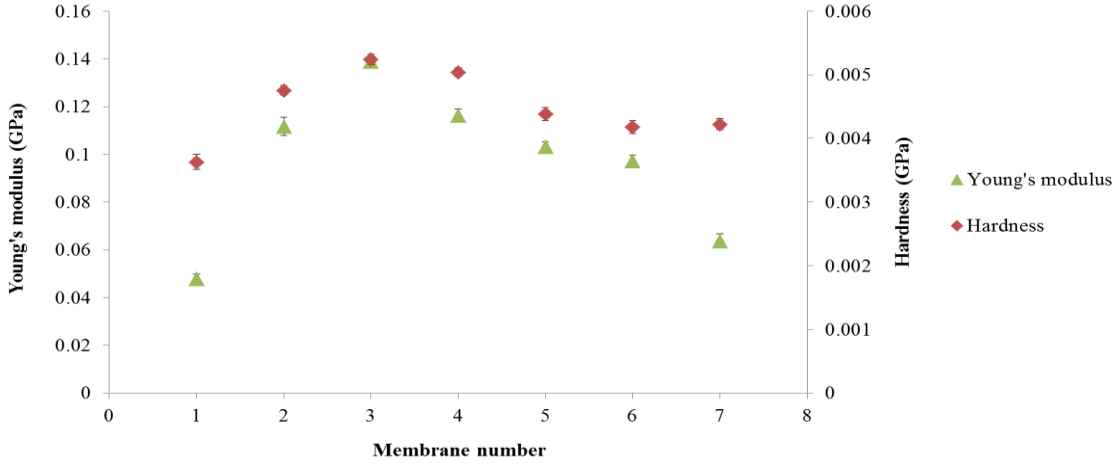

(b)

Figure 6.20. *Nanoindentation analysis results for the fabricated membranes (a) Force as a function of displacement (b) Young's modulus and hardness values (1:pristine PVC membrane, 2: PVC/0.25 Si-MWCNT membrane, 3: PVC/0.5 Si-MWCNT membrane, 4: PVC/1.0 Si-MWCNT membrane, 5: PVC/1.5 Si-MWCNT membrane, 6: PVC/2.0 Si-MWCNT membrane, 7: PVC/0.5 MWCNT-COOH membrane*)

As it can be seem in Figure 6.20a, maximum indentation depth of the fabricated depends on the amount of nanoparticle content of the membranes. The pure PVC membrane exhibited the highest maximum indentation depth of 2318 nm and with the increase of Si-MWCNT nanoparticles content, the maximum indentation depth decreased (Pakzad, Simonsen and Yassar, 2012). Addition of 0.5% of Si-MWCNT nanoparticles to the membrane matrix decreased the maximum indentation depth approximately by 35% (to 1500 nm), which means that under the same maximum load, pure PVC membrane deformed more than the PVC/Si-MWCNT nanocomposite membranes did. This reduction of the maximum indentation depth proved that there was a uniform distribution of Si-MWCNT nanoparticles in the casting solution and the strong bound between the Si-MWCNT nanoparticles and the PVC polymer which in turn enhance the mechanical behaviors of the membrane. However, further increase of Si-MWCNT nanoparticle amount resulted in an increase of the maximum indentation depth of the membrane, which might be attributed to the increase of the viscous nature of the membrane casting solution inhibiting the interaction between the polymer and the Si-MWCNT nanoparticles and creating stress-convergence points (Lee et al., 2013). In addition to this, the maximum indentation depth of PVC/0.5% MWCNT-COOH membrane was 2212 nm meaning that the deformation of the MWCNT-COOH added membrane was higher compared to that of Si-MWCNT modified membrane.

Young's modulus, which is the initial slope of the stress-strain curve, is a measure of resistance to deformation. According to Figure 6.20b, pristine PVC membrane had the lowest Young's modulus (≈ 0.047 GPa) among the fabricated membranes and as the percentage of Si-MWCNT nanoparticles increased, the Young's modulus tended to increase. Along with the incorporation of Si-MWCNT nanoparticles into the PVC matrix, the Young's modulus of the membranes was enhanced up to 75% corresponding to PVC/0.5% Si-MWCNT nanocomposite membrane with a value of 0.14 GPa, which means that resistance to deformation of pristine PVC membrane increased with the incorporation of Si-MWCNT nanoparticles under the applied force. The same trend was observed for the improvement of hardness values of the pristine PVC membrane, i.e., it increased from 0.0036 GPa to 0.0052 GPa with the addition of 0.5% Si-MWCNT. These results confirmed

that the addition of Si-MWCNT nanoparticles, which were uniformly dispersed in PVC matrix, were tightly bound with the polymer and improved the surface hardness as well as the elastic stiffness of the membrane. However, further increase of Si-MWCNT nanoparticles led to a decrease in the mechanical properties of the membrane. This might be attributed to the increase of the viscous nature of the membrane casting solution which inhibited the interaction between the polymer and the Si-MWCNT nanoparticles resulting in weak points in the membrane structure (Mahdi et al., 2016; Mirsa, Fu and Morgan, 2007; Lee et al., 2013). Furthermore, it can be observed from the figure that the Young Modulus and hardness values of the membrane fabricated using 0.5% MWCNT-COOH nanoparticles were found to be 0.063 GPa and 0.0042 GPa, respectively, which proved that the orientation of MWCNT with Silica particles greatly enhanced the mechanical property of the MWCNT so did the pure PVC membrane.

7. CONCLUSION

In the present thesis, a novel PVC based ultrafiltration membrane was developed by dispersing Si-MWCNT nanoparticles in the casting solution with varying amounts. The Si-MWCNT nanoparticles were synthesized by sol-gel method and the surface modification of MWCNT by Silica was confirmed by SEM, EDX and also FTIR analysis which verified the presence of Si-O group in the surface of Si-MWCNT. XRD analysis revealed that the synthesized Si-MWCNT has an amorphous structure.

Performance of PVC/Si-MWCNT membranes was studied in terms of pure water flux, sodium alginate and humic acid rejections and anti-fouling properties. The overall structures of the modified membranes were investigated in terms of morphological characteristics such as porosity; mean pore size, thickness, distribution of nanoparticles on the surface and in the cross-section of membranes, hydrophilicity, surface roughness, mechanical strength, crystallinity, thermal stability and surface composition.

The PVC/Si-MWCNT nanocomposite membrane addressed the trade-off between rejection and pure water flux performances for ultrafiltration. While maintaining a high SA and HA rejection performance (94% and 96% respectively), the water flux was increased (by 25% (around 400 L/m^2h by adding 0.5% Si-MWCNT) due to the hydrophilic properties introduced by the Si-MWCNT in the nanocomposite PVC membrane, which was also verified by the contact angle results and water uptake measurements and also the nodular structure enclosed by AFM images. The antifouling performance demonstrated that the blended membranes exhibited better antifouling properties reaching a FRR of 93% in the case of PVC/0.5%Si-MWCNT membrane and lower fouling resistances compared to those of pristine PVC membrane. Moreover, the SEM images indicated that finger-like pore structure of the modified nanocomposite membranes exhibited more connectivity between top and bottom layers, which led to a longer finger-like pore structure as well as a larger pore size compared to that of pure PVC membrane. EDX analysis showed that Si-MWCNT nanoparticles were evenly distributed along the cross-section and on the surface of the membranes at low concentrations up to 0.5%; however serious particle agglomeration occurred beyond 0.5% especially in the cross section area. FTIR spectrum of PVC and PVC/Si-MWCNT verified the existence of silica on the membrane surface by showing the

Si-O-Si and Si-CH groups. Based on the XRD results, PVC/Si-MWCNT nanocomposite membrane had amorphous structure which confirmed that Si-MWCNT nanoparticles were tightly bound with the PVC polymer. TGA results proved the thermal stability of the modified membranes at high temperature. Furthermore, PVC/Si-MWCNT nanocomposite membranes exhibited better mechanical strength in terms of hardness, stiffness and Young's modulus, which showed that membrane resistance to mechanical deformation under the applied force of stress was significantly enhanced by incorporating Si-MWCNT nanoparticles into the polymeric matrix resulting in an increase of membrane lifespan.

Table 7.1. *Comparison of the results found in this thesis with the reported data in the literature*

Resource	Membrane polymer	Nanoparticles	TMP (bar)	Membrane porosity (%)	Nanoparticle ratio (wt%)	Contact angle (°)	Pure water flux (L/m^2h)	Rejection (%)
Choi et al.	Polysulfone (PSf)	MWCNT	1	-	1.5	56.0	254	95
Wu et al.	Brominated polyphenylene (BPPO)	MWCNT	3	-	5.0	62.8	487	94
Majeed et al.	Polyacrylonitrile (PAN)	MWCNT	2	-	1.0	43.3	55	57
Yu et al.	Polyvinyldenefluride (PVDF)	3-aminopropyltriethoxysilane-MWCNT (A-MWCNT)	1	78	2.0	50.5	103	92
Vatanpour et al.	Polyvinyldenefluride (PVDF)	Polypyrrole (PPy)-MWCNT (PPY-MWCNT)	2	19	1.0	67.8	399	98
Sianipar et al.	Polysulfone (PSf)	Polydopamine-MWCNT	4	35	0.1	43.0	324	92
Zhang et al.	Polyvinyldenefluride (PVDF)	oxidized carbon nanotubes (OMWCNTs)	1	78	1.0	66.4	120	87
Rahimpour et al.	Polyether sulfone (PES)	MWCNT	3	-	0.5	57.6	184	94

Yu et al.	Polyvinyl chloride (PVC)	Nano-Silica	1	76	1.5	61.4	232	90
Present thesis	Polyvinyl chloride (PVC)	Si-MWCNT	0.69	90	0.5	54.0	400	94-96

REFERENCES

Abdel-Baset, T., Elzayat, M., and Mahrous, S. (2016). Characterization and optical and dielectric properties of polyvinyl chloride/silica nanocomposites films. *International Journal of Polymer Science*., **1**, 1-13.

Abdallah, H., Jamil, T. S., Shaban, A. M., Mansor, E. S., Souaya, E. R. (2018). Influence of the polyacrylonitrile proportion on the fabricated UF blend membranes' performance for humic acid removal. *Journal of Polymer Engineering*., **38**, 129-136.

Adato, R., Aksu, S., and Altug, H. (2015). Engineering mid-infrared nanoantennas for surface enhanced infrared absorption spectroscopy. *Materials Today.*, **18**, 436-446.

Al-Hobaib, A. S., Al-Sheetan, K. M., Shaik, M. R., Al-Suhybani, M. (2017). Modification of thin-film polyamide membrane with multi-walled carbon nanotubes by interfacial polymerization. *Applied Water Science*., **7**, 4341-4350.

Albert, D. E. (2015). Methods for verifying medical device cleanliness. In *Developments in surface contamination and cleaning* (109-128). William Andrew Publishing.

Alsalhy, Q., Algebory, S., Alwan, G. M., Simone, S., Figoli, A., Drioli, E. (2011). Hollow fiber ultrafiltration membranes from poly (vinyl chloride): preparation, morphologies, and properties. *Separation Science and Technology*., **46**, 2199-2210.

Arsuaga, J. M., Sotto, A., del Rosario, G., Martínez, A., Molina, S., Teli, S. B., Abajo, J. (2013). Influence of the type, size, and distribution of metal oxide particles on the properties of nanocomposite ultrafiltration membranes. *Journal of Membrane Science.*, **428**, 131-141.

Arumugham, T., Amimodu, R. G., Kaleekkal, N. J., Rana, D. (2019). Nano CuO/g-C_3N_4 sheets-based ultrafiltration membrane with enhanced interfacial affinity, antifouling and protein separation performances for water treatment application. *Journal of Environmental Sciences.*, **82**, 57-69.

Aryanti, P. T. P., Yustiana1b, R., Purnama, R. E. D., Wenten, I. G. (2015). Performance and characterization of PEG400 modified PVC ultrafiltration membrane. *Membrane Water Treatment.*, **6**, 379-392.

Bai, L., Liang, H., Crittenden, J., Qu, F., Ding, A., Ma, J., Li, G. (2015). Surface modification of UF membranes with functionalized MWCNTs to control membrane fouling by NOM fractions. *Journal of Membrane Science.*, **492**, 400-411.

Bai, H., Wang, X., Zhou, Y., Zhang, L. (2012). Preparation and characterization of poly (vinylidene fluoride) composite membranes blended with nano-crystalline cellulose. *Progress in Natural Science: Materials International.*, **22**, 250-257.

Baker, R. W., and Updated by Staff. (2000). Membrane technology. *Kirk Othmer Encyclopedia of Chemical Technology*.

Bhadra, M., and Mitra, S. (2013). Nanostructured membranes in analytical chemistry. *TrAC Trends in Analytical Chemistry.*, **45**, 248-263.

Bhatnagar, A., Kumar, E., and Sillanpää, M. (2010). Nitrate removal from water by nano-alumina: Characterization and sorption studies. *Chemical Engineering Journal.*, **163**, 317-323.

Bhavsar, V., and Tripathi, D. (2018). Structural, optical, and aging studies of biocompatible PVC-PVP blend films. *Journal of Polymer Engineering.*, **38**, 419-426.

Bisutti, I., Hilke, I., and Raessler, M. (2004). Determination of total organic carbon–an overview of current methods. *TrAC Trends in Analytical Chemistry.*, **23**, 716-726.

Bottino, A., Capannelli, G., Comite, A., Ferrari, F., Firpo, R., Venzano, S. (2009). Membrane technologies for water treatment and agroindustrial sectors. *Comptes Rendus Chimie.*, **12**, 882-888.

Bruschke, H. (1995). Industrial application of membrane separation processes. *Pure and applied chemistry.*, **67**, 993-1002.

Calabrò, V., and Basile, A. (2011). Fundamental membrane processes, science and engineering. In *Advanced Membrane Science and Technology for Sustainable Energy and Environmental Applications* (pp. 3-21): Elsevier.

Celik, E., and Choi, H. (2011). Carbon nanotube/polyethersulfone composite membranes for water filtration. In *Modern Applications in Membrane Science and Technology* (pp. 257-269): ACS Publications.

Chartoff, R. P., Menczel, J. D., and Dillman, S. H. (2009). Dynamic mechanical analysis (DMA). *Therm. Anal. Polym*, 387-495.

Chen, J. P., Mou, H., Wang, L. K., Matsuura, T., Wei, Y. (2011). Membrane separation: basics and applications. In *Membrane and desalination technologies* (pp. 271-332). Humana Press, Totowa, NJ.

Choi, J.-H., Jegal, J., and Kim, W.-N. (2006). Fabrication and characterization of multi-walled carbon nanotubes/polymer blend membranes. *Journal of Membrane Science.,* **284**, 406-415.

Chowdhury, Z. Z., Sagadevan, S., Johan, R. B., Shah, S. T., Adebesi, A., Md, S. I., Rafique, R. F. (2018). A review on electrochemically modified carbon nanotubes (CNTs) membrane for desalination and purification of water. *Materials Research Express.*, **5**, 102001.

Cui, W., Du, F., Zhao, J., Zhang, W., Yang, Y., Xie, X., Mai, Y. W. (2011). Improving thermal conductivity while retaining high electrical resistivity of epoxy composites by incorporating silica-coated multi-walled carbon nanotubes. *Carbon.*, **49**, 495-500.

Das, N., and Maiti, H. S. (2009). Ceramic membrane by tape casting and sol–gel coating for microfiltration and ultrafiltration application. *Journal of Physics and Chemistry of Solids.*, 70, 1395-1400.

Dao, T. D., Mericq, J.-P., Laborie, S., Cabassud, C. (2013). A new method for permeability measurement of hydrophobic membranes in Vacuum Membrane Distillation process. *water research.*, **47**, 2096-2104.

Das, R., Hamid, S. B. A., Ali, M. E., Ismail, A. F., Annuar, M., Ramakrishna, S. (2014). Multifunctional carbon nanotubes in water treatment: the present, past and future. *Desalination.,* **354**, 160-179.

Demirel, E., Zhang, B., Papakyriakou, M., Xia, S., Chen, Y. (2017). Fe2O3 nanocomposite PVC membrane with enhanced properties and separation performance. *Journal of membrane science.*, **529**, 170-184.

Ding, Z., Liu, X., Liu, Y., Zhang, L. (2016). Enhancing the compatibility, hydrophilicity and mechanical properties of polysulfone ultrafiltration membranes with lignocellulose nanofibrils. *Polymers*, **8**, 349.

Drioli, E., and Giorno, L. (Eds.). (2010). *Comprehensive membrane science and engineering* (Vol. **1**). Newnes.

Duarte, A. P., and Bordado, J. C. (2016). Smart composite reverse-osmosis membranes for energy generation and water desalination processes. In *Smart Composite Coatings and Membranes* (pp. 329-350). Woodhead Publishing.

Dwivedi, C., Pandey, I., Pandey, H., Ramteke, P. W., Pandey, A. C., Mishra, S. B., Patil, S. (2017). Electrospun nanofibrous scaffold as a potential carrier of antimicrobial therapeutics for diabetic wound healing and tissue regeneration. In *Nano-and Microscale Drug Delivery Systems* (pp. 147-164). Elsevier.

El–Safty, S. A., and Hoa, N. D. (2012). Organic–Inorganic Mesoporous Silica Nanotube Hybrid Anodic Alumina Membranes for Ultrafine Filtration of Noble Metal Nanoparticles. In *Noble Metals*. IntechOpen.

Eren, E., Sarihan, A., Eren, B., Gumus, H., Kocak, F. O. (2015). Preparation, characterization and performance enhancement of polysulfone ultrafiltration membrane using PBI as hydrophilic modifier. *Journal of Membrane Science.*, **475**, 1-8.

Erkan, H. S., Turan, N. B., and Engin, G. Ö. (2018). Membrane bioreactors for wastewater treatment. In *Comprehensive Analytical Chemistry* (Vol. **81**, pp. 151-200). Elsevier.

Han, M.-J., and Nam, S.-T. (2002). Thermodynamic and rheological variation in polysulfone solution by PVP and its effect in the preparation of phase inversion membrane. *Journal of Membrane Science.*, **202**, 55-61.

Fane, A. G., Wang, R., and Hu, M. X. (2015). Synthetic membranes for water purification: status and future. *Angewandte Chemie International Edition.*, **54**, 3368-3386.

Fersi, C., Gzara, L., and Dhahbi, M. (2009). Flux decline study for textile wastewater treatment by membrane processes. *Desalination.*, **244**, 321-332.

Goh, P. S., Ng, B. C., Lau, W. J., Ismail, A. F. (2015). Inorganic nanomaterials in polymeric ultrafiltration membranes for water treatment. *Separation & Purification Reviews.*, **44**, 216-249.

Hamingerova, M., Borunsky, L., and Beckmann, M. (2015). Membrane Technologies for Water and Wastewater Treatment on the European and Indian Market. Techview Report of Fraunhofer Center for International Management and Knowledge Economy.

Hilal, N., and Wright, C. J. (2018). Exploring the current state of play for cost-effective water treatment by membranes. *npj Clean Water*, **1**,1-8.

Hossieny, N. (2010). Morphology and Properties of Polymer/Carbon Nanotube Nanocomposite Foams Prepared by Supercritical Carbon Dioxide.

Hsu, Y.-W., Wu, C.-C., Wu, S.-M., Su, C.-C. (2017). Synthesis and Properties of Carbon Nanotube-Grafted Silica Nanoarchitecture-Reinforced Poly (Lactic Acid). *Materials.,* **10**, 829.

Hübschen, G., Altpeter, I., Tschuncky, R., Herrmann, H. G. (Eds.). (2016). *Materials characterization using Nondestructive Evaluation (NDE) methods*. Woodhead publishing.

Idris, A., Zain, N. M., and Noordin, M. (2007). Synthesis, characterization and performance of asymmetric polyethersulfone (PES) ultrafiltration membranes with polyethylene glycol of different molecular weights as additives. *Desalination.,* **207**, 324-339.

Islam, M. S., Deng, Y., Tong, L., Faisal, S. N., Roy, A. K., Minett, A. I., Gomes, V. G. (2016). Grafting carbon nanotubes directly onto carbon fibers for superior mechanical stability: Towards next generation aerospace composites and energy storage applications. *Carbon.*, **96**, 701-710.

Jankhah, S. (2018). Technology trends in membrane filtration use. *Filtration and Separation.,* **55**, 30-33.

Jose, A. J., Kappen, J., and Alagar, M. (2018). Polymeric membranes: Classification, preparation, structure physiochemical, and transport mechanisms. In *Fundamental Biomaterials: Polymers* (pp. 21-35). Woodhead Publishing.

Kar, S., Bindal, R. C., and Tewari, P. K. (2012). Carbon nanotube membranes for desalination and water purification: Challenges and opportunities. *Nano Today.,* **7**, 385-389.

Kayyarapu, B., Kumar, Y., Mohommad, H. B., Neeruganti, O., Chekuri, R. (2016). Structural, thermal and optical properties of pure and Mn2+ doped poly (vinyl chloride) films. *Materials Research.,* **19**, 1167-1175.

Kayvani Fard, A., McKay, G., Buekenhoudt, A., Al Sulaiti, H., Motmans, F., Khraisheh, M., Atieh, M. (2018). Inorganic membranes: preparation and application for water treatment and desalination. *Materials.,* **11**, 74.

Kesting, R. E. (1990). The four tiers of structure in integrally skinned phase inversion membranes and their relevance to the various separation regimes. *Journal of applied polymer science.*, **41**, 2739-2752.

Khalid, A., Al-Juhani, A. A., Al-Hamouz, O. C., Laoui, T., Khan, Z., Atieh, M. A. (2015). Preparation and properties of nanocomposite polysulfone/multi-walled carbon nanotubes membranes for desalination. *Desalination.*, **367**, 134-144.

Khan, A., Sherazi, T. A., Khan, Y., Li, S., Naqvi, S. A. R., Cui, Z. (2018). Fabrication and characterization of polysulfone/modified nanocarbon black composite antifouling ultrafiltration membranes. *Journal of Membrane Science.*, **554**, 71-82.

Khulbe, K. C., Feng, C. Y., and Matsuura, T. (2007). Synthetic polymeric membranes: characterization by atomic force microscopy. *Springer Science and Business Media*.

Kim, E. S., Hwang, G., El-Din, M. G., Liu, Y. (2012). Developmnt of nanosilver and multi-walled carbon nanotubes thin-film nanocomposite membrane for enhanced water treatment. *Journal of membrane science.*, **394**, 37-48.

Kim, J. Y., Lee, H. K., and Kim, S. C. (1999). Surface structure and phase separation mechanism of polysulfone membranes by atomic force microscopy. *Journal of Membrane Science.*, **163**, 159-166.

Kim, M., Hong, J., Lee, J., Hong, C. K., Shim, S. E. (2008). Fabrication of silica nanotubes using silica coated multi-walled carbon nanotubes as the template. *Journal of colloid and interface science*, **322**, 321-326.

Kools, W. F. C. (1998). Membrane formation by phase inversion in multicomponent polymer systems. Mechanisms and morphologies.

Krishnamoorthy, R., and Sagadevan, V. (2015). Polyethylene glycol and iron oxide nanoparticles blended polyethersulfone ultrafiltration membrane for enhanced performance in dye removal studies. *e-Polymers.*, **15**, 151-159.

Laîné, J. M., Vial, D., and Moulart, P. (2000). Status after 10 years of operation—overview of UF technology today. *Desalination.*, **131**, 17-25.

Lee, A., Elam, J. W., and Darling, S. B. (2016). Membrane materials for water purification: design, development, and application. *Environmental Science: Water Research andTechnology.*, **2**, 17-42.

Lee, J., Jeong, S., and Liu, Z. (2016). Progress and challenges of carbon nanotube membrane in water treatment. *Critical reviews in environmental science and technology.,* **46**, 999-1046.

Lee, S., Choi, B. G., Choi, D., Park, H. S. (2014). Nanoindentation of annealed Naf ion/sulfonated graphene oxide nanocomposite membranes for the measurement of mechanical properties. *Journal of Membrane Science.,* **451**, 40-45.

Liew, K. M., Lei, Z. X., and Zhang, L. W. (2015). Mechanical analysis of functionally graded carbon nanotube reinforced composites: a review. *Composite Structures.*, **120**, 90-97.

Lonsdale, H. K. (1982). The growth of membrane technology. *Journal of membrane science.*, **10**, 81-181.

Low, Z. X., Wang, Z., Leong, S., Razmjou, A., Dumée, L. F., Zhang, X., Wang, H. (2015). Enhancement of the antifouling properties and filtration performance of poly (ethersulfone) ultrafiltration membranes by incorporation of nanoporous titania nanoparticles. *Industrial and Engineering Chemistry Research.*, **54**, 11188-11198.

Liu, X., Peng, Y., and Ji, S. (2008). A new method to prepare organic–inorganic hybrid membranes. *Desalination.*, **221**, 376-382.

Liu, H., Gong, C., Wang, J., Liu, X., Liu, H., Cheng, F., Wen, S. (2016). Chitosan/silica coated carbon nanotubes composite proton exchange membranes for fuel cell applications. *Carbohydrate polymers.*, **136**, 1379-1385.

Loganathan, S., Valapa, R. B., Mishra, R. K., Pugazhenthi, G., Thomas, S. (2017). Thermogravimetric analysis for characterization of nanomaterials. In *Thermal and Rheological Measurement Techniques for Nanomaterials Characterization* (pp. 67-108). Elsevier.

Low, Z.-X., Razmjou, A., Wang, K., Gray, S., Duke, M., Wang, H. (2014). Effect of addition of two-dimensional ZIF-L nanoflakes on the properties of polyethersulfone ultrafiltration membrane. *Journal of Membrane Science.,* **460**, 9-17.

Ma, L., Dong, X., Chen, M., Zhu, L., Wang, C., Yang, F., Dong, Y. (2017). Fabrication and water treatment application of carbon nanotubes (CNTs)-based composite membranes: a review. *Membranes.*, **7**, 16.

Mahdi, E., Chaudhuri, A. K., and Tan, J.-C. (2016). Capture and immobilisation of iodine (I 2) utilising polymer-based ZIF-8 nanocomposite membranes. *Molecular Systems Design & Engineering.*, **1**, 122-131.

Mallakpour, S., and Shafiee, E. (2017). The synthesis of poly (vinyl chloride) nanocomposite films containing ZrO2 nanoparticles modified with vitamin B1 with the aim of improving the mechanical, thermal and optical properties. *Designed monomers and polymers.*, **20**, 378-388.

Marbelia, L., Bilad, M. R., Bertels, N., Laine, C., Vankelecom, I. F. (2016). Ribbed PVC–silica mixed matrix membranes for membrane bioreactors. *Journal of membrane science.*, **498**, 315-323.

Martín, A., Arsuaga, J. M., Roldán, N., De Abajo, J., Martínez, A., Sotto, A. (2015). Enhanced ultrafiltration PES membranes doped with mesostructured functionalized silica particles. *Desalination.*, **357**, 16-25.

Misra, R., Fu, B. X., and Morgan, S. E. (2007). Surface energetics, dispersion, and nanotribomechanical behavior of POSS/PP hybrid nanocomposites. *Journal of Polymer Science Part B: Polymer Physics.*, **45**, 2441-2455.

Mittal, P., Jana, S., and Mohanty, K. (2011). Synthesis of low-cost hydrophilic ceramic–polymeric composite membrane for treatment of oily wastewater. Desalination., **282**, 54-62.

Mohamed, M. A., Jaafar, J., Ismail, A., Othman, M., Rahman, M. (2017). Fourier transform infrared (FTIR) spectroscopy. In *Membrane Characterization* (pp. 3-29): Elsevier.

Mohammad, A. W., Hilal, N., Lim, Y. P., Amin, I. N. H. M., Raslan, R. (2011). Atomic force microscopy as a tool for asymmetric polymeric membrane characterization. *Sains Malaysiana.*, **40**, 237-244.

Molyanyan, E., Aghamiri, S., Talaie, M., Iraji, N. (2016). Experimental study of pure and mixtures of CO 2 and CH 4 adsorption on modified carbon nanotubes. *International journal of environmental science and technology.*, **13**, 2001-2010.

Mulder, J. (2012). *Basic principles of membrane technology*. Springer Science and Business Media.

Murugesan, V. (2017). *Optimization of Nanocomposite Membrane for Membrane Distillation* (Doctoral dissertation, Université d'Ottawa/University of Ottawa).

Nagavarma, B. V. N., Yadav, H. K., Ayaz, A. V. L. S., Vasudha, L. S., Shivakumar, H. G. (2012). Different techniques for preparation of polymeric nanoparticles-a review. *Asian J. Pharm. Clin. Res.*, **5**, 16-23.

Nagy, E. (2018). *Basic Equations of Mass Transport Through a Membrane Layer*: Elsevier.

Ng, L. Y., Mohammad, A. W., Leo, C. P., Hilal, N. (2013). Polymeric membranes incorporated with metal/metal oxide nanoparticles: a comprehensive review. *Desalination.,* **308**, 15-33.

Nicolaisen, B. (2003). Developments in membrane technology for water treatment. *Desalination.,* **153**, 355-360.

Nikje, M. M. A., and Yaghoubi, A. (2014). Preparation and properties of polyurethane/functionalized multi-walled carbon nanotubes rigid foam nanocomposites. *Polimery.,* **59**, 776-782.

Noble, R. D. (1987). An overview of membrane separations. *Separation science and technology.*, **22**, 731-743.

Nunes, S. P., and Peinemann, K. V. (2001). *Membrane technology*. Wiley-vch.

Orooji, Y., Faghih, M., Razmjou, A., Hou, J., Moazzam, P., Emami, N., Jin, W. (2017). Nanostructured mesoporous carbon polyethersulfone composite ultrafiltration membrane with significantly low protein adsorption and bacterial adhesion. *Carbon.,* **111**, 689-704.

Pakzad, A., Simonsen, J., and Yassar, R. (2012). Elastic properties of thin poly (vinyl alcohol)–cellulose nanocrystal membranes. *Nanotechnology.,* **23**, 085706.

Pendergast, M. M., and Hoek, E. M. (2011). A review of water treatment membrane nanotechnologies. *Energy & Environmental Science.,* **4**, 1946-1971.

Peyravi, M., Jahanshahi, M., Rahimpour, A., Javadi, A., Hajavi, S. (2014). Novel thin film nanocomposite membranes incorporated with functionalized TiO2 nanoparticles for organic solvent nanofiltration. *Chemical Engineering Journal.*, **241**, 155-166.

Pendergast, M. M., and Hoek, E. M. (2011). A review of water treatment membrane nanotechnologies. *Energy and Environmental Science.*, **4**, 1946-1971.

Pinnau, I., and Freeman, B. D. (2000). for Membrane Separations. In *Encyclopedia of Separation Science* (pp. 1755-1764). Academic Press.

Purkait, M. K., Sinha, M. K., Mondal, P., Singh, R. (2018). *Stimuli Responsive Polymeric Membranes: Smart Polymeric Membranes* (Vol. **25**). Academic Press.

Qin, X., and Subianto, S. (2017). Electrospun nanofibers for filtration applications. In *Electrospun Nanofibers* (pp. 449-466). Woodhead Publishing.

Rahimpour, A., Jahanshahi, M., Khalili, S., Mollahosseini, A., Zirepour, A., Rajaeian, B. (2012). Novel functionalized carbon nanotubes for improving the surface properties and performance of polyethersulfone (PES) membrane. *Desalination.*, **286,** 99-107.

Rajendran, S., Prabhu, M. R., and Rani, M. U. (2008). Characterization of PVC/PEMA based polymer blend electrolytes. *International journal of electrochemical science.*, **3**, 282-290.

Raman, N., Sudharsan, S., and Pothiraj, K. (2012). Synthesis and structural reactivity of inorganic–organic hybrid nanocomposites–a review. J*ournal of Saudi Chemical Society*., **16**, 339-352.

Ramoraswi, N. O. (2014). *Physical and Chemical Properties of Carbon Nanotubes and Silica Nano-composites on the Photo-catalytic Activity of Titania Nanoparticles for Selected Organic Pollutants* (Doctoral dissertation, University of KwaZulu-Natal, Durban).

Rana, D., and Matsuura, T. (2010). Surface modifications for antifouling membranes. *Chemical reviews.*, **110**, 2448-2471.

Rashid, M., and Ralph, S. F. (2017). Carbon nanotube membranes: synthesis, properties, and future filtration applications. *Nanomaterials.*, **7**, 99.

Rosa, M. J., and De Pinho, M. N. (1997). Membrane surface characterisation by contact angle measurements using the immersed method. *Journal of Membrane Science.*, **131**, 167-180.

Roy, K., Anjali, T., and Sujith, A. (2017). Asymmetric membranes based on poly (vinyl chloride): effect of molecular weight of additive and solvent power on the morphology and performance. *Journal of materials science.*, **52**, 5708-5725.

Sabir, A., Shafiq, M., Islam, A., Sarwar, A., Dilshad, M. R., Shafeeq, A., Jamil, T. (2015). Fabrication of tethered carbon nanotubes in cellulose acetate/polyethylene glycol-400 composite membranes for reverse osmosis. *Carbohydrate polymers.*, **132**, 589-597.

Saha, A. K., Das, S., Bhatta, D., Mitra, B. C. (1999). Study of jute fiber reinforced polyester composites by dynamic mechanical analysis. *Journal of applied polymer science.*, **71**, 1505-1513.

Saki, S., and Uzal, N. (2018). Preparation and characterization of PSF/PEI/CaCO 3 nanocomposite membranes for oil/water separation. *Environmental Science and Pollution Research.*, **25**, 25315-25326.

Saraswathi, M. S. S. A., Nagendran, A., and Rana, D. (2019). Tailored polymer nanocomposite membranes based on carbon, metal oxide and silicon nanomaterials: a review. *Journal of Materials Chemistry A.*, **7**, 8723-8745.

Saraswathi, M. S. S. A., Rana, D., Nagendran, A., Alwarappan, S. (2018). Custom-made PEI/exfoliated-MoS2 nanocomposite ultrafiltration membranes for separation of bovine serum albumin and humic acid. *Materials Science and Engineering: C.*, **83**, 108-114.

Scott, K. (1995). Introduction to membrane separations. *Handbook of industrial membranes: introduction to membrane separation. 2rd ed. Elsevier Advanced Technology*, 3-185.

Seader, J. D., Henley, E. J., and Roper, D. K. (2006). Separation process principles.

Si, M., Feng, D., Qiu, L., Jia, D., Elzatahry, A. A., Zheng, G., Zhao, D. (2013). Free-standing highly ordered mesoporous carbon–silica composite thin films. *Journal of Materials Chemistry A.*, **1**, 13490-13495.

Sianipar, M., Kim, S. H., Min, C., Tijing, L. D., Shon, H. K. (2016). Potential and performance of a polydopamine-coated multiwalled carbon nanotube/polysulfone nanocomposite membrane for ultrafiltration application. *Journal of industrial and engineering chemistry.*, **34**, 364-373.

Sile-Yuksel, M., Tas, B., Koseoglu-Imer, D. Y., Koyuncu, I. (2014). Effect of silver nanoparticle (AgNP) location in nanocomposite membrane matrix fabricated with different polymer type on antibacterial mechanism. *Desalination.*, **347**, 120-130.

Silva, T. L., Morales-Torres, S., Figueiredo, J. L., Silva, A. M. (2015). Multi-walled carbon nanotube/PVDF blended membranes with sponge-and finger-like pores for direct contact membrane distillation. *Desalination.*, **357**, 233-245.

Singh, R. (2014). *Membrane technology and engineering for water purification: application, systems design and operation*. Butterworth-Heinemann.

Singh, R., Kumar, R., and Ahuja, I. S. (2017). Thermal analysis for joining of dissimilar polymeric materials through friction stir welding.

Sgreccia, E., Chailan, J. F., Khadhraoui, M., Di Vona, M. L., Knauth, P. (2010). Mechanical properties of proton-conducting sulfonated aromatic polymer membranes: stress–strain tests and dynamical analysis. *Journal of Power Sources.*, **195**, 7770-7775.

Sridhar, S., Bee, S., and Bhargava, S. K. (2014). Membrane-based gas separation: principle, applications and future potential. *Chem. Eng. Dig.*, 1-25.

Strathmann, H. (1981). Membrane separation processes. *Journal of membrane science.*, **9**, 121-189.

Strathmann, H. (2000). Membrane separation processes, 1. Principles. *Ullmann's Encyclopedia of Industrial Chemistry*.

Stanojević, M., Lazarević, B., and Radić, D. (2003). Review of membrane contactors designs and applications of different modules in industry. *FME Transactions.*, **31**, 91-98.

Tai, M. H., Gao, P., Tan, B. Y. L., Sun, D. D., Leckie, J. O. (2014). Highly efficient and flexible electrospun carbon–silica nanofibrous membrane for ultrafast gravity-driven oil–water separation. *ACS applied materials and interfaces.*, **6**, 9393-9401.

Teow, Y., Ooi, B., Ahmad, A., Lim, J. (2012). Mixed-matrix membrane for humic acid removal: influence of different types of TiO2 on membrane morphology and performance. *International Journal of Chemical Engineering and Applications.*, **3**, 374.

Ulbricht, M. (2006). Advanced functional polymer membranes. *Polymer.*, **47**, 2217-2262.

Van der Bruggen, B. (2018). Microfiltration, ultrafiltration, nanofiltration, reverse osmosis, and forward osmosis. In *Fundamental Modelling of Membrane Systems* (pp. 25-70): Elsevier.

Van der Bruggen, B., Vandecasteele, C., Van Gestel, T., Doyen, W., Leysen, R. (2003). A review of pressure-driven membrane processes in wastewater treatment and drinking water production. *Environmental progress.*, **22**, 46-56.

Vatanpour, V., Ghadimi, A., Karimi, A., Khataee, A., Yekavalangi, M. E. (2018). Antifouling polyvinylidene fluoride ultrafiltration membrane fabricated from embedding polypyrrole coated multiwalled carbon nanotubes. *Materials Science and Engineering: C.*, **89**, 41-51.

Vatanpour, V., Madaeni, S. S., Moradian, R., Zinadini, S., Astinchap, B. (2012). Novel antibifouling nanofiltration polyethersulfone membrane fabricated from embedding TiO2 coated multiwalled carbon nanotubes. *Separation and purification technology.*, **90**, 69-82.

Vinci, R. P., and Vlassak, J. J. (1996). Mechanical behavior of thin films. *Annual Review of Materials Science.*, **26**, 431-462.

Visakh, P. M., Markovic, G., and Pasquini, D. (Eds.). (2016). *Recent Developments in Polymer Macro, Micro and Nano Blends: Preparation and Characterisation*. Woodhead Publishing.

Wang, K., Addiego, F., Bahlouli, N., Ahzi, S., Rémond, Y., Toniazzo, V., Muller, R. (2012). Analysis of thermomechanical reprocessing effects on polypropylene/ethylene octene copolymer blends. *Polymer degradation and stability.*, **97**, 1475-1484.

Wang, K., Abdalla, A. A., Khaleel, M. A., Hilal, N., Khraisheh, M. K. (2017). Mechanical properties of water desalination and wastewater treatment membranes. *Desalination.*, **401**, 190-205.

Wang, P., Ma, J., Wang, Z., Shi, F., Liu, Q. (2012). Enhanced separation performance of PVDF/PVP-g-MMT nanocomposite ultrafiltration membrane based on the NVP-grafted polymerization modification of montmorillonite (MMT). *Langmuir.*, **28**, 4776-4786.

Wang, X., Du, Z., Zhang, C., Li, C., Yang, X., Li, H. (2008). Multi-walled carbon nanotubes encapsulated with polyurethane and its nanocomposites. *Journal of Polymer Science Part A: Polymer Chemistry.*, **46**, 4857-4865.

Wang, Z., Xu, L., Qi, C., Zhao, C. (2018). Fabrication of MWCNTs-polysulfone composite membranes and its application in the removal of bisphenol A. *Materials Research Express.*, **5**, 065101.

Whitehead, P. (2018). Total Organic Carbon (TOC) and its Measurement https://www.elgalabwater.com/blog/total-organic-carbon-toc 27 Mar 2018.

Wu, G., Gan, S., Cui, L., Xu, Y. (2008). Preparation and characterization of PES/TiO2 composite membranes. *Applied Surface Science.,* **254**, 7080-7086.

Wu, H., Tang, B., and Wu, P. (2010). Novel ultrafiltration membranes prepared from a multi-walled carbon nanotubes/polymer composite. *Journal of Membrane Science.,* **362**, 374-383.

Wu, Z., Faiz, R., Li, T., Kingsbury, B. F., Li, K. (2013). A controlled sintering process for more permeable ceramic hollow fibre membranes. *Journal of membrane science.,* **446**, 286-293.

Wei, G., Chen, S., Fan, X., Quan, X., Yu, H. (2015). Carbon nanotube hollow fiber membranes: high-throughput fabrication, structural control and electrochemically improved selectivity. *Journal of Membrane Science.*, **493**, 97-105.

Yadav, K. (2009). Diagnosis of the failure of ultrafiltration membranes used in the dairy industry.

Yang, Y., Qiu, S., Cui, W., Zhao, Q., Cheng, X., Li, R. K. Y., Mai, Y.-W. (2009). A facile method to fabricate silica-coated carbon nanotubes and silica nanotubes from carbon nanotubes templates. *Journal of materials science.,* **44**, 4539-4545.

Yang, Y., Zhang, H., Wang, P., Zheng, Q., Li, J. (2007). The influence of nano-sized TiO2 fillers on the morphologies and properties of PSF UF membrane. *Journal of Membrane Science.*, **288**, 231-238.

Yin, J., and Deng, B. (2015). Polymer-matrix nanocomposite membranes for water treatment. *Journal of membrane science.,* **479**, 256-275.

Young, S. K., and Mauritz, K. A. (2001). Dynamic mechanical analyses of Nafion/organically modified silicate nanocomposites. *Journal of Polymer Science Part B: Polymer Physics.*, **39**, 1282-1295.

Yu, Z., Liu, X., Zhao, F., Liang, X., Tian, Y. (2015). Fabrication of a low-cost nano-SiO2/PVC composite ultrafiltration membrane and its antifouling performance. *Journal of Applied Polymer Science*, **132**, 1-11.

Yun, S., and Oyama, S. T. (2011). Correlations in palladium membranes for hydrogen separation: a review. *Journal of membrane science.*, **375**, 28-45.

Zahid, M., Rashid, A., Akram, S., Rehan, Z. A., Razzaq, W. (2018). A comprehensive review on polymeric nano-composite membranes for water treatment. *J Membrane Sci Technol.*, **8**, 179-198.

Zare, S., and Kargari, A. (2018). Membrane properties in membrane distillation. In *Emerging Technologies for Sustainable Desalination Handbook* (pp. 107-156). Butterworth-Heinemann.

Zargar, M., Hartanto, Y., Jin, B., Dai, S. (2017). Polyethylenimine modified silica nanoparticles enhance interfacial interactions and desalination performance of thin film nanocomposite membranes. *Journal of Membrane Science.,* **541**, 19-28.

Zhang, J., Xu, Z., Shan, M., Zhou, B., Li, Y., Li, B., Qian, X. (2013). Synergetic effects of oxidized carbon nanotubes and graphene oxide on fouling control and anti-fouling mechanism of polyvinylidene fluoride ultrafiltration membranes. *Journal of Membrane Science.,* **448**, 81-92.

Zhang, X., Chen, Y., Konsowa, A. H., Zhu, X., Crittenden, J. C. (2009). Evaluation of an innovative polyvinyl chloride (PVC) ultrafiltration membrane for wastewater treatment. *Separation and purification technology.*, **70**, 71-78.

Zhao, S., Yan, W., Shi, M., Wang, Z., Wang, J., Wang, S. (2015). Improving permeability and antifouling performance of polyethersulfone ultrafiltration membrane by incorporation of ZnO-DMF dispersion containing nano-ZnO and polyvinylpyrrolidone. *Journal of Membrane Science.,* **478**, 105-116.

Zhou, D., Zhu, L., Fu, Y., Zhu, M., Xue, L. (2015). Development of lower cost seawater desalination processes using nanofiltration technologies A review. *Desalination.,* **376**, 109-116.

Zhou, H., Zhang, C., Li, H., Du, Z. (2011). Fabrication of silica nanoparticles on the surface of functionalized multi-walled carbon nanotubes. *Carbon.,* **49**, 126-132.

Zhu, K., and Wang, G. (2018). Fabrication of high-performance ultrafiltration membranes using zwitterionic carbon nanotubes and polyethersulfone. *High Performance Polymers.*, **30**, 602-611.

Xu, Z., Wu, T., Shi, J., Teng, K., Wang, W., Ma, M., Fan, J. (2016). Photocatalytic antifouling PVDF ultrafiltration membranes based on synergy of graphene oxide and TiO2 for water treatment. *Journal of Membrane Science.*, **520**, 281-293.

RESUME

Name and surname	: Chahrazed MAHMOUDI
Foreign language	: Arabic, French, English
Place and Year of Birth	: Algeria/ 1995
Email	: mahmoudichahrazedmaster@gmail.com

Education and Professional Background:

- 2014-2017, Bachelor's Degree, University of Hassiba Ben Bouali Algeri, Faculty of Science and Technology, Department of Process Engineering.
- 2017 – Ongoing, Degree of Master of Science, University of Hassiba Ben Bouali Algeria, Faculty of Science and Technology, Department of Chemical Engineering.
- 2018-2019, Erasmus Program, Degree of Master of Science, Eskisehir Technical University, School of Natural Sciences, Department of Chemical engineering.